

ISVR Technical Memorandum

SCIENTIFIC PUBLICATIONS BY THE ISVR

Technical Reports are published to promote timely dissemination of research results by ISVR personnel. This medium permits more detailed presentation than is usually acceptable for scientific journals. Responsibility for both the content and any opinions expressed rests entirely with the author(s).

Technical Memoranda are produced to enable the early or preliminary release of information by ISVR personnel where such release is deemed to be appropriate. Information contained in these memoranda may be incomplete, or form part of a continuing programme; this should be borne in mind when using or quoting from these documents.

Contract Reports are produced to record the results of scientific work carried out for sponsors, under contract. The ISVR treats these reports as confidential to sponsors and does not make them available for general circulation. Individual sponsors may, however, authorize subsequent release of the material.

COPYRIGHT NOTICE

(c) ISVR University of Southampton All rights reserved.

ISVR authorises you to view and download the Materials at this Web site ("Site") only for your personal, non-commercial use. This authorization is not a transfer of title in the Materials and copies of the Materials and is subject to the following restrictions: 1) you must retain, on all copies of the Materials downloaded, all copyright and other proprietary notices contained in the Materials; 2) you may not modify the Materials in any way or reproduce or publicly display, perform, or distribute or otherwise use them for any public or commercial purpose; and 3) you must not transfer the Materials to any other person unless you give them notice of, and they agree to accept, the obligations arising under these terms and conditions of use. You agree to abide by all additional restrictions displayed on the Site as it may be updated from time to time. This Site, including all Materials, is protected by worldwide copyright laws and treaty provisions. You agree to comply with all copyright laws worldwide in your use of this Site and to prevent any unauthorised copying of the Materials.

UNIVERSITY OF SOUTHAMPTON
INSTITUTE OF SOUND AND VIBRATION RESEARCH
DYNAMICS GROUP

Applications of Bio-Feedback to Muscle Models

by

F.M. Colacino, E. Rustighi and B.R. Mace

ISVR Technical Memorandum No: 993

December 2010

Authorised for issue by
Professor Brian Mace
Group Chairman

© Institute of Sound & Vibration Research

Table of Contents

Abstract.....	4
1. Aim	5
2. Background	5
3. Model description	7
3.1 <i>Musculotendon System</i>	9
3.1.1 <i>Muscle activation dynamics</i>	10
3.1.2 <i>Active muscle Force-Length relationship</i>	11
3.1.3 <i>Passive muscle Force-Length relationship</i>	12
3.1.4 <i>Muscle Force-Velocity relationship</i>	12
3.1.5 <i>Total Force-Length-Velocity relationship for muscles</i>	13
3.1.6 <i>Tendon Force-Length relationship</i>	14
3.1.7 <i>Musculotendon unit dynamics</i>	14
3.2 <i>Limb Anatomy</i>	16
3.3 <i>Nervous System</i>	17
3.3.1 <i>Spinal Cord and Sensory Organs</i>	17
3.3.2 <i>The Renshaw Inhibition (β-loop)</i>	18
3.3.3 <i>The Golgi-Tendon Organs</i>	18
3.3.4 <i>Muscle Spindles</i>	19
3.3.5 <i>Considerations on the Sensory Organs</i>	22
3.3.6 <i>Motoneuron Pool</i>	22
4. Measurements	23
4.1 <i>Aim</i>	23
4.2 <i>Experimental Setup</i>	23
4.2.1 <i>Data Logger Setup</i>	24
4.2.2 <i>Strain Gauge Load Cell Calibration</i>	24
4.3 <i>Trials & Protocol</i>	24
5. Model Implementation	28
5.1 <i>Parameter Estimation</i>	32
5.1.1 <i>Loading and Pre-processing of Experimental Data</i>	33
5.1.2 <i>Parameter Initialisation</i>	36
5.1.3 <i>Optimisation Algorithm</i>	41
5.1.4 <i>Data Output and Plotting</i>	45

6. Data Analysis and Results	46
6.1 Estimated Values	46
6.2 Model Validation.....	56
6.3 Static Values.....	62
6.4 Operating range of Muscle Fibres.....	66
7. Discussion.....	67
8. Conclusions	69
Acknowledgements.....	70
References	71
Appendix A.....	74
Appendix B.....	85
Appendix C.....	91

Abstract

An EMG-driven musculoskeletal model is implemented to estimate subject-specific musculoskeletal parameters such as the optimal physiological muscle length, the tendon slack length and the maximum isometric muscle force of flexor and extensor muscle groups crossing the wrist, as well as biomechanical indexes to quantify the muscle operating range, the stiffness of the musculotendon actuators, and the contribution of the muscle fibers to the joint moment.

Twelve healthy subjects (11 males and 1 female, mean age 31.1 ± 8.7 years) were instructed to perform isometric maximum voluntary contractions of wrist flexors and extensors. Recorded EMGs were used as input to the model and the root mean square error (RMSE) between measured and predicted torque was minimised to estimate the subject-specific musculotendon parameters. The model was validated and the RMSE and the normalised RMSE calculated during estimation and validation phases are compared.

Estimated subject-specific musculoskeletal parameters vary in a physiologically realistic range, while the biomechanical indexes are consistent with previously published data.

The proposed methodology proved to be effective for the in-vivo estimation of physiological parameters of the musculotendon complex and has potential as an investigative tool to distinguish aetiological differences among subjects affected by musculoskeletal disorders.

1. Aim

The main research idea consists in the implementation and validation of a neuromusculoskeletal model of a one degree of freedom wrist joint with the aim to investigate the interaction between musculotendon system and neural signals controlling muscle contraction.

The outcome of the research provides investigational opportunities to quantify limb function and the relative contribution of model subcomponents and could be exploited to enhance the understanding of the mutual role of Central Nervous System (CNS), peripheral receptors and musculoskeletal system during motor tasks as well as for the development of rehabilitation protocols or the implementation of closed loop algorithms for functional electrical stimulation (FES).

To pursue the aim of the research, a topological musculoskeletal model of a single degree of freedom wrist joint was developed. Electromyograms (EMGs) and exerted torques in flexion/extension, recorded in healthy subjects during maximum voluntary contractions (MVCs) of selected wrist flexors and extensors, were used as input to the model in order to estimate in-vivo subject-dependent musculotendon parameters. The complete neuromusculoskeletal model was finally experimentally validated.

2. Background

An experimentally validated neuromusculoskeletal model, made up of mathematical relationships describing the interaction between nervous system (neuro-), muscles and tendons (-musculo-), and limb anatomy (-skeletal), is an essential tool to analyse the interplay of muscle architecture, joint geometry and neural pathways and is able to provide additional insights into the dynamic interactions between these elements and between the system and the environment that would be difficult or even impossible to obtain from physiological studies alone (Pearson et al., 2006). Many rehabilitation techniques are currently used for people with spinal cord injury, stroke, head injuries, as well as cerebral palsy and multiple sclerosis (Langhorne et al., 2009; Peckham and Knutson, 2005). Nevertheless, in terms of motor recovery “a large amount of research is required to define much more clearly the interventions that carry benefit in a routine clinical setting” (Langhorne et al., 2009). Neuromusculoskeletal modelling represents a promising approach for assessing the interplay between sensory function and the musculoskeletal system (Pearson et al., 2006). Modelling the neuronal and mechanical elements underlying human movements can give insightful indications for the design of more physiological fine-tuned rehabilitation protocols.

Extensive work has been carried out to develop both accurate musculoskeletal and sensory organs models. Musculoskeletal models developed so far can be mainly categorised in inverse dynamic models and forward dynamic models (Buchanan et al., 2004; Erdemir et al., 2007; Lloyd et al., 2009). Inverse dynamic models use data collected in a motion analysis laboratory (i.e. force and kinematic data) to determine joint moments and forces for a given scaled musculotendon geometrical model. Forward dynamic models use recorded EMGs as the activation signal of muscles in a scaled musculotendon geometrical model in order to predict force and kinematic data. There is yet another approach which merges the two above and is used to calibrate and validate a musculoskeletal model (Koo et al., 2002; Lloyd et al., 2009): a hybrid forward and inverse dynamic

model, where recorded force and kinematic data are used to calculate joint moments (inverse dynamics approach) which are successively compared to the joints moments calculated using recorded EMGs as input (forward dynamics approach). A numerical optimisation is then used to estimate subject-specific musculotendon parameters.

So far, models of the sensory organs have been elaborated and numerically tested with simplified representation of the musculoskeletal components (Lan, 2002; Lan et al., 2005; Lin and Crago, 2002; Mileusnic et al., 2006; Prochazka et al., 1997a, b; Shao and Buchanan, 2008). On the other hand, regarding complete neuromusculoskeletal modelling (i.e. merged musculoskeletal models and neural pathways) the main effort has been spent in studying locomotion with either oversimplified musculoskeletal models or no direct experimental validation, this latter conducted by comparing simulated results with data available from different studies (Frigon and Rossignol, 2006; Paul et al., 2005; Pearson et al., 2006). Less has been investigated with regards to the upper limbs in term of complete neuromusculoskeletal models. To be mentioned are three works. The first work (Koo and Mak, 2006) only includes spindle and spinal cord models in a musculoskeletal model of the elbow, but experiments were performed with only one subject. The second work (Song et al., 2008) comprises a full musculoskeletal model of the upper limb, but only spindles and Golgi tendon organs were considered as sensory organs and did not have any closed-loop among the components It was validated by comparison with literature results and no experimental work was carried out. The third work (Lan et al., 2005) contains a simplified model of the elbow and more detailed models of sensory organs and their interaction at the spinal level, but a sensitivity analysis of various reflex gains and external loading conditions was carried out only computationally while no experimental work was conducted. With regard to investigations aimed to characterise the musculoskeletal structure of either the whole upper limb or wrist only, previous experimental studies as well as models can be found in (Delp et al., 1996; Garner and Pandy, 2001; Gonzalez et al., 1997; Holzbaur et al., 2005; Lemay and Crago, 1996; Loren et al., 1996).

In this framework, the development and validation of a complete neuromusculoskeletal model characterised by a closed-loop system made up of CNS, musculoskeletal system and peripheral receptors would enable a deeper understanding of motor task planning and execution (e.g. control of the end-target equilibrium positions during reaching movements). By integrating and analysing the role of the known spinal pathways responsible for the muscular excitation and the control of movement, it will be possible to understand their relative criticality in motor task regulation in either healthy subjects or patients. A direct monitoring of any single component of the system (e.g. a single muscle or a single group of sensory receptors) and analysis of the functional effects of removing or modifying this component in a functional context will allow magnitude and timing of motor activity to be investigated in a more systematic way (Pearson et al., 2006).

3. Model description

Figure 1 shows a simplified representation of the pathways involved in each volitional contraction. The nervous system (i.e. brain, spinal cord and peripheral receptors) receives, elaborates and sends signals to muscles (i.e. musculotendon system), which contract to generate forces and, once coupled with limb anatomy, torques responsible for the limb rotation.

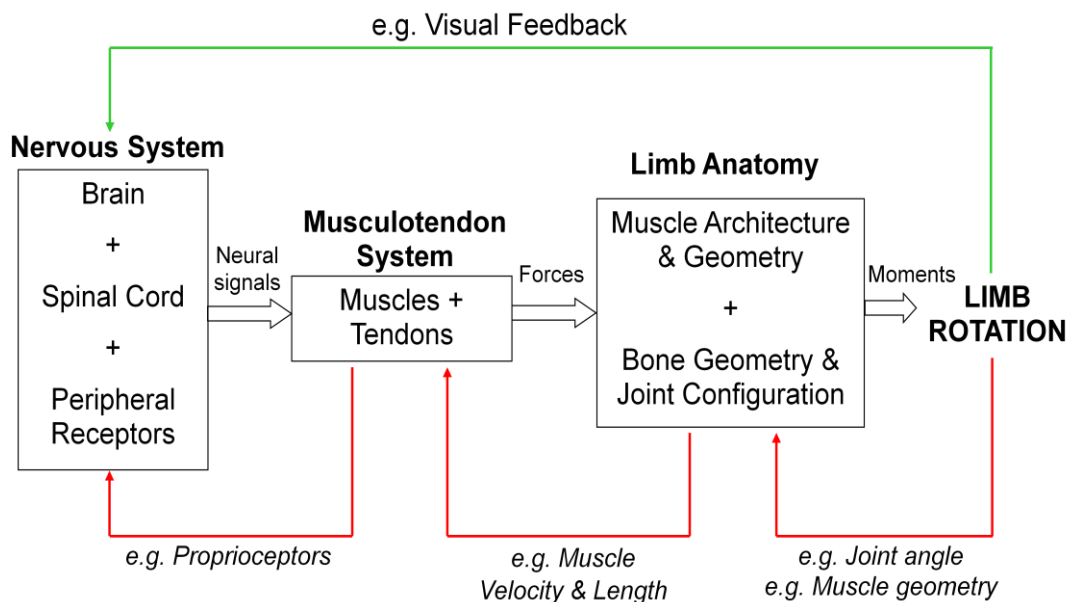


Figure 1 – Schematic representation of the pathways involved in volitional contractions.

Figure 2 shows a more detailed description of how the subcomponents relate each other. The instantaneous angular position of a human limb is thus determined by a closed-loop system organised hierarchically. A limb, characterised by its anatomy (i.e. muscle architecture and geometry as well as bone geometry and joint configuration), is actuated by muscles, wrapped in a complex manner around each joint, whose contraction dynamics is elicited by an activation signal. This in turn is related to a neural signal coming from the spinal cord which results from the interaction between train of impulses coming from the peripheral receptors (also called sensory organs) located inside the muscle (e.g. Muscle Spindles), the tendons (e.g. Golgi Tendon Organs), the skin (e.g. cutaneous reflex), the spinal cord itself (e.g. Renshaw Cells), and descending commands coming from the brain, as well as from the correspondent sensory organs of the antagonist muscles (agonist and antagonist muscles influence each other). Hence, sensory inputs from peripheral receptors directly influence subsequent motor output during the movement of a limb, and natural sensors, such as those found in the skin, muscles, tendons, and joints play an important synergistic role in determining complex motor functions (Sinkjaer et al., 2003).

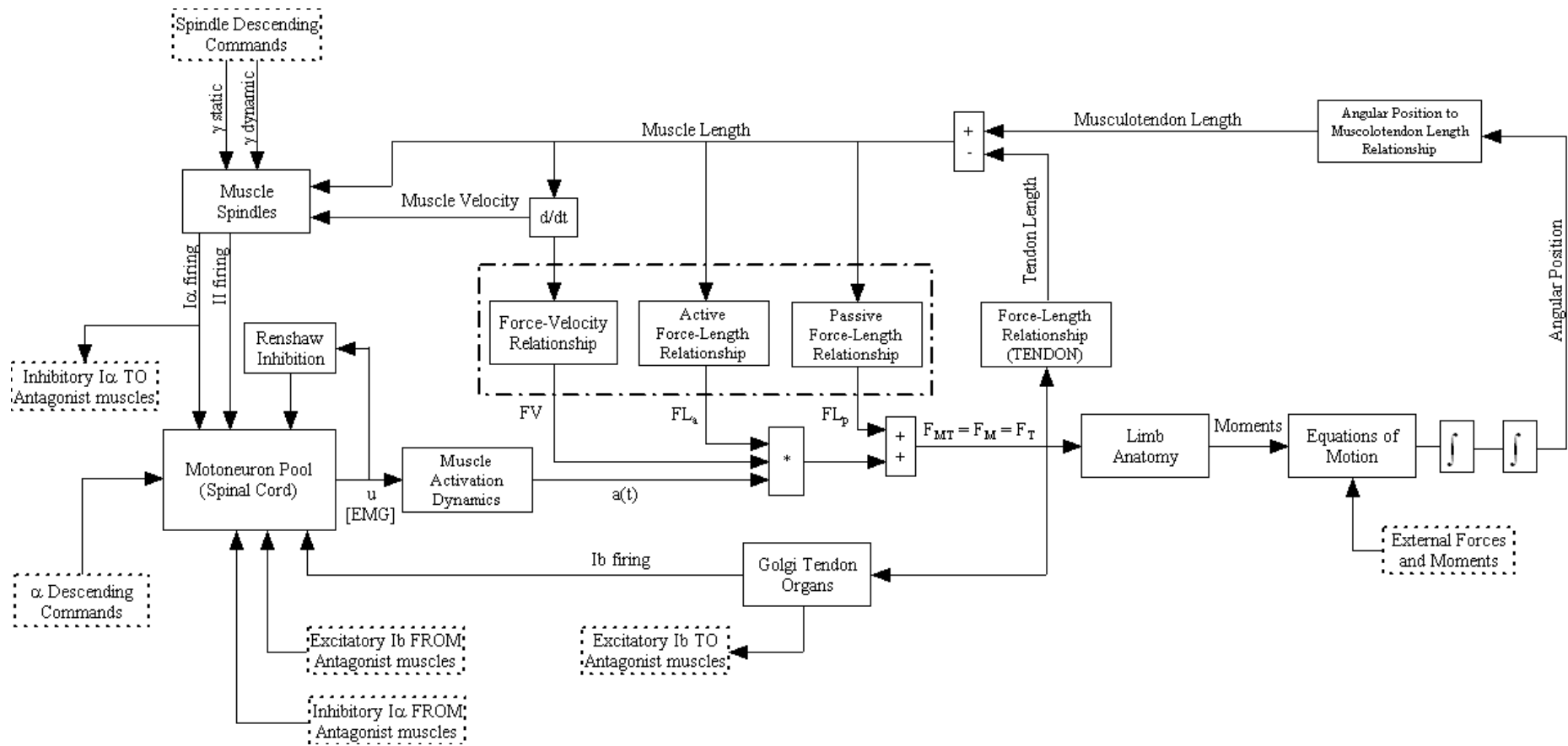


Figure 2 – Schematic diagram of the neuromusculoskeletal model of a single musculotendon unit. See Schmidt (1978) for more details.

3.1 Musculotendon System

The instantaneous total force, F_{MT} , exerted by a musculotendon unit was calculated by means of a lumped Hill-type musculotendon model (Zajac, 1989)

$$F_{MT}(\theta, t) = F_M(\theta, t) = F_T(\theta, t) = [\widetilde{F}L_\alpha(\theta, t) \cdot \widetilde{F}V(\theta, t) \cdot a(t) + \widetilde{F}L_p(\theta, t)] \cdot F_{oM} \quad (1)$$

where t is time, θ is the angular position of the wrist, F_M is the muscle force, F_T is the tendon unit force, $\widetilde{F}L_\alpha$ is the normalised active muscle force-length relationship, $\widetilde{F}L_p$ is the normalised passive muscle force-length relationship, $\widetilde{F}V$ is the normalised muscle force-velocity relationship, F_{oM} is the maximum isometric muscle force and $a(t)$ is the activation level obtained from linear envelope processing of raw EMG signals. Muscle and tendon were considered in series connection, while pennation angle* was disregarded for this joint (Garner and Pandy, 2001). The tilde (~) symbol is superimposed to indicate normalised quantities. Normalisations were operated according to the scaling approach adopted in (Zajac, 1989), thus referring muscle lengths to the optimal muscle fibre length L_{oM} , muscle velocities to the muscle maximum velocity V_{MAX} and forces to the maximum isometric muscle force F_{oM} .

The above mentioned quantities will be described in more details hereafter. Refer to Table 1 for parameter values. Units are in the SI unless otherwise stated.

* Muscles and tendons are geometrically arranged as to form the so-called *pennation angle*. In general, its influence on the transmission of the force between muscle and tendon is neglected when its value is less than 20°. In the other cases, the relationship between tendon force, F_T , and muscle force, F_M , is:

$$F_T = F_M \cos(\phi)$$

with ϕ being the pennation angle given by:

$$\phi(t) = \sin^{-1} \left(\frac{L_{oM} \sin \phi_o}{L_M(t)} \right)$$

and ϕ_o being the pennation angle at the optimal muscle length L_{oM} .

Table 1 – Model Parameters

	Units	Value	Reference
Muscle Activation Dynamics			
A (constant in the range [-3 .. 0])		Estimated	(Buchanan et al., 2004)
τ_{act}	[s]	0.05	(Zajac, 1989)
τ_{deact}	[s]	0.08	(Zajac, 1989)
Active muscle Force-Length relationship			
d		0.56	(Lan, 2002)
k		-1/d ²	(Lan, 2002)
λ		0.15	(Buchanan et al., 2004)
Muscle Force-Velocity relationship			
aa		1.5	(Lan, 2002)
bb		8	(Lan, 2002)
cc		0.0866	(Lan, 2002)
Muscle Volume, Mass and Density			
Density	[g/cm ³]	1.06	(Mendez and Keys, 1960)
Flexor Carpi Ulnaris (±SD)	[cm ³]	37.1 (±13.6)	(Holzbaur et al., 2007)
Flexor Carpi Radialis (±SD)	[cm ³]	34.8 (±17.1)	(Holzbaur et al., 2007)
Flexor Digitorum Superficialis (±SD)	[cm ³]	74.2 (±27.4)	(Holzbaur et al., 2007)
Extensor Carpi Radialis Longus (±SD)	[cm ³]	37.5 (±19)	(Holzbaur et al., 2007)
Flexor Carpi Ulnaris	[kg]	0.0393	
Flexor Carpi Radialis	[kg]	0.0369	
Flexor Digitorum Superficialis	[kg]	0.0786	
Extensor Carpi Radialis Longus	[kg]	0.0397	

3.1.1 Muscle activation dynamics

Every muscle actively contracts when activated by a neural excitation. The process that transforms neural excitation in muscle force is referred to as activation dynamics.

The EMG[†] signal was related to muscle activation $a(t)$ as in Buchanan et al. (2004). A normalized, rectified, filtered EMG, $nrEMG(t)$, was first transformed to the neural excitation $u(t)$ by means of a first-order differential equation, that is

$$\frac{du(t)}{dt} + \left[\frac{1}{\tau_{act}} \cdot (\beta + (1 - \beta) \cdot nrEMG(t)) \right] \cdot u(t) = \frac{1}{\tau_{act}} \cdot nrEMG(t), \quad (2)$$

where the constant β ($0 < \beta < 1$) was set as in Zajac (1989) equal to

$$\beta = \frac{\tau_{act}}{\tau_{deact}} \quad (3)$$

[†] Electrical potential generated by muscle cells when these cells are both mechanically active and at rest.

with τ_{act} and τ_{deact} time constants defining the build-up in activation for excited or relaxed muscle. In particular, a relaxed muscle ($u(t) = 0$) activates more slowly than an excited one ($u(t) = 1$), that is $\tau_{act} < \tau_{deact}$.

Then, $u(t)$ was related to the muscle activation $a(t)$ according to the following non-linear relationship

$$a(t) = \frac{e^{Au(t)} - 1}{e^A - 1} \quad (4)$$

where the constant A must be determined during a calibration process.

3.1.2 Active muscle Force-Length relationship

The active muscle Force-Length relationship $\widetilde{F}L_a(\theta, t)$ was described as follows (Lan, 2002)

$$\widetilde{F}L_a(\theta, t) = k \cdot \widetilde{L}_M(\theta, t)^2 - 2 \cdot k \cdot \widetilde{L}_M(\theta, t) + k + 1. \quad (5)$$

It represents an activation-dependent parabolic curve normalised with respect to the maximum isometric muscle fibre force, F_{oM} , and is a function of the normalised muscle length, $\widetilde{L}_M(\theta, t)$, normalised by the optimal physiological muscle length $L_{oM}(t)$ ($\widetilde{L}_M(\theta, t) = \frac{L_M(\theta, t)}{L_{oM}}$). In turn, $L_{oM}(t)$ varies with the level of activation $a(t)$ according to the following relationship (Buchanan et al., 2004)

$$L_{oM}(t) = L_{oM}\{\lambda[1 - a(t)] + 1\}. \quad (6)$$

The term λ defines the amount of optimal fibre length increase as activation decreases. The factor k is related to a scaling factor d as follows

$$k = -\frac{1}{d^2}.$$

The maximum isometric muscle force, F_{oM} , is the force developed by a muscle when it is maximally stimulated at its optimal physiological length, $L_{oM}(t)$.

As Figure 3a shows, equation (5) describes a downward parabola with vertex located at $\widetilde{L}_M = 1$ and $\widetilde{F}L_a = 1$, whose branches intersect the normalised muscle length axis (i.e. x-axis) at $(1-d)$ and $(1+d)$. Figure 3b, instead, shows the same curve at different activation levels.

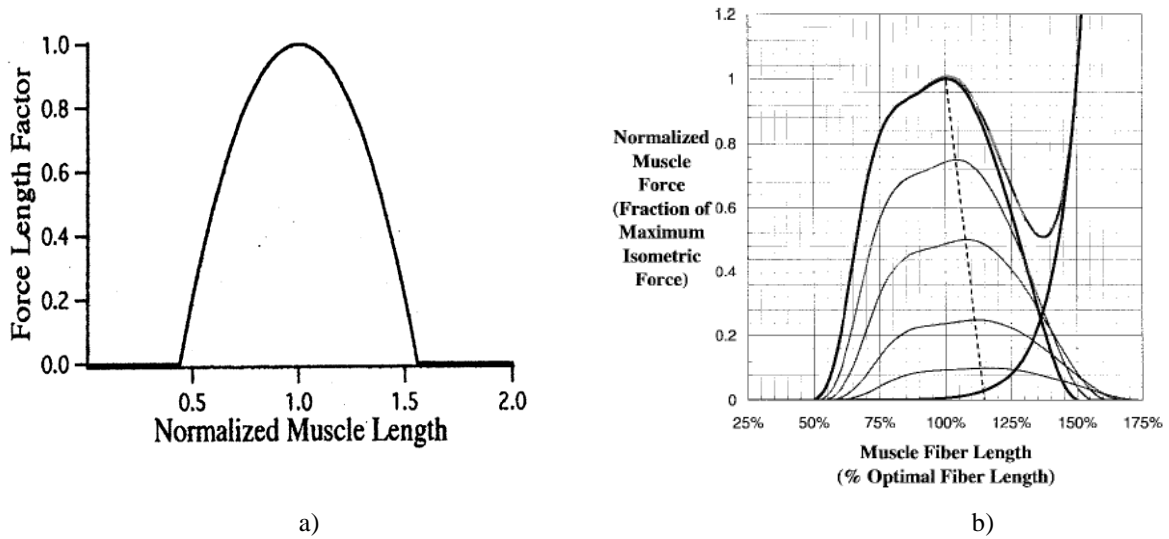


Figure 3 - Active muscle Force-Length relationship. a) 100% activation (i.e. muscle maximally stimulated). Taken from Lan (2002); b) How the curve modifies at different activation levels. Taken from Buchanan et al. (2004).

3.1.3 Passive muscle Force-Length relationship

The passive muscle force-length relationship describes the elastic properties of the muscle fibres when they are stretched beyond the optimal muscle length L_{OM} . It is given by (Buchanan et al., 2004)

$$\widetilde{FL}_p(\theta, t) = \frac{e^{10(\widetilde{L}_M(\theta, t)-1)}}{e^5} \quad (7)$$

where $\widetilde{FL}_p(\theta, t)$ is the passive muscle force normalised with respect to the maximum isometric muscle fibre force, F_{OM} , and $\widetilde{L}_M(\theta, t)$ is the muscle length normalised with respect to the optimal physiological muscle length, $L_{OM}(t)$. Figure 4 shows \widetilde{FL}_p , \widetilde{FL}_a and their sum: the total force \widetilde{F}_{tot} .

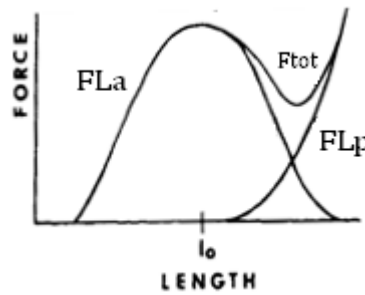


Figure 4 – Active (FL_a), passive (FL_p) and total (F_{tot}) force-length relationships. Modified from Winter (2005).

3.1.4 Muscle Force-Velocity relationship

Muscle fibres present viscous properties described by the following relationship (Lan, 2002)

$$\widetilde{FV}(\theta, t) = \frac{aa}{1 + e^{[bb(\widetilde{V}_M(\theta, t)-cc)]}} \quad (8)$$

where $\widehat{FV}(\theta, t)$ is the force-velocity relationship normalised with respect to the maximum isometric muscle fibre force, F_{OM} , aa , bb , and cc are appropriate constants and $\widehat{V}_M(\theta, t)$ is the muscle velocity normalised with respect to the maximal contraction velocity $V_{max}(t) = 10 \cdot L_{OM}(t)$ (Zajac, 1989). By this formula, both eccentric (i.e. lengthening) and concentric (i.e. shortening) contractions are taken into account. As plotted in Figure 5a, this curve ranges from -1 to 1 on the normalized velocity axis (i.e. x-axis) and from 0 to 1.5 on the normalized force-velocity axis (i.e. y-axis), being equal to 1 at $\widehat{V}_M = 0$. Figure 5b shows its activation-dependent characteristic.

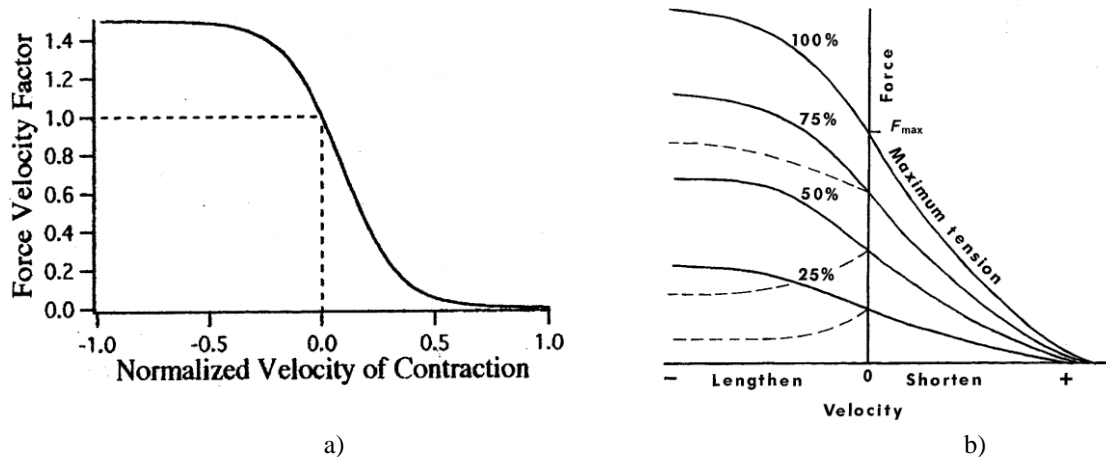


Figure 5 – Force-velocity relationship. Taken from a) Lan (2002); b) Winter (2005).

3.1.5 Total Force-Length-Velocity relationship for muscles

Being the muscle force contemporary dependent upon both length and velocity, a three-dimensional plot describing their effects is shown in Figure 6. For clarity, the surface shown is plotted at 100% activation level with no passive elastic force-length relationship.

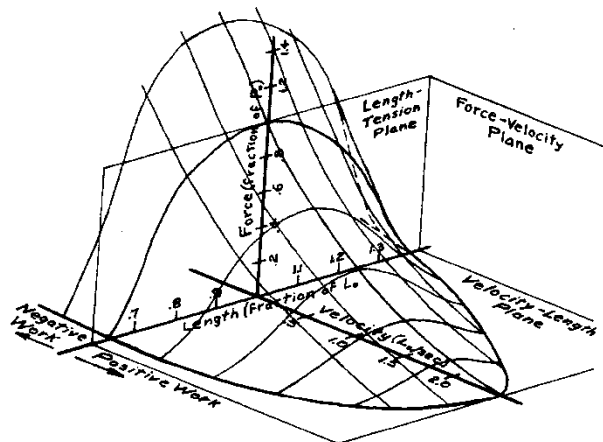


Figure 6 – Total force-length-velocity relationship (passive properties not shown). Taken from Winter (2005).

3.1.6 Tendon Force-Length relationship

Tendons are in series connection with muscles, so they both sense the same force. The normalised tendon force, $\tilde{F}_{KT}(\theta, t)$, is given by (Buchanan et al., 2004)

$$\begin{cases} \tilde{F}_{KT} = 0 & \varepsilon \leq 0 \\ \tilde{F}_{KT} = 1480.3 \cdot \varepsilon^2 & 0 < \varepsilon < 0.0127 \\ \tilde{F}_{KT} = 37.5 \cdot \varepsilon - 0.2375 & \varepsilon \geq 0.0127 \end{cases} \quad (9)$$

where $\tilde{F}_{KT}(\theta, t)$ is normalised with respect to the maximum isometric muscle fibre force, F_{oM} , and $\varepsilon(\theta, t)$ is the tendon strain defined as

$$\varepsilon(\theta, t) = \frac{L_T(\theta, t) - L_{TS}}{L_{TS}} \quad (10)$$

In equation (10), $L_T(\theta, t)$ is the tendon length while L_{TS} is the tendon slack length, the length beyond which a tendon starts carrying load (i.e. $\varepsilon > 0$). As shown in Figure 7, the tendon force-length relationship comprises a quadratic region (for small deformations) and a linear region (for larger deformations).

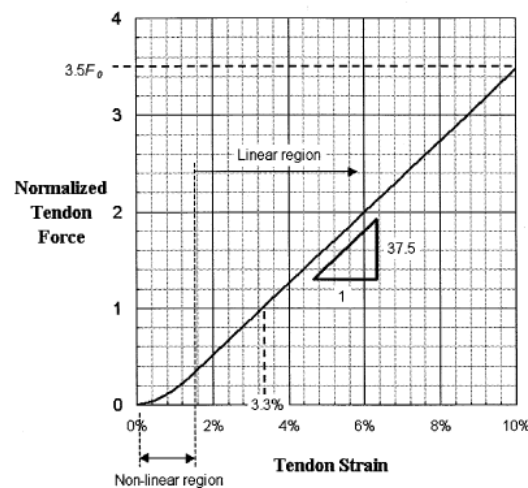


Figure 7 – Tendon force-length relationship. Taken from Buchanan et al. (2004).

3.1.7 Musculotendon unit dynamics

The muscle (with its mass) and the tendon connected in series behave as a critically damped mass-spring-damper system (Winter, 2005). A recognised lumped parameter model used to mimic the musculotendon dynamics is the Hill model (Figure 8), where non-linear elastic properties are condensed in springs (i.e. TE = tendon elasticity, SE = muscle series elasticity, PE = muscle parallel elasticity), non-linear viscous properties are condensed in dashpots (i.e. B(v)), while the actuating properties are delegated to the actin-myosin contractile machinery (i.e. CE = contractile element) (Winter, 2005; Yamaguchi, 2001; Zajac, 1989).

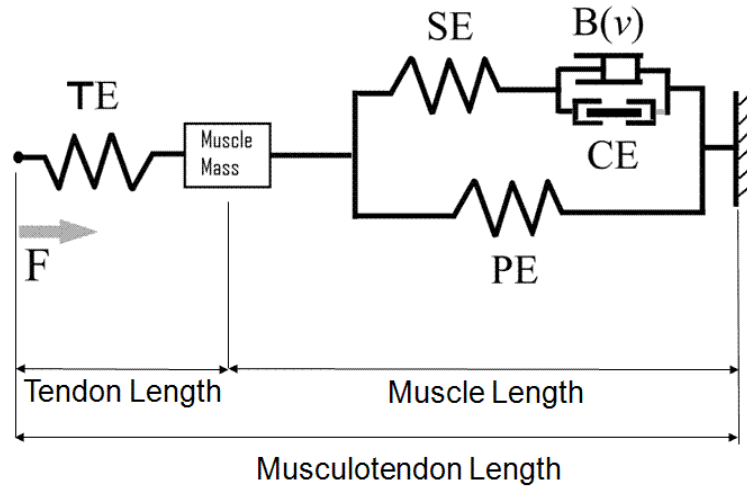


Figure 8 – Lumped parameter model of the musculotendon unit.

In the present study, a slightly different model was implemented so that neither the dynamics of the musculotendon unit nor the physiological meaning of its components were affected (see section ‘Model Implementation’ for details). Indeed, for long-tendon actuators (as those in the arms) muscle series elasticity (i.e. SE) can be neglected (Zajac, 1989), thus a lumped model for muscle like the one in Figure 9 was used

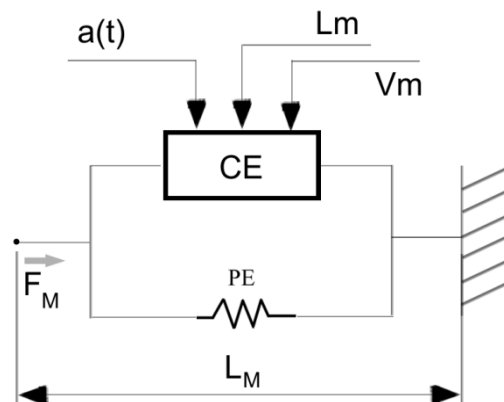


Figure 9 – Modified Hill model (adapted from (Zajac, 1989)).

In it, the properties of the muscle tissue were represented by two main components: one dependent only on the current muscle length, $L_M(\theta, t)$, velocity, $V_M(\theta, t)$, and activation, $a(t)$ (i.e. equations (2) to (6) and equation (8)); the other (i.e. PE) dependent on the non-linear passive elastic properties of the muscle (i.e. equation (7)). Hence, the total force $F_M(\theta, t)$ in equation (1) results from the sum of these components and acts on the muscle mass thought as concentrated and located between the muscle and the tendon fibres (see 5. Model Implementation for more details).

3.2 Limb Anatomy

Musculoskeletal geometry plays an important role in determining muscle velocity and muscle length, which are the main variables for the force-length and the force-velocity relationships. As schematically shown in Figure 2, the musculotendon force F_{MT} given by equation (1), contributes to the joint moment once the muscle's moment arm is known.

On the other hand, muscle architecture and geometry as well as bone geometry and joint configuration represent very complex systems[‡]. Every single movement is always the result of the interaction between agonist and antagonist muscles acting contemporary. For this reason, many musculotendon units, as the one shown in Figure 8, are usually involved even for a single degree of freedom movement. Muscles are connected to bones, via the tendons, in a complex manner since they bend or wrap around other structures at some joint configurations. Moreover, the insertion points vary with joint positions, and this influences the moment arms, which in turn are a function of the muscle's length. Another aspect to consider is that most joints do not act as simple hinges, but they allow a combination of rotation and translation, so that their centre of rotation changes with the angular position. As a consequence, the moment arms change as well. Finally, many of the parameters describing the limb anatomy are subject-dependent.

Commercially available modelling software such as SIMM (Software for Interactive Musculoskeletal Modelling – MusculoGraphics Inc. Chicago, USA) or AnyBody (AnyBody Technology, Denmark) provide the user with a library of bones, muscles, ligaments and other tissues which can be assembled by means of a graphical user interface. The library contains average-sized components based on cadaveric data (Delp et al., 1990). These musculoskeletal models must then be scaled to fit size and body proportions of the individual under study. The scaling task can be performed by means of anatomical markers and motion capture sessions or by means of medical imaging techniques, such as computed tomography (CT) or magnetic resonance imaging (MRI). For more details see (Blemker et al., 2007; Lloyd et al., 2009; Winby et al., 2008).

For the case under study, moment arms (*MAs*) and the musculotendon length changes (ΔL_{MT}) as a function of joint angle were obtained via polynomial curve fits of actual measurements (Lemay and Crago, 1996). The following relationships were then used in order to link the joint angle, θ , to the moment arm and the musculotendon length change

$$MA(\theta) = a_0 + a_1\theta + a_2\theta^2 + a_3\theta^3 + a_4\theta^4 + a_5\theta^5 \quad (11)$$

$$\Delta L_{MT}(\theta) = b_0 + b_1\theta + b_2\theta^2 + b_3\theta^3 \quad (12)$$

where θ is in radians, ΔL_{MT} in cm, while a_i and b_i coefficients are specified in (Lemay and Crago, 1996).

As defined in this latter work, a positive moment arm is a wrist flexion moment. The wrist angle is defined as zero with the hand in neutral orientation and goes positive as the hand is flexed. The muscle length change is defined to be zero at $\theta = -70^\circ$, and goes positive with wrist flexion for a lengthening muscle.

[‡] A good source of data can be found in Delp and Loan (1995) and in Yamaguchi (1990).

3.3 Nervous System

Even though the nervous system has not been included in the present study (except for what concerns EMGs), this paragraph contains information regarding spinal cord and sensory organs that might be useful for a follow up study aimed to develop a complete neuromusculoskeletal model.

All of the descriptions below are referred to the elbow joint, but their general validity holds.

3.3.1 Spinal Cord and Sensory Organs

The control of posture and movement is characterized by a hierarchical organisation. The central nervous system (CNS) consists of the brain and the spinal cord. All the remaining nervous tissue is referred to as the peripheral nervous system. The spinal cord integrates all the signals coming either from the brain or from the peripheral receptors (i.e. sensory organs). Indeed, the CNS centres and the motor organization can operate properly only if a series of an uninterrupted stream of impulses is received from specialized receptors.

The train of impulses is transmitted by the nerve fibres[§]. The transmission of the information from the CNS to the periphery takes place by efferent nerve fibres (succinctly, efferents). On the other hand, the nerve fibres of the motor receptors, which are responsible for transmitting the signals from the periphery to the spinal cord, are called afferent nerve fibres (succinctly, afferents)**.

Figure 10 shows the schematic representation of the elbow joint which will be referred to hereafter. It includes one flexor and one extensor muscle (subscripts f and e, respectively), the in-series attached tendons, the neural signals $u(t)$ (which elicit the muscle activation $a(t)$) transferred by the efferents, and two motoneurons, α_f and α_e .

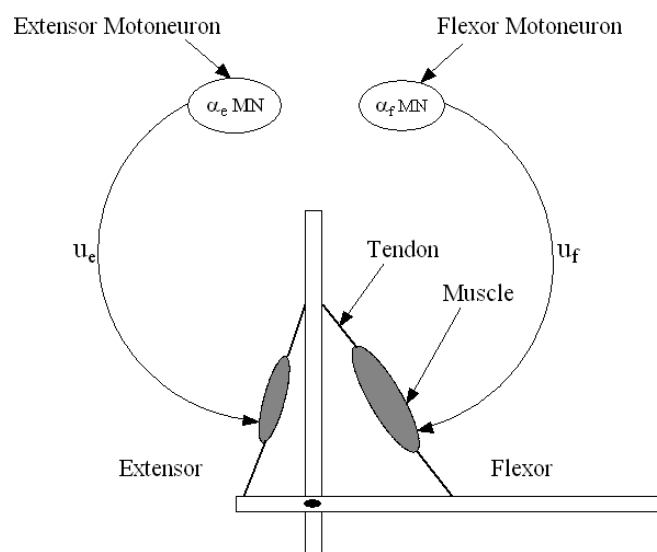


Figure 10 – Schematic representation of the elbow joint.

The reflex model that will be described in the following sections includes the Renshaw cells, the Golgi-tendon organs and the muscle spindles. Their role in exciting or inhibiting muscle activity will

[§] The nerves in the periphery of the body are bundles of axons. The axons are the branches departing from the soma. The soma is the cell body of the neuron. Soma and axons form the neurons. The neurons are the nerve cells of the nervous system. The neurons responsible for the motor function are called motoneurons. Neurons are connected with each other: the connection is called synapse. For more details refer to (Schmidt, 1978).

** The efferent nerve fibres depart from the neurons located into the spinal cord. In contrast, the afferent nerve fibres converge to the motoneurons to which are connected by synapses. The afferents' nerve cells are grouped in the ganglions located on the afferents and outside the spinal cord. For more details refer to (Schmidt, 1978).

be also described. Moreover, a description of the motoneuron pool organization and the influence of the antagonists on a motor task will be addressed.

3.3.2 The Renshaw Inhibition (β -loop)

Motoneurons are provided with a negative feedback which produces feedback inhibition. The signal leaving the motoneurons to be transferred by the afferents to the muscles is also fed back (by inhibitory interneurons called Renshaw cells) to the same motoneurons to form the Renshaw inhibition (Figure 11).

This feedback guarantees protection against too powerful excitations. Indeed, as the motoneuron activity increases (which causes a muscle activity increase), the Renshaw cells also become more excited, thus increasing their inhibitory effect after a short latent period (due to the interneuron's activity). By this arrangement, weak motoneuron activity is transferred undisturbed to the muscle, while too strong excitation is dampened to prevent hyperactivity of the muscles.

The β -pathway is modelled using a gain as in Lan et al. (2005).

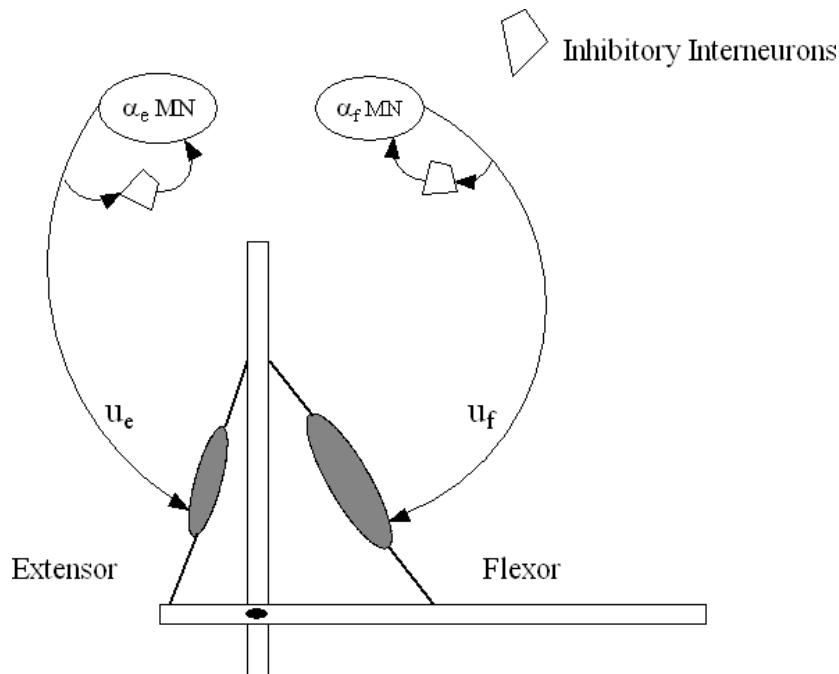


Figure 11 – The inhibitory Renshaw cells realise a negative feedback to control the motoneuron activity.

3.3.3 The Golgi-Tendon Organs

They are activated by changes in muscle tension. Their main role is to keep muscle tension constant and protect against overloading, acting to prevent too rapid rise in tension. For this reason, the Golgi organs produce inhibition of the homonymous motoneurons and excitation of the antagonist motoneurons due to their connection mediated by interneurons^{††}.

Figure 12 schematically shows the elbow joint and the *lb* afferent pathways of the tendon organs. A marked increase in muscle tension increases the impulse frequency in the correspondent afferent, *lb*, thus producing the inhibition of the correspondent muscle (via the inhibitory interneuron). At the same time, this affects the correspondent antagonist muscle which results excited (via the excitatory interneuron) by the same change in impulse frequency. The resulting net effect is a weaker

^{††} Interneurons are interposed neurons along a connection path.

excitation of the agonist muscle and a stronger excitation of the antagonist muscle, thus acting as a force-control system that keeps the muscle tension constant.

In the same way, when the tension in the muscle decreases, the impulse frequency in Ib decreases and so does the inhibitory effect for the agonist muscle (i.e. the tension in muscle tends to increase again) as well as the excitatory effect for the antagonist muscle. In this case, the resulting net effect is a stronger excitation of the agonist muscle and a weaker excitation of the antagonist muscle, thus acting as a force-control system as well.

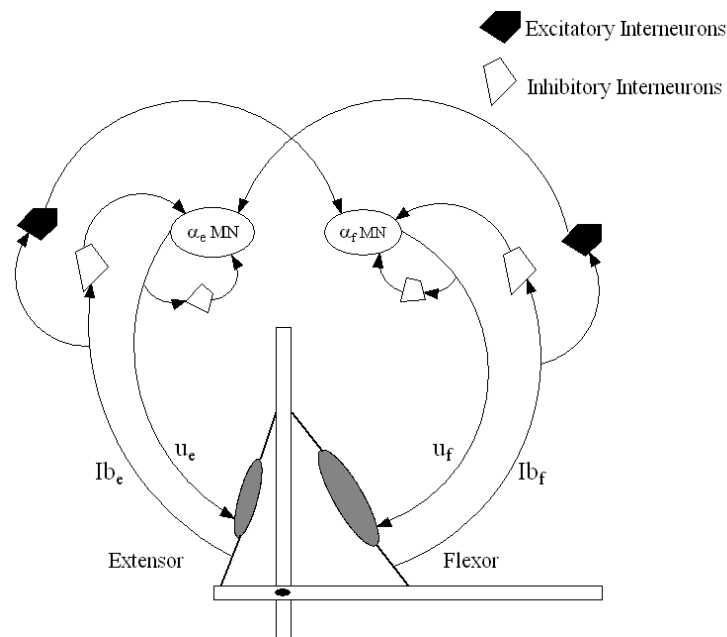


Figure 12 – Golgi tendon organs pathways Ib to flexor motoneurons (α_f MN) and extensor motoneurons (α_e MN).

The following piece-wise static linear relationship could be used to model the firing response of the tendon organs, Ib , to changes in tendon force (Song et al., 2008)

$$\begin{cases} Ib = \frac{646}{3} \cdot F_T & F_T < 3 \\ Ib = 114 \cdot F_T + 304 & F_T \geq 3 \end{cases} \quad (13)$$

where F_T is the tendon force in Newton^{**}.

3.3.4 Muscle Spindles

Each muscle contains two types of fibres: the extrafusal fibres and the intrafusal fibres. The former constitute the major part of the muscle, the latter are thinner and shorter and grouped in a spindle-shaped connective tissue capsule and are mechanically parallel to the extrafusal musculature. The extrafusal fibres are responsible for carrying loads and performing motor tasks, the muscle spindles represent the sensory organs of the muscle.

Figure 2 shows muscle spindles' inputs and outputs. Each one of them will be described next.

** An attractive alternative formulation based on a first-order dynamics and a delay can be found in (Prochazka et al., 1997a)

Changes in muscle length and velocity are sensed by the muscle spindles. The associated stretch reflex mechanism tends to automatically keep the muscle length constant. If the muscle and the muscle spindles it contains are stretched, then the impulse frequency transmitted to the CNS by the primary afferents $I\alpha$ increases. The firing rate is also higher when the length changes than when the muscle is kept at a fixed position. On the contrary, if the muscle shortens by contraction of the extrafusal muscle fibres, the tension on the muscle spindles is relaxed and the discharge rate decreases or even drop to zero.

As shown in Figure 13, the $I\alpha$ firing is transmitted directly to the homonymous motoneuron by the primary afferents, while it is transmitted to the antagonist (reciprocal) motoneuron by means of an inhibitory interneuron. The net effect of this interaction constitutes a length-control system. Indeed, if for example the flexor muscle is stretched, then the firing rate sent to the flexor motoneuron increases, thus exciting the flexor muscle, and the inhibition of the antagonist motoneuron increases due to the action of the inhibitory interneuron, thus relaxing the extensor muscle. At the same time, the extensor muscle shortens and this produces a decreased excitation of the correspondent motoneuron (i.e. relaxation of the extensor) as well as a decreased inhibition of the reciprocal motoneuron (i.e. easier excitation of the flexor). The final global effect is an increased activation of the flexor motoneurons, because the homonymous excitation increases and the reciprocal antagonist inhibition decreases, and the contemporary reduction of the antagonist motoneuron activity, because the homonymous excitation decreases and the reciprocal antagonist inhibition increases. The resulting increased activation of the flexor tends to compensate its lengthening.

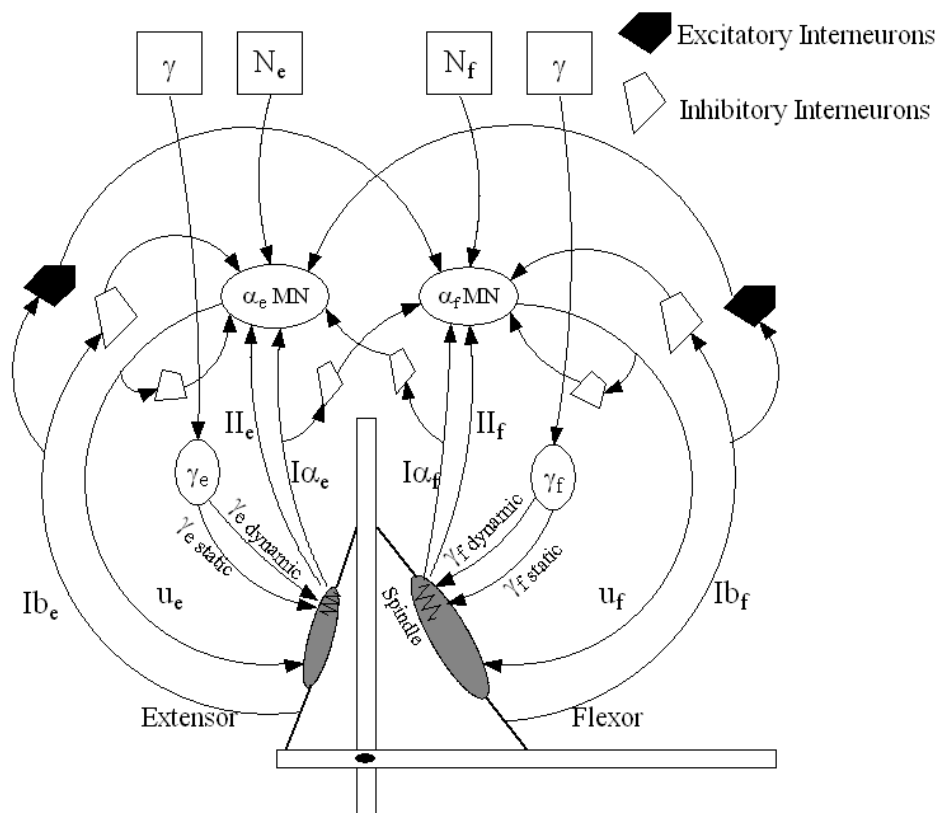


Figure 13 – Muscle spindle's pathways to flexor motoneurons (α_f MN) and extensor motoneurons (α_e MN). Primary ($I\alpha$) and secondary (II) afferents and descending control signals N_e , N_f and γ are shown.

Due to a secondary sensory innervation, another signal, *II* firing, is sent to the motoneurons from the muscle spindles (Figure 13). Its firing is mainly linked to the joint position: its value changes with the position and remains constant at a fixed position, thus tracking down the joint position.

Another characteristic of the muscle spindles is their motor innervation. The intrafusal muscle fibres, just as the extrafusal fibres, possess a motor innervation, the γ fibres, which transmit the so-called γ -command to the muscle spindles. By exciting the intrafusal muscle fibres, and thus stretching their central portion, a stronger activation of the homonymous motoneuron is obtained by an increase of the discharge rate of the primary afferent $I\alpha$. The contrary applies when the intrafusal fibres are relaxed. This means that the threshold of the stretch receptor can be varied by intrafusal "pretensioning". For example, when intrafusal contraction occurs, the threshold is lowered and the muscle spindle reacts more sensitively when the muscle is stretched. Figure 2 and Figure 13 also show the static and dynamic γ innervations. Fusimotor neurons are classified as static or dynamic according to the type of intrafusal muscle fibres they innervate and their physiological effects on the responses of the Ia and II sensory neurons innervating the central, non-contractile part of the muscle spindle^{§§}.

The most comprehensive muscle spindle's mathematical models can be found in (Lin and Crago, 2002; Mileusnic et al., 2006). Nevertheless, many authors use simpler versions when such a component has to be integrated in a complete neuromusculoskeletal model. Hence, the muscle spindle firing characteristics can be modelled as follows (Koo and Mak, 2006)

$$I\alpha = \begin{cases} G_V (V_M (t - T_{SRD}))^{0.6} + G_L (L_M (t - T_{SRD}) - L_M (0)) + I\alpha_o & \text{for } v_M (t) \geq 0 \\ -G_V |V_M (t - T_{SRD})|^{0.6} + G_L (L_M (t - T_{SRD}) - L_M (0)) + I\alpha_o & \text{for } v_M (t) < 0 \end{cases} \quad (14)$$

where $I\alpha$ is the primary afferent firing rate, L_M is the muscle length, V_M is the muscle velocity, $L_M(0)$ is the muscle length in its initial position, $I\alpha_o$ is the background firing rate (equal to 6.45 impulse/sec), T_{SRD} is the stretch reflex delay (equal to 30 msec), and G_V and G_L are the dynamic and static gain of the spindle model, respectively. In particular, these two latter parameters are related to the descending γ -motoneuron activation command sent to the muscle spindles, thus their value can be changed or left constant (equal to 4.3 and 2, respectively).

It is worth noting that the previous model disregards the influence of the *II* firing.

^{§§} Muscle spindles are composed of 3-12 intrafusal muscle fibres, of which there are three types: dynamic nuclear bag fibres (bag₁ fibres); static nuclear bag fibres (bag₂ fibres); nuclear chain fibres and the axons of sensory neurons.

The static axons innervate the chain or bag₂ fibres. They increase the firing rate of Ia and II afferents at a given muscle length (see schematic of fusimotor action below). The dynamic axons innervate the bag₁ intrafusal muscle fibres. They increase the stretch-sensitivity of the $I\alpha$ afferents by stiffening the bag₁ intrafusal fibres. Several theories, based on recordings from spindle afferents, have been proposed to describe how the CNS controls gamma fusimotor neurons:

1) *Alpha-gamma co-activation*. Here it is posited that gamma motoneurons are activated in parallel with alpha motoneurons to maintain the firing of spindle afferents when the extrafusal muscles shorten (Vallbo and al-Falahe, 1990).

2) *Fusimotor set*: gamma motoneurons are activated according to the novelty or difficulty of a task. Whereas static gamma motoneurons are continuously active during routine movements such as locomotion, dynamic gamma motoneurons tend to be activated more during difficult tasks, increasing Ia stretch-sensitivity (Prochazka, 1996).

3) *Fusimotor template of intended movement*. Static gamma activity is a "temporal template" of the expected shortening and lengthening of the receptor-bearing muscle. Dynamic gamma activity turns on and off abruptly, sensitizing spindle afferents to the onset of muscle lengthening and departures from the intended movement trajectory (Taylor et al., 2006).

3.3.5 Considerations on the Sensory Organs

The sensory organs (i.e. Renshaw cells, Golgi tendons, and muscle spindles) are in general characterized by a dynamics with gains (adjustable by the higher motor centres) and delays. A typical example can be found in (Prochazka et al., 1997a).

One can decide to simplify the model by substituting the dynamic relationships with static ones, and/or disregarding the delays, and/or regulating the gains or leave them constant.

3.3.6 Motoneuron Pool

The spinal cord is the site where the motoneuron activity takes place and where all the signals coming from agonist and antagonist sensory organs as well as descending commands converge to or depart from. Its output is the activation $u(t)$ (see equation (1)).

One model suitable to describe the motoneuron pool would be the one proposed by Lan et al. (2005). In this work a simple model with no delays for each feedback sensory pathway was used, while a first-order dynamics was considered to model the background activation of the motoneuron pool, $c(t)$, elicited by the descending command $N_e(t)$ and $N_f(t)$ for extensors and flexors, respectively (Figure 13)

$$\begin{aligned} \frac{dc_f(t)}{dt} &= -\frac{1}{\tau_{N_f}} c_f(t) + \frac{1}{\tau_{N_f}} N_f(t) & 0 \leq N_f(t) \leq 1 \\ \frac{dc_e(t)}{dt} &= -\frac{1}{\tau_{N_e}} c_e(t) + \frac{1}{\tau_{N_e}} N_e(t) & 0 \leq N_e(t) \leq 1 \end{aligned} \quad (15)$$

where τ_{N_f} and τ_{N_e} are the time constants correspondent to flexor (subscript f) and extensor (subscript e) muscles, respectively.

The final output of the motoneuron pool is thus given by the sum of all excitatory (positive) and inhibitory (negative) signals coming from the sensory organs, that is

$$\begin{aligned} u_f(t) &= \frac{c_f(t)}{1 + c_f(t)g_f} (1 + s_f \cdot I\alpha_f - r_f \cdot I\alpha_e) \\ u_e(t) &= \frac{c_e(t)}{1 + c_e(t)g_e} (1 + s_e \cdot I\alpha_e - r_e \cdot I\alpha_f) \end{aligned} \quad (16)$$

where s_f and s_e are stretch reflex gains, r_f and r_e represent the gains of the inhibition signal coming from the antagonist afferents, g_f and g_e are the Renshaw cell gains. For all the parameter values see Lan et al. (2005).

4. Measurements

4.1 Aim

Gathering EMG signals and torques exerted by the hand in order to calibrate and validate the numerical model of the human wrist. EMG signals from two muscle groups (flexors and extensors) as well as joint moments and positions will be used to estimate subject-specific musculotendon parameters. Measured torques will be also used to validate the model by comparison with the predicted joint moments.

4.2 Experimental Setup

An instrumented armchair allowed seven hand positions with the wrist angle in the range of $+30^\circ$ (flexion) -30° (extension) with 10° intervals (Figure 14).

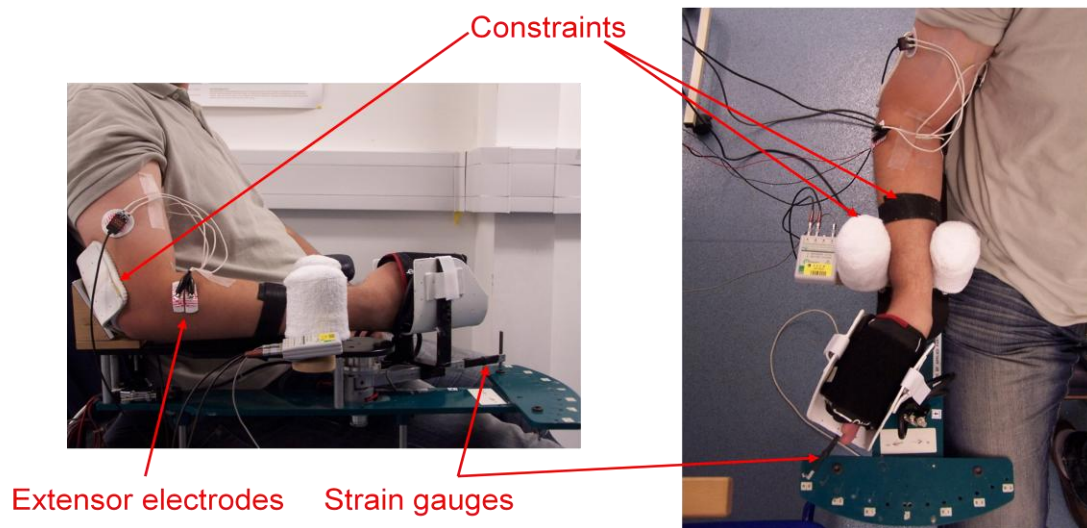


Figure 14 – Test rig.

A CE approved Data Logger from MIE Medical Research Ltd was used as a data acquisition system. The Data Logger, powered by a single standard AA battery (1.5V or 3.6 V), is a portable stand-alone device which stores data on standard memory cards (MMC). It is connected to a PC via an opto-isolated RS232 serial cable (supplied with the device) only during the preliminary programming procedure (see section *Task to be performed*). The Data Logger comprises a sub-miniature pre-amplifier (gain equal to 1000) to be used close to the muscle site under test. The pre-amplifier receives EMG signals from bipolar surface electrodes applied on the skin in the range of mV. The amplifier output is in the range of 0 to 5 V. The Data Logger is CE certified to Medical Devices Directive.

The exerted torques was measured by a calibrated strain gauge load cell (whose signal was in the range of mV) connected to an amplifier (Fylde FE-369-TA). The load cell was powered with 2 V by an external power supply. The amplified signal (gain equal to 500) was recorded by the same Data Logger. A customised cable was used to connect the load cell both to the power supply and the Data Logger.

The test rig was provided with a potentiometer to measure the angle of the hand. Since isometric contractions were performed, the pre-calibrated positions of the armchair were used to determine the angle and no signals were recorded from the potentiometer. Anyway, its shaft axis served as a reference for aligning the wrist rotation axis.

All of the signals were collected synchronously at 1000 Hz.

4.2.1 Data Logger Setup

Prior to data collection, the Data Logger must be programmed (e.g. required sampling rate, active channels, etc.). This process was performed by using the proprietary software (MyoDat) supplied with the device. The device was thus connected to a PC via an opto-isolated RS232 serial cable (also supplied). Once the programming was completed, and the subject prepared with all of the transducers connected, the transducers' functionality and/or their optimal placement was checked real-time. Instead, data acquisition was carried out "blindly" with the Data Logger disconnected from the PC (this is a feature of the Data Logger). 4 out of 8 channels were programmed: channel 1 to 3 were set to record EMGs, while channel 4 was set to record the signal coming from the load cell.

4.2.2 Strain Gauge Load Cell Calibration

Four strain gauges mounted in a full bridge configuration were fixed on a rectangular bar (Figure 14) and used as load cell. The resistance of each resistor was equal to 120 Ω and the full bridge required 2 V power supply (provided by an external source).

Weights from zero to 4.8 kg were hung to one end of a rope (by means of a pulley) in five different step experiments during which the voltage measured by the load cell was recorded together with the correspondent weight. The other end of the rope was tied up, at a distance of 6 inches (0.1524 m) from the potentiometer rotation axis, to the shaft onto which the strain gauges were mounted.

Measured voltage related linearly with applied weights (Voltage = $m \cdot \text{Weight} + c$) and coefficients were interpolated for each experiment. Final values ($m = 22.6 \text{ mV/Kg}$; $c = -420 \text{ mV}$) were then obtained by averaging those obtained from each single experiment.

Finally, the calibrated torque T_{SG} in Nm was equal to

$$T_{SG} = \frac{(\text{Measured Voltage} - c)}{m} \cdot g \cdot \text{arm}$$

where g is the gravitational acceleration in m/s^2 and arm is equal to 0.1524 m (6 inches).

All of the measurements for the calibration procedure were recorded by using the MIE Data Logger and the voltage was amplified 500 times using a Fylde FE-369-TA amplifier.

4.3 Trials & Protocol

The experimentation was approved by the Human Experimentation Safety Committee (approval number: 998) and informed consent was obtained from each subject.

Twelve healthy subjects (mean age 31.1 ± 8.7 years) were instructed to perform three isometric MVCs at each position for 5 s for both flexors and extensors, with 10 sec rest between two subsequent contractions. Totally, 14 measurements were recorded for each subject: 7 positions for flexors and 7 positions for extensors. As Figure 14 shows, the hand was in neutral orientation, while forearm, arm (vertical), elbow (flexed at 90°), and shoulder were immobilised. A typical experiment generated a plot like the one in Figure 15 which shows the torque measured together with EMGs.

This specific measurement refers to a flexion trial as it can be inferred by the EMG waveforms: the flexor EMG is synchronous with the exerted torque while the extensor EMG is mainly flat throughout the experiment.

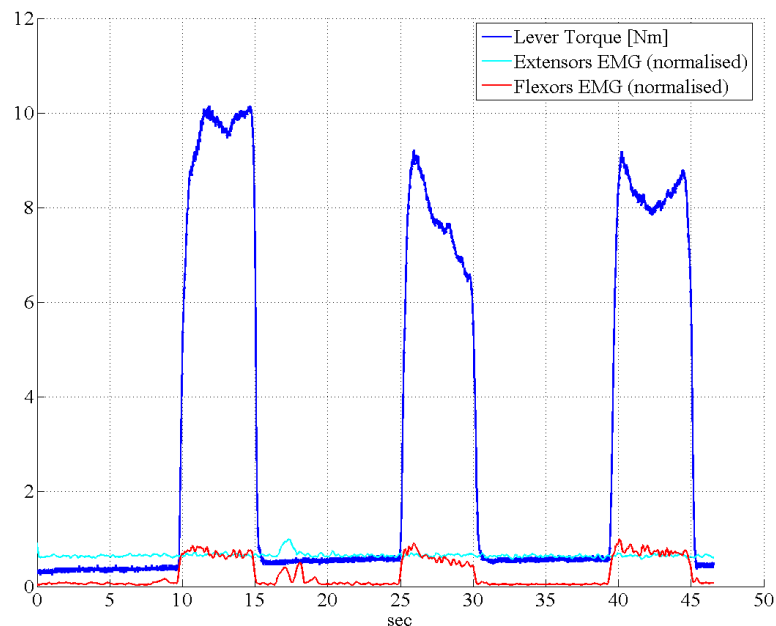


Figure 15 – A typical experiment during which torque as well as EMGs are recorded.

Surface EMG electrodes were positioned equidistant from the motor point of flexor carpi ulnaris (FCU), flexor carpi radialis and flexor digitorum superficialis to measure EMG signals for flexion. They were placed on a line from the medial epicondyle of the elbow to the radial styloid process (base of the thumb), one third distal of the medial epicondyle. The extensor EMG electrodes were positioned close to the motor point of extensor carpi radialis longus (ECRL) as follows: on a line from the lateral epicondyle of the elbow to the 2nd metacarpal, 5-7cm distal of the lateral epicondyle. Positions are better illustrated in Figure 16.

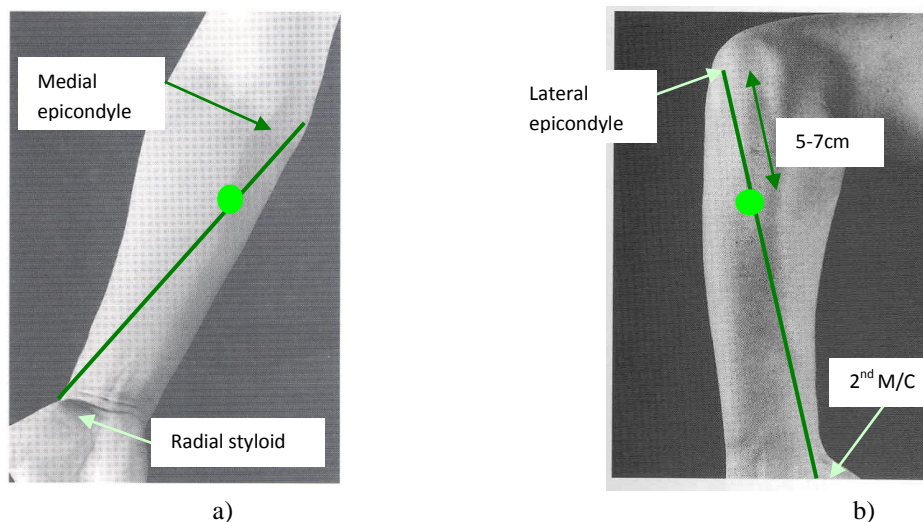


Figure 16 – EMG electrode positions for a) flexor muscles and b) extensor muscles.

Prior to each trial, a set of preliminary actions had to be performed. These follow:

1. Electrodes' placement
 - a. Determine whether the subject is right-handed or left-handed.
 - b. Wipe clean electrodes' site on the subjects' arm.
 - c. Locate electrodes' positions (according to instructions above) and apply them on the dry skin.
2. Arm position
 - a. Fix the height of the chair arm to a natural position for the shoulder (relaxed).
 - b. Align wrist joint with potentiometer shaft axis.
 - c. Fix elbow constraint.
 - d. Fix forearm by:
 - i. Strap.
 - ii. Two-point gauzed constraint.
 - e. Place air splint around the hand (its middle position in correspondence with the knuckles).
 - f. Make sure that the electrodes remain untouched.
3. Electrical connections
 - a. Wire electrodes and connect them to the Data Logger.
 - b. Connect the strain gauge socket.
 - c. Ensure 2 Volts are supplied to the strain gauges.
4. Measurements setup
 - a. Offset the voltmeter reading to ZERO by screwing the offset screw on the front panel of the amplifier.
 - b. Choose 500 as amplification gain (make sure that the gain screw is at its lowest position).
 - c. IMPORTANT: make sure that the voltmeter reading is positive while the strain gauges are loaded.
 - d. Inflate the cuff so that hand and fingers movements are constrained, without discomfort of the subject.
5. Carry out experiments
 - a. Flexion-extension MVCs are carried out within the range -30/+30 degrees at 10 degrees interval (0 degree corresponds to the hand placed vertically, aligned with the forearm and having the palm facing the subject).
 - b. For each muscle group (flexors and extensors), the subject is requested to perform THREE maximal isometric contractions for 5 sec at each position with 10 sec rest in between.
 - c. Perform 30 sec random contractions at 20F (flexor-side) degrees for flexors and at 20E (extensor-side) degrees for extensors.

As a good practice:

1. Inflate the air splint JUST BEFORE the experiment to avoid discomfort due to long compression.
2. Recommend the subjects NOT TO CONTRACT OTHER MUSCLES (only those of the forearm).
3. Recommend the subjects to keep the FINGERS STRAIGHT.

4. DEFLATE THE AIR SPLINT after half of the experiments has been carried out to avoid discomfort due to long compression.
5. Always MAKE SURE THAT THE VOLTMETER READING IS POSITIVE while loading the strain gauges.

The following control of contra-indications was assured throughout the experiments.

- Attachments to subjects:

Hand washing is obligatory. The electrode site was prepared by removing dead skin using commercially available alcohol swipes. The abrasion was performed carefully such that even a red skin was highly unlikely. Once the skin was dry, pre-gelled self-adhesive electrodes could be attached. To prevent movement artifacts, a micropore tape to attach the pre-amp cable to the skin was used. The subjects taking part in an experiment were asked for previous symptoms of allergy to surface electrodes. In case of positive answer, the experiment cannot be performed. The consent form to be completed prior each experimentation will specifically request these details to each subject. In case of unexpected allergy during the experiment, the subject is able to immediately terminate the test.

- No physical hazards:

The rig is constituted of an instrumented armchair which allows setting different wrist positions. To measure isometric contractions, with the hand in a predetermined position, the subject can either push the handle against a constraint or try to maintain the same position against the action of applied weights, not exceeding 20% of maximum force measured in the preliminary phase. The former solution was chosen.

The subjects taking part in an experiment were healthy with no arthritis or previous wrist injury. In these latter cases, the experiment cannot be performed. The consent form to be completed prior each experimentation will specifically request these details to each subject.

In case wrist pain or aggravation occurs, the test rig as well as the tasks to be performed allows the subject to immediately terminate the experiment with no further risks.

- No electrical hazards:

No electric stimuli were sent to the subjects. All of the equipment used for the experiments was fully tested and isolated electrically.

5. Model Implementation

In case of maximum voluntary contractions (MVCs) the origin and the insertion point of a musculotendon unit remain fixed, as schematically shown in Figure 17. As a consequence, the musculotendon length L_{MT} is constant and equal to

$$L_{MT}(\theta) = L_{oMT} + \Delta L_{MT}(\theta). \quad (17)$$

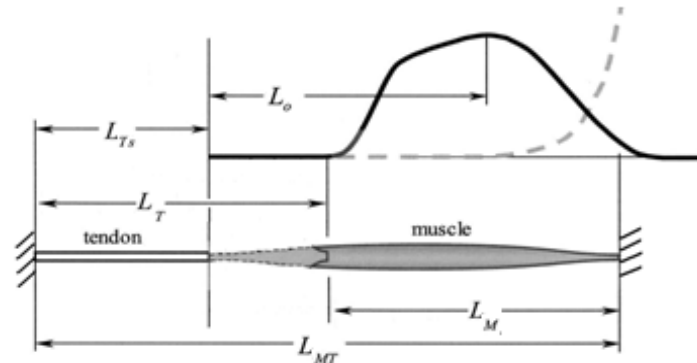


Figure 17 – For a given position, the musculotendon length L_{MT} is constant while both the muscle length, L_M , and the tendon length, L_T , mutually change.

Thus, for a given joint angle the musculotendon length changes of an amount equal to ΔL_{MT} (equation (12)) with respect to its maximally elongated musculotendon length, L_{oMT}^{***} . In turn, L_{oMT} is a function of the optimal physiological muscle length, $L_{oM}(t)$, and the tendon slack length, L_{TS} , as given by the following equation (Lan, 2002; Lemay and Crago, 1996)

$$L_{oMT} = L_{TS} + 1.2 \cdot L_{oM} \quad (18)$$

$L_{oM}(t)$ and L_{TS} together with the maximum isometric muscle force, F_{oM} , are characteristic of a specific musculotendon unit and need to be known or estimated.

Finally, the instantaneous muscle length, $L_M(\theta, t)$ in case of MVCs is equal to

$$L_M(\theta, t) = L_{MT}(\theta) - L_T(\theta, t) \quad (19)$$

or

$$L_M(\theta, t) = L_{oMT} + \Delta L_{MT}(\theta) - L_T(\theta, t) \quad (20)$$

once equation (17) has been substituted into equation (19).

In case one limb extremity moves (i.e. no MVCs), equation (20) becomes

*** As reported in Lemay and Crago (1996), the maximal physiological musculotendon length (different from the musculotendon length which changes with joint configuration) is obtained by measuring the distance from origin to insertion as the joints are set to the extremes of the physiologically realistic range of motion.

$$L_M(\theta, t) = L_{oMT} + \Delta L_{MT}(\theta) - L_T(\theta, t) - x_{ext}(t) \quad (21)$$

where $x_{ext}(t)$ is an external length change due to the limb movement. In the present study no limb movement has been included, thus $x_{ext}(t)$ was set equal to zero.

For MVCs (i.e. $x_{ext}(t) = 0$), once L_{TS} and L_{oM} are given (or estimated) and $\Delta L_{MT}(\theta)$ has been determined from equation (12), the only unknown of equation (21) remains $L_T(\theta, t)$, which is calculated integrating the differential equation governing the musculotendon dynamics. Thus, the implemented model can be schematically represented as in the following figure

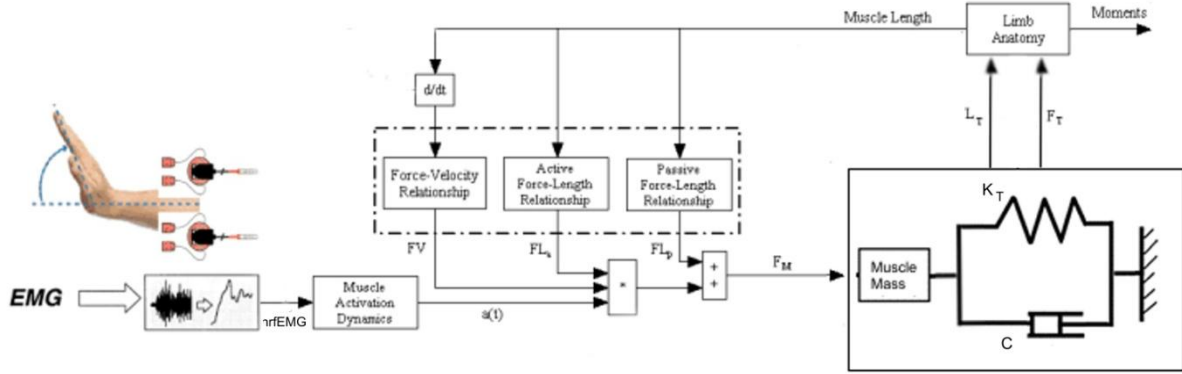


Figure 18 – Schematic representation of the musculoskeletal model.

In this work, a dashpot $C(\theta, t)$ connected in parallel to the spring $K_T(\theta, t)$ representing the tendon was added to the model in Figure 8 for numerical stability. Thus, in Figure 18 the muscle force $F_M(\theta, t)$, calculated from equation (1) with $F_M = \tilde{F}_M \cdot F_{oM}$, acts on the muscle mass, M_m , and thus on the tendon unit comprising a spring in parallel with a dashpot. $L_T(\theta, t)$ can be finally determined by integrating the following differential equation

$$F_M(\theta, t) = M_m \cdot \ddot{L}_T(\theta, t) + C(\theta, t) \cdot \dot{L}_T(\theta, t) + F_{K_T}(\theta, t) \quad (22)$$

where $F_{K_T}(\theta, t)$ is the tendon force contribution due to the spring and is calculated from equations (9) and (10) with $F_{K_T} = \tilde{F}_{K_T} \cdot F_{oM}$, while $C(\theta, t)$ is the viscous coefficient due to the dashpot whose value has been set equal to

$$C(\theta, t) = \sqrt{4 \cdot M_m \cdot K_T(\theta, t)} \quad (23)$$

with K_T given by

$$K_T(\theta, t) = \frac{F_{K_T}(\theta, t)}{L_T(\theta, t)}. \quad (24)$$

Equation (23) assures that the system behaves as a critically-damped second order system (Khoo, 1999) which is a physiological requirement (Winter, 2005).

The term M_m was set equal to 0.1546 kg (sum of the masses of flexor muscles in Table 1) and 0.0397 kg for the flexors and extensors, respectively. Anyway, the system showed to be insensitive to a wide range of different values of this parameter.

In summary, as Figure 18 shows, recorded EMGs determine the muscle activation level, which contributes to generate the muscle force, $F_M(\theta, t)$, together with the F-L and F-V relationships. In turn, $F_M(\theta, t)$ acts on the muscle mass and the tendon unit. Finally, exerted moments and instantaneous muscle length $L_M(\theta, t)$ are obtained by the tendon force, $F_T(\theta, t)$

$$F_T(\theta, t) = C(\theta, t) \cdot \dot{L}_T(\theta, t) + F_{K_T}(\theta, t) \quad (25)$$

which interacts with limb anatomy described by equations (11), (12) and (17) to (21) to generate joint moments.

The model of one musculotendon unit as implemented in Simulink is shown in Figure 19 where all of the equations described so far have been represented in block diagrams.

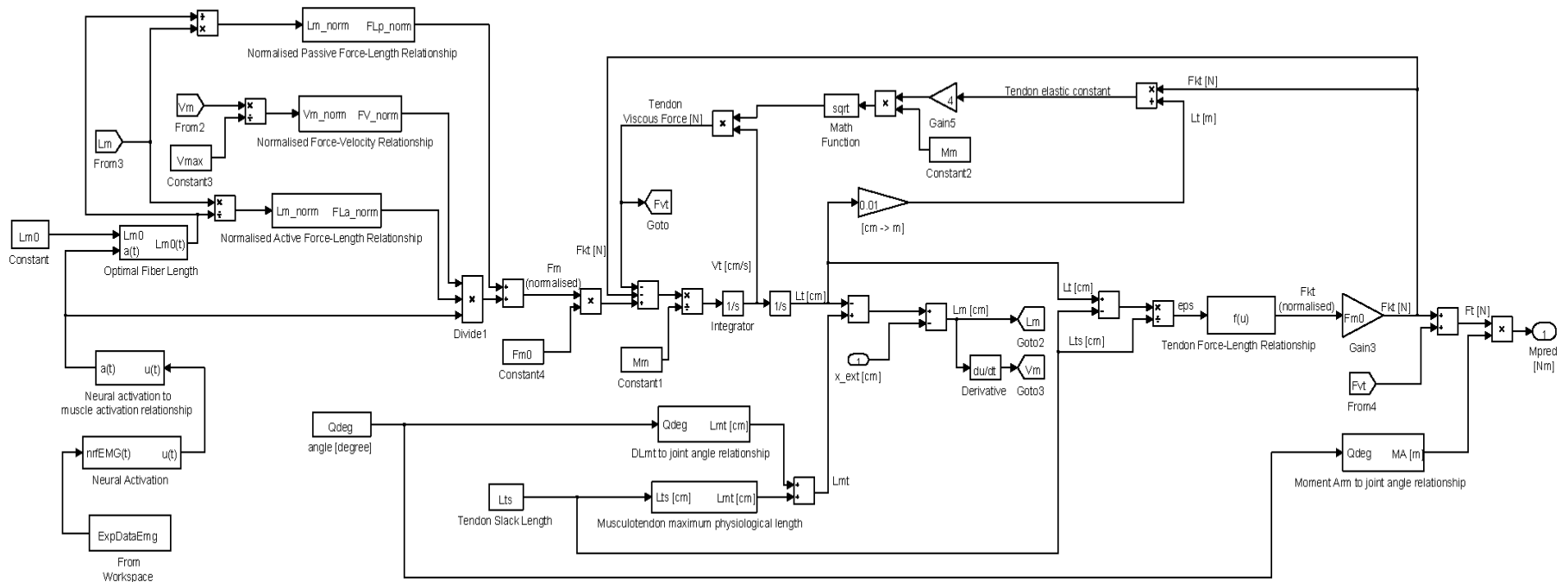


Figure 19 – Simulink implementation of the musculoskeletal model for a single musculotendon unit.

5.1 Parameter Estimation

The described model needs the following musculoskeletal parameters to be known or estimated:

- The optimal physiological muscle length, $L_{oM}(t)$;
- The maximum isometric muscle force, F_{oM} ;
- The tendon slack length, L_{TS} ;

Three more parameters have been added to the previous ones:

- The coefficient A as in equation (4);
- The moment arm, $MA(\theta)$;
- The musculotendon length change, $\Delta L_{MT}(\theta)$;

The latter two parameters were allowed a 10% variation with respect to values obtained from equations (11) and (12) in order to take into account possible inaccuracies in the determination of the wrist angle.

Figure 20 schematically shows the algorithm utilised for the estimation of the six parameters above. Having constructed the model (enclashed in the dashed rectangle in Figure 20), the EMGs were used as input, while the predicted joint moments were compared to the moments exerted by the limb and measured by means of the strain gauge load cell. The root mean square error (RMSE) between predicted and measured joint moments was used as the objective function to be minimised for the estimation of the six parameters. In particular, the RMSE was set equal to:

$$RMSE = \sqrt{\frac{\sum_{i=1}^N (M_{pred}(i) - M_{meas}(i))^2}{N}} \quad (26)$$

where N was the total number of samples in one trial, $M_{pred}(i)$ and $M_{meas}(i)$ are respectively the torque calculated by the model and the torque measured at instant i .

It must be specified that 6 out of 7 experiments recorded for each subject were used for the estimation process. Specifically, measurements at 0° were only used for the validation process and were not included during the estimation phase.

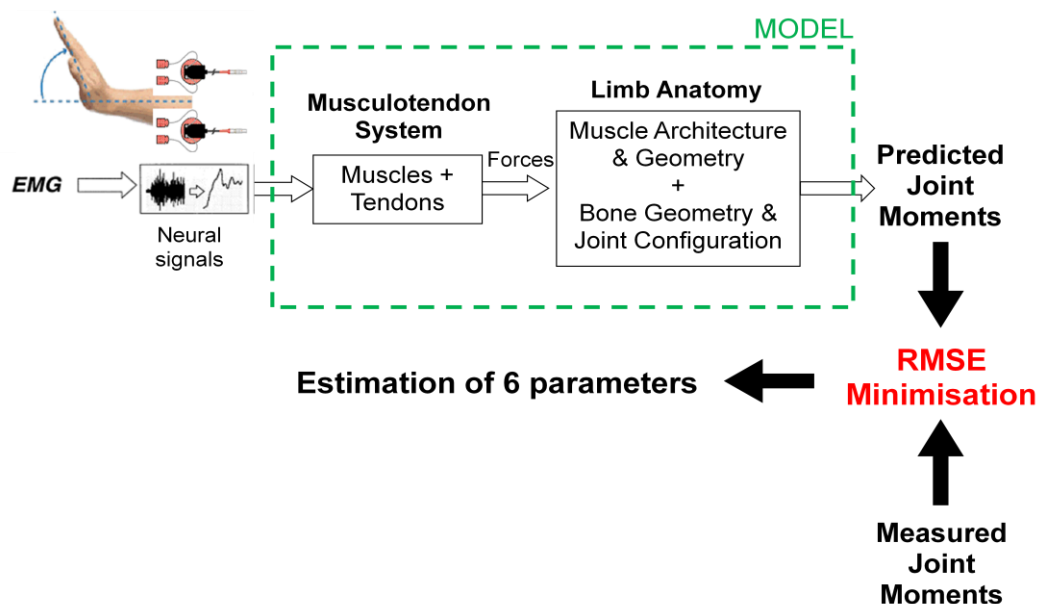


Figure 20 – Scheme of the optimisation process.

The Matlab code used for parameter estimation will be described next and relevant pieces of code will be embedded in the text. In order to give an overview of how the entire Matlab code operates, Figure 21 schematically illustrates its execution sequence. The file “ParamEst_ConOpt_soton.m” contains the MAIN program and recalls other functions (Sub-levels I and II in Figure 21) and it is made up of four cells performing the following tasks:

1. Load and Pre-process Experimental Data;
2. Initialise parameters;
3. Run Identification;
4. Output Data.

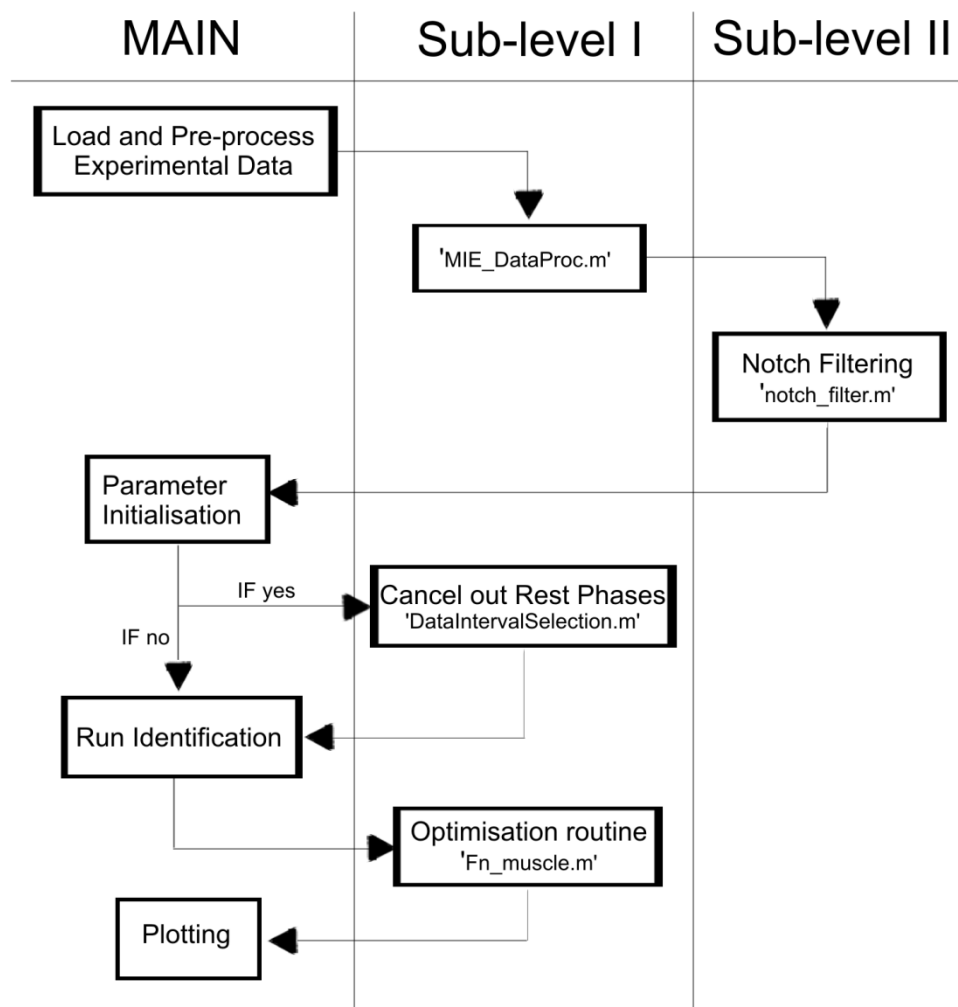


Figure 21 – Sequence of operations performed by the Matlab code.

5.1.1 Loading and Pre-processing of Experimental Data

The first cell of the MAIN program (below) executes the following commands:

- Load experimental data to be processed;
- Define the window of data to be used (i.e. variables `fsample`, `lsample`, `sample_int`);
- Calls the function “MIE_DataProc.m”.

```

%% Load and Pre-process Experimental Data
clear all

global Lm0 Fm0 Lts A DLmt MA k e thetap thetap_init T tauact taudeact emg
global Mpred Mtot lambda aa bb cc fsample lsample sample_int Mtot_new
global emg_new MuscleGroup

[file_name,path_name]=uigetfile('*.mat','Select file');
load([path_name,file_name]);

fsample=500; % first sample to be included
lsample=length(data); % last sample to be included
sample_int=lsample-fsample+1; % sample interval to be processed

MIE_DataProc

```

The “MIE_DataProc.m” function (Sub-level I) performs two tasks:

- Calculate the linear envelope profile of the EMG signals;
- Calculate the calibrated torques from the load cell signal.

The code for the first task is follows:

```

T1=1;
fc_smooth=3; % cutoff frequency Butterworth filter
Fs=1000; % sampling frequency

%% EMG processing

% raw EMG signal recorded with MIE processed with Simpon's commands
fc=[50:50:Fs/2-1];
b=notch_filter(fc,T1,Fs);
emg1=filtfilt(b,1,data(:,2)); % Extensors, notch filtering
emg2=filtfilt(b,1,data(:,3)); % Flexors, notch filtering
emg1_detr=detrend(emg1)/std(emg1); % Extensors, detrend
emg2_detr=detrend(emg2)/std(emg2); % Flexors, detrend
emg1_rect=abs(emg1_detr); % Extensors, rectified
emg2_rect=abs(emg2_detr); % Flexors, rectified
[b_smooth,a_smooth]=butter(2,fc_smooth/Fs*2); % Butterworth Filter
emg1_env=filtfilt(b_smooth,a_smooth,emg1_rect); %Extensors, linear envelope
emg2_env=filtfilt(b_smooth,a_smooth,emg2_rect); %Flexors, linear envelope

emg1_env_norm=emg1_env(fsample:lsample)/max(emg1_env(fsample:lsample));
emg2_env_norm=emg2_env(fsample:lsample)/max(emg2_env(fsample:lsample));

```

In the first task, raw EMG data (contained in the variable named “data”) were processed to calculate the correspondent linear envelope profile mimicking the muscle tension waveform.

The signals were first notch filtered to eliminate any influence of the mains electricity¹⁰. The following code (Sub-level II) was used to generate the coefficients of the notch filter which enable the cancellation of the mains influence with intervals of 50 Hz.

```
function b=notch_filter(fc,T1,Fs);  
  
N=floor(T1*Fs/2);  
t=[-N:N]/Fs;  
h=zeros(size(t));  
for i=1:length(fc);  
h0=cos(2*pi*t*fc(i));  
h1=h0.*(1+cos(pi/N*[-N:N]))/2;  
h1=h1/sum(h1.*h0);  
h=h+h1;  
end  
b=zeros(size(h));  
b(N+1)=1;  
b=b-h;
```

The notch filter coefficients were then passed as the numerator of the `filtfilt` function that generated the variables `emg1` and `emg2` for extensor and flexor EMGs, respectively. In this case, an all-zero filter (FIR) was used as 1 was entered as value for the denominator coefficients. After filtering the data in the forward direction, `filtfilt` reverses the filtered sequence and runs it back through the filter with Zero-phase distortion (i.e. the EMG signal is not shifted in time).

Successively, eventual linear trends over time of the EMGs were removed and referred to the standard deviation of the signals which were then rectified.

The EMGs were subsequently lowpass filtered by means of a second order Butterworth filter. The command “[`b_smooth`,`a_smooth`]=`butter`(2,`fc_smooth`/`Fs`*2)” returns the zeros and poles of the filter characterised by a normalised cutoff frequency of 0.006 which corresponds to a value of 3 Hz. The force generated by the muscle is typically in the range of 3 to 10 Hz, thus this lowpass filter enables to correlate the EMG with the muscle force filtering out the high frequency components (Buchanan et al., 2004).

As reported in Koo and Mak (2005) for elbow muscles “*The theoretical basis of linear envelope processing is that the frequency characteristics of muscle twitches could be regarded as a second order, critically damped, low-passed system (Milner-Brown et al., 1973). Since each twitch can be considered to be the impulse response of an active motor unit associated with a motor unit action potential (MUAP) impulse, the full-wave-rectified EMG can be considered as a summation of MUAPs of various amplitudes, whereas, muscle tension can be considered as a graded summation of the twitches resulting from all active motor units. It has been reported that the contracting time of a twitch for different muscles ranged between 20 and 90 ms (Buchthal and Schmalbruch, 1970; Milner-Brown et al., 1973). Since the cut-off frequency of 3 Hz of a second-order Butterworth filter corresponds approximately to a contracting time of 50 ms, which can be regarded as the averaged value reported in the literature, it represents a reasonable selection for the elbow muscles*”.

¹⁰ This procedure was redundant since the MIE Data Logger, as a medical approved device, is shielded from the mains electricity frequency (50 Hz). Anyway, it may result useful in case of custom setups.

The same choice was made for wrist muscles and the Butterworth filter coefficients were then applied to the EMG signals by means of a second `filtfilt` command which generated the new variables `emg1_env` and `emg2_env`.

Finally, the EMGs recorded during MVC trials were normalised with respect to the peak EMG value obtained during the corresponding experiment (the final EMG values range between 0 and 1).

The second task of file “MIE_DataProc.m” calculates the calibrated values of the torque exerted by the hand and recorded using the strain gauge load cell. Refer to section ‘4.2.2 Strain Gauge Load Cell Calibration’ for details on the following code.

```
%% Torque calculation

% Calibration coefficients (slope m, constant c) are obtained as the mean
% of the interpolating values
m=(22+22+23+23+23)/5;
c=(-420-420-420-420-420)/5;

% Strain Gauge Torque
arm=6*0.0254; % [m]
lev_torque=((data(:,5)-c)/m)*9.81*arm; %[Nm] lever torque

lev_torque=lev_torque(fsample:lsample);

% Time vector
time=data(fsample:lsample,1);
```

5.1.2 Parameter Initialisation

The aim of the second cell of the MAIN program is the initialisation of the variable used for the subsequent optimisation routine.

The first part sets the parameters values as in Table 1.

```
%% Initialise Parameters

% Activation dynamics parameters from Zajac (1989),
% Critical Review of Biomedical Engineering
tauact=0.05; % [s]
taudeact=0.08; % [s]

% Muscle dynamics parameters
lambda=0.15; % from Buchanan 2004
aa=1.5; % from Lan 2002 & 2005
bb=8; % from Lan 2002 & 2005
cc=0.0866; % from Lan 2002 & 2005
d=0.56; % from Lan 2002
k=-1/d^2; % from Lan 2002
```

```
T=time(2,1)-time(1,1);
```

The second part initialises the vector of the six parameters to be estimated (PHI_init) by asking the user to specify:

- The initial estimates of the four parameters: $Lm0$, $Fm0$, Lts and A ;
- The muscle group to be analysed (flexors or extensors);
- The value of the angle at which the hand was positioned for the specific experiment (Q_{deg}).

These two latter information were then used to set the initial estimates for the two remaining parameters to be estimated – the moment arm, MA , and the musculotendon length change, $DLmt$ – according to equations (11) and (12) from Lemay and Crago (1996). In particular, the relationships contained therein for the Extensor Carpi Radialis Longus (ECRL) and for the Flexor Carpi Ulnaris (FCU) were used to initialise these two latter values in case of extension or flexion, respectively. Finally, it must be pointed out that the sign of the values for the extensors was changed for convenience with respect to the convention used in (Lemay and Crago, 1996).

It is worth noting that by definition the sign of the joint angles are considered positive for flexions and negative for extensions, thus the wrist angular position, Q_{deg} , was set accordingly by means of the first `if` cycle. The measured torque, M_{tot} , was considered positive no matter of the group of muscles.

```
% Input initial estimates of parameters to be estimated
PHI = zeros(6,1); % initialise parameter vector

Lm0 = input('Enter initial guess of parameter Lm0 (cm) >>');
Fm0 = input('Enter initial guess of parameter Fm0 (N) >>');
Lts = input('Enter initial guess of parameter Lts (cm) >>');
A = input('Enter initial guess of parameter A (must be between -3 and...
0) >>');
MuscleGroup = input('Enter muscle group (e for extensors, f for...
flexors) >>', 's');
Qdeg = input('Enter wrist angular position (degrees) >>');

if Qdeg~=0
    side=input('Hands on flexor or extensor side? (enter f or e) >>', 's');
    if MuscleGroup=='e' && side=='e' || MuscleGroup=='f' && side=='e'
        Qdeg = -Qdeg;
    end
end

Mtot=lev_torque; % [Nm]

if MuscleGroup=='e'
    emg=emg1_env_norm;
else
    emg=emg2_env_norm;
end
```

```

Cut = input('Do you want to cut off phases at rest? (y,n)>>','s');
if Cut=='y'
    DataIntervalSelection
else
    Mtot_new=Mtot;
    emg_new=emg;
    time_new=time;
end

Q=0.01745329*Qdeg; % degrees to radians conversion

if MuscleGroup=='e'
    % Moment arm/angle relationship EXTENSOR CARPI RADIALIS LONGUS (ECRL)
    % from Lemay & Crago (1996)
    a1ECRL=-1.02;
    a2ECRL=0.31;
    a3ECRL=0.12;
    a4ECRL=-0.12;
    a5ECRL=-0.03;
    a6ECRL=0.03;
    MA=a1ECRL+a2ECRL*Q+a3ECRL*Q^2+a4ECRL*Q^3+a5ECRL*Q^4+a6ECRL*Q^5;

    % Musculotendon length/angle relationship EXTENSOR CARPI RADIALIS
    % LONGUS (ECRL), from Lemay & Crago (1996)
    b0ECRL=1.35;
    b1ECRL=0.98;
    b2ECRL=-0.12;
    b3ECRL=-0.007;
    DLmt=b0ECRL+b1ECRL*Q+b2ECRL*Q^2+b3ECRL*Q^3;

else
    % Moment arm/angle relationship FLEXOR CARPI ULNARIS (FCU)
    % from Lemay & Crago (1996)
    a1FCU=1.90;
    a2FCU=0.14;
    a3FCU=-0.55;
    a4FCU=0.20;
    a5FCU=0.22;
    a6FCU=-0.12;
    MA=a1FCU+a2FCU*Q+a3FCU*Q^2+a4FCU*Q^3+a5FCU*Q^4+a6FCU*Q^5;

    % Musculotendon length/angle relationship FLEXOR CARPI ULNARIS (FCU)
    % from Lemay & Crago (1996)
    b0FCU=-2.0;
    b1FCU=-1.86;
    b2FCU=-0.089;
    b3FCU=0.08;
    DLmt=b0FCU+b1FCU*Q+b2FCU*Q^2+b3FCU*Q^3;

end

if MuscleGroup=='e'
    thetap_init=[Lm0; Fm0; Lts; A; -DLmt; -MA]

```

```

else
    thetap_init=[Lm0; Fm0; Lts; A; DLmt; MA]
end

```

It must be specified that the variable `Cut` (and the relative `if` cycle) allows one to choose whether or not to include the phases at rest during each experiment by means of the function `DataIntervalSelection.m`. As reported below, flexible values of the recorded EMGs were used as a threshold to distinguish rest from contraction phases. In particular, a difference of 0.2 between two EMG values separated by 400 samples on the ascending part of the data was used to identify the instants at which a contraction could be considered as begun, while a difference of 0.04 between two EMG values separated by 400 samples on the descending part of the same data was used to identify the instants at which a contraction could be considered as terminated.

```

% DataIntervalSelection.m

samples=400; % sample interval to evaluate the gradient

% IF cycle to identify the FIRST sample on the ascending part of the FIRST
% contraction
jjj=0;
for i=1:13000-fsample
    if i<=(length(emg)-samples)
        if (emg(i+samples)-emg(i))>0.2
            ind1=i;
            break
        end
    end
end

% IF cycle to identify the LAST sample on the descending part of the
% FIRST contraction
jjj=0;
for i=13001-fsample:19000-fsample
    if i<=(length(emg)-samples)
        if Mtot(i) < 1
            if abs((emg(i+samples)-emg(i)))<0.04
                ind2=i+samples;
                break
            end
        end
    end
end

% IF cycle to identify the FIRST sample on the ascending part of the
% SECOND contraction
jjj=0;
for i=19001-fsample:28000-fsample
    if i<=(length(emg)-samples)
        if (emg(i+samples)-emg(i))>0.2
            ind3=i;

```

```

        break
    end
end
end

% IF cycle to identify the LAST sample on the descending part of the
% SECOND contraction
jjj=0;
for i=28001-fsample:35000-fsample
    if i<=(length(emg)-samples)
        if Mtot(i) < 1
            if abs((emg(i+samples)-emg(i)))<0.04
                ind4=i+samples;
                break
            end
        end
    end
end

% IF cycle to identify the FIRST sample on the ascending part of the
% THIRD contraction
jjj=0;
for i=35001-fsample:43000-fsample
    if i<=(length(emg)-samples)
        if (emg(i+samples)-emg(i))>0.2
            ind5=i;
            break
        end
    end
end

% IF cycle to identify the LAST sample on the descending part of the
% THIRD contraction
jjj=0;
for i=43001-fsample:sample_int-fsample
    if i<=(length(emg)-samples)
        if Mtot(i) < 1
            if abs((emg(i+samples)-emg(i)))<0.04
                ind6=i+samples;
                break
            end
        end
    end
end

% FOR cycle to re-size the variables
jjj=0;
for i=ind1:ind2
    jjj=jjj+1;
    Mtot_new(jjj,1)=Mtot(i);
    emg_new(jjj,1)=emg(i);
    time_new(jjj,1)=time(i);
end

```

```

jjj=ind2-ind1;
for i=ind3:ind4
    jjj=jjj+1;
    Mtot_new(jjj,1)=Mtot(i);
    emg_new(jjj,1)=emg(i);
    time_new(jjj,1)=time(i);
end
jjj=(ind4-ind3)+(ind2-ind1);
for i=ind5:ind6
    jjj=jjj+1;
    Mtot_new(jjj,1)=Mtot(i);
    emg_new(jjj,1)=emg(i);
    time_new(jjj,1)=time(i);
end

sample_int=length(Mtot_new);

```

5.1.3 Optimisation Algorithm

The third cell of the MAIN program launches the identification routine to estimate the six unknown parameters. The algorithm used to perform the minimisation of the objective function J employed a gradient descent approach by means of the Matlab (The Mathworks, Inc.) function “fmincon” which finds the minimum of constrained nonlinear multivariable functions starting at an initial estimate.

The specific syntax for the fmincon function is neglected here (the reader can refer to the Matlab User Guide), instead the relevant features are commented hereafter.

fmincon minimises the objective function J calculated in `Fn_muscle.m` starting at the initial values specified in vector `PHI_init` subject to the linear inequalities $A_{ineq} * PHI \leq b_{ineq}$ and a set of lower and upper bounds (i.e. `lb` and `ub`) on the design variables in vector `PHI`, so that the solution is always in the range $lb \leq PHI \leq ub$.

In particular, lower and upper bounds for $L_{oM}(t)$, F_{oM} and L_{TS} were set considering a reasonable physiologically realistic range (Garner and Pandey, 2001; Holzbaur et al., 2005), that is in the range 1 to 10 cm for $L_{oM}(t)$, 20 to 2000 N for F_{oM} and 10 to 40 cm for L_{TS} ; parameter A was allowed to vary in the range [-3; 0] as in (Buchanan et al., 2004) – to be noted that -0.001 was used instead of zero for numerical reasons; parameters $MA(\theta)$ and $\Delta L_{MT}(\theta)$ were allowed a 10% variation with respect to their initial values calculated from equations (11) and (12) and specified in vector `PHI_init`. Moreover, by means of the linear inequalities $A_{ineq} * PHI \leq b_{ineq}$, $L_{oM}(t)$ values were also constrained to be less than or equal to the L_{TS} values as from data reported in literature (Garner and Pandey, 2001, 2003; Holzbaur et al., 2005; Winters and Stark, 1988).

All these bounds and constraints were passed to the user-defined function 'Fn_muscle' and used by the fmincon function for the minimisation process. The final estimated values of the six parameters are stored in the vector `PHI`. A series of other informative outputs regarding the estimation process are provided depending on the options specified (commands in square brackets).

```

%% Run Identification

% Finds a constrained minimum the objective function J defined by the
% function "Fn_muscle".

% Constrained optimization bounds (lb=lower bounds, ub=upper bounds)
if MuscleGroup=='e'
    lb=[1; 20; 10; -3; 1.1*PHI_init(5); 0.9*PHI_init(6)];
    ub=[inf; 2000; 40; -0.001; 0.9*PHI_init(5); 1.1*PHI_init(6)];
else
    lb=[1; 20; 10; -3; 1.1*PHI_init(5); 0.9*PHI_init(6)];
    ub=[10; 2000; 40; -0.001; 0.9*PHI_init(5); 1.1*PHI_init(6)];
end

Aineq=[1, 0, -1, 0, 0, 0];
bineq=0;

% fmincon finds the minimum of constrained nonlinear multivariable function
[PHI, fval, exitflag, output, lambda, grad, hessian] = ...
fmincon('Fn_muscle', PHI_init, Aineq, bineq, [], [], lb, ub)

```

The user-defined function `Fn_muscle.m` defines the model being employed for estimating the parameters and returns to `fmincon` the value of the objective function J (equation (26)) at every iteration during the optimisation process. A vector of six parameters, $PHI(i)$ with $i = 1, \dots, 6$, is formed at each iteration starting at specified initial values considering the specified lower and upper bounds as well as the inequality constraints; then it is used in the discrete version of the constructed model; finally the objective function J is evaluated. This process is repeated iteratively until the optimal combination for the six parameters has been found.

In order to solve numerically the differential equations of the musculotendon model made up of equations (1) to (12) and (17) to (24), the finite difference method was used and the complete model was converted in a finite difference form by using the backward-difference rule (Hildebrand, 1968). Specifically, the first order derivatives of a function $f(i)$ with samples spaced by T were approximated as

$$f'(i) = \frac{f(i) - f(i-1)}{T},$$

while the second order derivatives took the form

$$f''(i) = \frac{f(i) - 2 \cdot f(i-1) + f(i-2)}{T^2}.$$

The Matlab code used to perform the estimation process is reported below. In it, each equation in discrete form was referred to its corresponding continuous version of the previous paragraphs (equations (1) to (12) and (17) to (24)) by appropriate comments. It is worth noting that the implementation sequence reflects the Simulink scheme shown in Figure 19. Finally, an error check

was introduced to stop the simulation in case negative values of the muscle length L_M occur during the optimisation process.

```

function J=Fn_muscle(PHI)

global k e Fpred Lm u T tauact taudeact emg a Lts MuscleGroup
global Mpred Mtot lambda aa bb cc FLa_norm FLp_norm FV_norm sample_int
global Mtot_new emg_new

% Variables' preallocation
Lm=zeros(sample_int,1);
u=zeros(sample_int,1);
a=zeros(sample_int,1);
FLp_norm=zeros(sample_int,1);
FLa_norm=zeros(sample_int,1);
Vm=zeros(sample_int,1);
FV_norm=zeros(sample_int,1);
Fpred=zeros(sample_int,1);
Mpred=zeros(sample_int,1);
Vt=zeros(sample_int,1);
Lt(1,1)=Lts;
Lt(2,1)=Lts;
Lt(3:sample_int,1)=zeros(sample_int-2,1);
Fvt=zeros(sample_int,1);
Fkt=zeros(sample_int,1);
eps=zeros(sample_int,1);
Fkt_norm=zeros(sample_int,1);

if MuscleGroup=='e'
    MM=0.077; % [kg]
else
    MM=0.126; % [kg]
end

% Discrete form of the musculotendon model
for i=3:sample_int

    % Neural signal - EQUATIONS (2) and (3)
    u(i)=((1/tauact)*emg_new(i-1)-u(i-1))*((1/tauact)*((tauact/taudeact)+...
    (1-(tauact/taudeact))*emg_new(i-1)))*T+u(i-1);

    % Activation signal - EQUATION (4)
    a(i)=((exp(PHI(4)*u(i))-1)/(exp(PHI(4))-1));

    % Normalised active force-length relationship - EQUATIONS (5) and (6)
    FLa_norm(i)=k*(Lm(i-1)/(PHI(1)*(lambda*(1-a(i))+1)))^2-...
    2*k*(Lm(i-1)/(PHI(1)*(lambda*(1-a(i))+1)))+k+1;

    % Normalised passive force-length relationship - EQUATIONS (7) and (6)

```

```

FLp_norm(i)=(exp(10*(Lm(i-1)/(PHI(1)*...
(lambda*(1-a(i))+1))-1))/exp(5));

% Normalised force-velocity relationship - EQUATIONS (8) and (6)
Vm(i-1)=(Lm(i-1)-Lm(i-2))/T; % [cm/s] muscle velocity
FV_norm(i)=(aa/(1+exp(bb*((Vm(i-1)/(10*PHI(1)*...
(lambda*(1-a(i))+1))-cc)))));

% Predicted total force -> Fm=Fm0*(FLp_norm+FLa_norm*FV_norm*a)
% EQUATION (1)
Fm(i)=PHI(2)*(FLp_norm(i)+FLa_norm(i)*FV_norm(i)*a(i));

% Tendon viscous force Fvt - EQUATIONS (23) and (24)
Vt(i-1)=(Lt(i-1)-Lt(i-2))/T; % [cm/s] tendon velocity
Fvt(i)=Vt(i-1)*sqrt(4*MM*(Fkt(i-1)/(0.01*Lt(i-1)))); % [N]

% Tendon length - EQUATION (22)
Lt(i)=(Fm(i)-Fvt(i)-Fkt(i-1))*T^2/MM+2*Lt(i-1)-Lt(i-2); % [cm]

% Tendon deformation - EQUATION (10)
eps(i)=(Lt(i)-PHI(3))/PHI(3);

% Normalised tendon elastic force - EQUATION (9)
if eps(i)<=0
    Fkt_norm(i)=0;
elseif eps(i)<0.0127
    Fkt_norm(i)=1480.3*eps(i)^2;
else
    Fkt_norm(i)=37.5*eps(i)-0.2375;
end

% Actual tendon elastic force -> Fkt=Fkt_norm*FoM
Fkt(i)=Fkt_norm(i)*PHI(2); % [N]

% Predicted total moment -> Mpred=(Fkt+Fvt)*MomentArm
Mpred(i)=(Fkt(i)+Fvt(i))*PHI(6); % [Ncm]

% Muscle length - EQUATIONS (18) and (20)
Lm(i)=PHI(5)+1.2*PHI(1)+PHI(3)-Lt(i); % [cm]

% Error check
if Lm(i)<0
    error('opt:Lm:Lm_negative','Lm has negative values.')
end
end

Mpred=Mpred/100; % [Ncm -> Nm] => Nm=Ncm/100

% Error between measured moment (Mtot) and predicted moment (Mpred)
e = Mtot_new - Mpred; %compute criterion function

```

```
% Objective function to be minimised
J = sqrt(sum(e.^2)/sample_int);
```

5.1.4 Data Output and Plotting

The fourth (and last) cell of the MAIN program displays the final estimated parameters as well as the RMSE and normalised RMSE (NRMSE) values calculated from the estimation. Finally, the measured torque (M_{tot}), the predicted torque (M_{pred}) and the linear envelope of the EMG are plotted together.

```
%% Data Output & Plotting

disp(' ');
disp('Final Parameter Values (Lm0 [cm], Fm0 [N], Lts [cm],A [-... 3,..,0],...
Dlmt [cm], MA [cm]):');
disp(PHI);

RMSE=sqrt(sum(e.^2)/length(e))
NRMSE=RMSE/(max(Mtot)-min(Mtot))*100

figure
grid on
hold on
if Cut=='n'
    plot(time_new,Mtot_new,time_new,Mpred,time_new,emg_new,'LineWidth',2);
else
    plot(time_new(1:ind2-ind1),Mtot_new(1:ind2-ind1),time_new((ind2-...
ind1)+1:(ind4-ind3)+(ind2-ind1)),Mtot_new((ind2-ind1)+1:(ind4-ind3)+(ind2-...
ind1)), 'b',time_new((ind4-ind3)+(ind2-ind1)+1:(ind6-ind5)+(ind4-...
ind3)+(ind2-ind1)),Mtot_new((ind4-ind3)+(ind2-ind1)+1:(ind6-ind5)+(ind4-...
ind3)+(ind2-ind1)), 'b', 'LineWidth',2)
    plot(time_new(1:ind2-ind1),Mpred(1:ind2-ind1), 'g',time_new((ind2-...
ind1)+1:(ind4-ind3)+(ind2-ind1)),Mpred((ind2-ind1)+1:(ind4-ind3)+(ind2-...
ind1)), 'g',time_new((ind4-ind3)+(ind2-ind1)+1:(ind6-ind5)+(ind4-...
ind3)+(ind2-ind1)),Mpred((ind4-ind3)+(ind2-ind1)+1:(ind6-ind5)+(ind4-...
ind3)+(ind2-ind1)), 'g', 'LineWidth',2)
    plot(time_new(1:ind2-ind1),emg_new(1:ind2-ind1), 'r',time_new((ind2-...
ind1)+1:(ind4-ind3)+(ind2-ind1)),emg_new((ind2-ind1)+1:(ind4-ind3)+(ind2-...
ind1)), 'r',time_new((ind4-ind3)+(ind2-ind1)+1:(ind6-ind5)+(ind4-...
ind3)+(ind2-ind1)),emg_new((ind4-ind3)+(ind2-ind1)+1:(ind6-ind5)+(ind4-...
ind3)+(ind2-ind1)), 'r', 'LineWidth',2)
end
set(gca,'fontsize',24,'fontname','times')
set(gcf,'color',[1 1 1],'position',[1 1 1680 891])
xlabel('Seconds','fontsize',24,'fontname','times')
legend('Measured Torque [Nm]','Estimated Torque [Nm]','Normalized Enveloped
EMG','Location','Best')
if MuscleGroup=='e'
    title('Extensors','fontsize',24,'fontname','times')
else
    title('Flexors','fontsize',24,'fontname','times')
end
```

6. Data Analysis and Results

Results for flexors and extensors were analysed by focusing on:

1. The values of the estimated parameters which are expected to vary in a physiologically realistic range.
2. Validation of the model and the estimated parameters by comparison of the RMSE and the NRMSE values obtained during both the estimation and the validation phase.
3. The comparison of static values of measured and estimated torques at each angle with those reported in the literature.
4. The operating range of the muscle fibres.

In what follows, the word ‘flexors’ means FCU, FCR and FDS as lumped together, unless specified otherwise, while the word ‘extensors’ is used as synonym of ECRL.

6.1 Estimated Values

As previously described, the musculotendon model needs the following musculoskeletal parameters to be known or estimated: the optimal physiological muscle length, $L_{oM}(t)$; the maximum isometric muscle force, F_{oM} ; the tendon slack length, L_{TS} ; the coefficient A as in equation (4); the moment arm, $MA(\theta)$; the musculotendon length change, $\Delta L_{MT}(\theta)$.

As expected, the quality of recorded EMG signals was different from subject to subject due to the large number of aspects that may influence these measurements¹¹. In the case of flexors, data from three subjects (3, 6 and 11) did not show any significant variation between phases at rest and during contractions and thus were neglected. Among the other nine subjects, only two (subject 7 and 12) showed a low firing level at rest, while the EMGs of the remaining seven subjects were characterised by a high firing level (up to half of its range, i.e. circa 0.5) when no contractions occurred. In the case of extensors, data from two subjects (5 and 11) were neglected for the same reason, while all of the remaining ten subjects showed high firing level at rest. In order not to obtain a biased estimate for the subjects with high firing level at rest, the above parameters were estimated by exclusively using data in correspondence of the contraction phases, while a flexible value of the recorded EMG was used as a threshold to distinguish rest from contraction phases: EMG values above the threshold meant contraction. For this reason, at each position in the range $[-30^\circ, \dots, +30^\circ]$ rest phases were cropped and only data in correspondence of the contractions were used for the estimation. The threshold value was set by the function `DataIntervalSelection.m` as specified in the section “5.1.2 Parameter Initialisation”.

Table 2 lists the estimated values for flexors and extensors – average over the six positions in the range $[-30^\circ, \dots, +30^\circ]$ (without measurements at 0°) with standard deviation (SD) – of the first four of the above parameters for each subject and compare them to values of the corresponding parameters as listed in (Garner and Pandy, 2001; Holzbaur et al., 2005). More specifically, since the flexor electrodes were positioned equidistant from the motor point FCU, FCR and FDS, it was assumed that the recorded EMG represented the summative signal coming from these three muscles. Hence, values of L_{oM} and L_{TS} from (Garner and Pandy, 2001; Holzbaur et al., 2005) reported in Table 2 represent the average over those listed therein, while the F_{oM} values represent the sum of the corresponding quantities listed in the same works. In particular, values of L_{oM} and

¹¹ Recording EMGs is not a trivial task. For example, subject concentration might affect the outcome of the measurements. See (Merletti and Parker, 2004) for far more details on this topic.

L_{TS} referred to (Holzbaur et al., 2005) are averages over values for FCU, FCR, and FDS, while values of F_{OM} represent the sum for the same muscles. At the same time, values of L_{OM} and L_{TS} referred to (Garner and Pandey, 2001) are averages over values for FCU and FCR, while values of F_{OM} represent the sum for the same muscles. For extensors, instead, values for ECRL as reported in the same references were used. Finally, values in (Holzbaur et al., 2005) were used as initial estimates for the corresponding parameters during the optimisation process.

Figure 22, Figure 23 and Figure 24 respectively show values of L_{OM} , F_{OM} and L_{TS} as in Table 2 in a chart format. For flexors, individual average estimated values for L_{OM} ranged from 5.99 cm to 9.96 cm, for F_{OM} from 339.99 N to 899.38 N, for L_{TS} from 19.47 cm to 25.73 cm. For extensors, individual average estimated values for L_{OM} ranged from 7.74 cm to 11.89 cm, for F_{OM} from 340.56 N to 1032.60 N, for L_{TS} from 22.13 cm to 22.26 cm.

The estimated values of the parameter A , constrained to vary between -3 and 0 as in (Buchanan et al., 2004), ranged from -2.11 to 0 for flexors (mean -0.56, SD ± 0.52) and from -0.35 to 0 for extensors (mean -0.56, SD ± 0.41).

The estimated values of $\Delta L_{MT}(\theta)$ and $MA(\theta)$ for both flexors and extensors of the 12 subjects are listed in Table 3. As specified already, their estimation was constrained in the range $\pm 10\%$ with respect to values obtained from equations (11) and (12) as in (Lemay and Crago, 1996). Figure 28 and Figure 29 show the comparison between the values estimated and those calculated using these latter equations. In particular, Figure 28 compares reference and estimated values of muscle length changes at different angles for FCU and ECRL. Likewise, Figure 29 compares moment arm values at different angles for FCU and ECRL.

As already reported in section 5.1.2 *Parameter Initialisation*, the FCU and ECRL values given in (Lemay and Crago, 1996) were used to initialise both the parameters $\Delta L_{MT}(\theta)$ and $MA(\theta)$ for flexors and extensors, respectively. Moreover, it should be mentioned that the sign of the extensor values was changed for convenience with respect to the convention used in the cited paper.

In order to verify the consistency of the experiments, subject 2 performed the same experiments five times with 10 days interval. The average estimated values (\pm SD) for L_{OM} , F_{OM} and L_{TS} were respectively 9.56 (± 0.46) cm, 733.77 (± 49.19) N and 24.73 (± 0.30) cm for flexors and 10.70 (± 1.69) cm, 1032.6 (± 74.27) N and 22.20 (± 0.02) cm for extensors.

Table 2 – Estimated parameters L_{oM} , F_{oM} , L_{TS} , and A for the 12 subjects in comparison with data from the literature.

		Subject												(Holzbaur et al., 2005)	(Garner and Pandy, 2001)
		1	2	3	4	5	6	7	8	9	10	11	12		
FLEXORS															
L_{oM} [cm]	Mean	7.38	9.93		7.08	5.99		7.73	9.84	9.44	9.96		9.65	6.65*	4.54**
	±SD	1.66	0.71	BAD SIGNALS	2.08	2.34	BAD SIGNALS	1.16	0.27	1.36	0.10	BAD SIGNALS	0.85		
F_{oM} [N]	Mean	371.96	842.92	BAD SIGNALS	339.94	354.60	BAD SIGNALS	470.67	495.34	899.38	526.96	BAD SIGNALS	625.86	429.5†	929.63††
	±SD	27.09	129.93		20.09	162.99		161.42	110.27	416.28	56.39		130.92		
L_{TS} [cm]	Mean	24.76	25.19	BAD SIGNALS	19.47	24.31	BAD SIGNALS	25.72	25.43	24.15	25.42	BAD SIGNALS	25.73	29.08*	27.11**
	±SD	0.39	0.60		0.22	0.77		0.03	0.26	0.81	0.09		0.04		
A	Mean	-2.11	-0.31	BAD SIGNALS	-0.51	-1.17	BAD SIGNALS	0.00	-0.62	-0.03	-0.20	BAD SIGNALS	-0.04		
	±SD	0.75	0.79		0.99	1.26		0.00	0.66	0.08	0.27		0.10		
EXTENSORS															
L_{oM} [cm]	Mean	9.09	10.70	7.74	8.59		8.39	7.82	11.89	9.41	8.03		9.77	8.1‡	8.96‡
	±SD	2.60	1.69	0.81	1.16	BAD SIGNALS	2.83	1.12	6.20	4.22	1.31	BAD SIGNALS	3.06		
F_{oM} [N]	Mean	682.89	1032.60	378.35	340.56	BAD SIGNALS	684.84	442.19	793.37	688.74	804.52	BAD SIGNALS	797.25	304.9‡	268.42‡
	±SD	315.85	74.27	24.79	67.32		157.35	134.84	261.72	267.64	293.24		193.78		
L_{TS} [cm]	Mean	22.13	22.20	22.18	22.14	BAD SIGNALS	22.21	22.19	22.25	22.21	22.26	BAD SIGNALS	22.23	22.4‡	26.8‡
	±SD	0.06	0.02	0.02	0.02		0.02	0.04	0.04	0.03	0.03		0.03		
A	Mean	0.00	-0.07	0.00	-0.09	BAD SIGNALS	0.00	0.00	-0.12	-0.10	-0.51	BAD SIGNALS	-0.21		
	±SD	0.00	0.10	0.00	0.13		0.00	0.00	0.11	0.15	0.47		0.19		

* Average over values for Flexor Carpi Ulnaris (FCU), Flexor Carpi Radialis (FCR), and Flexor Digitorum Superficialis (FDS).

† Sum of values for Flexor Carpi Ulnaris (FCU), Flexor Carpi Radialis (FCR), and Flexor Digitorum Superficialis (FDS).

** Average over values for Flexor Carpi Ulnaris (FCU) and Flexor Carpi Radialis (FCR).

†† Sum of values for Flexor Carpi Ulnaris (FCU) and Flexor Carpi Radialis (FCR).

‡ Values for Extensor Carpi Radialis Longus (ECRL).

Optimal Physiological Muscle Length - L_{oM} [cm]

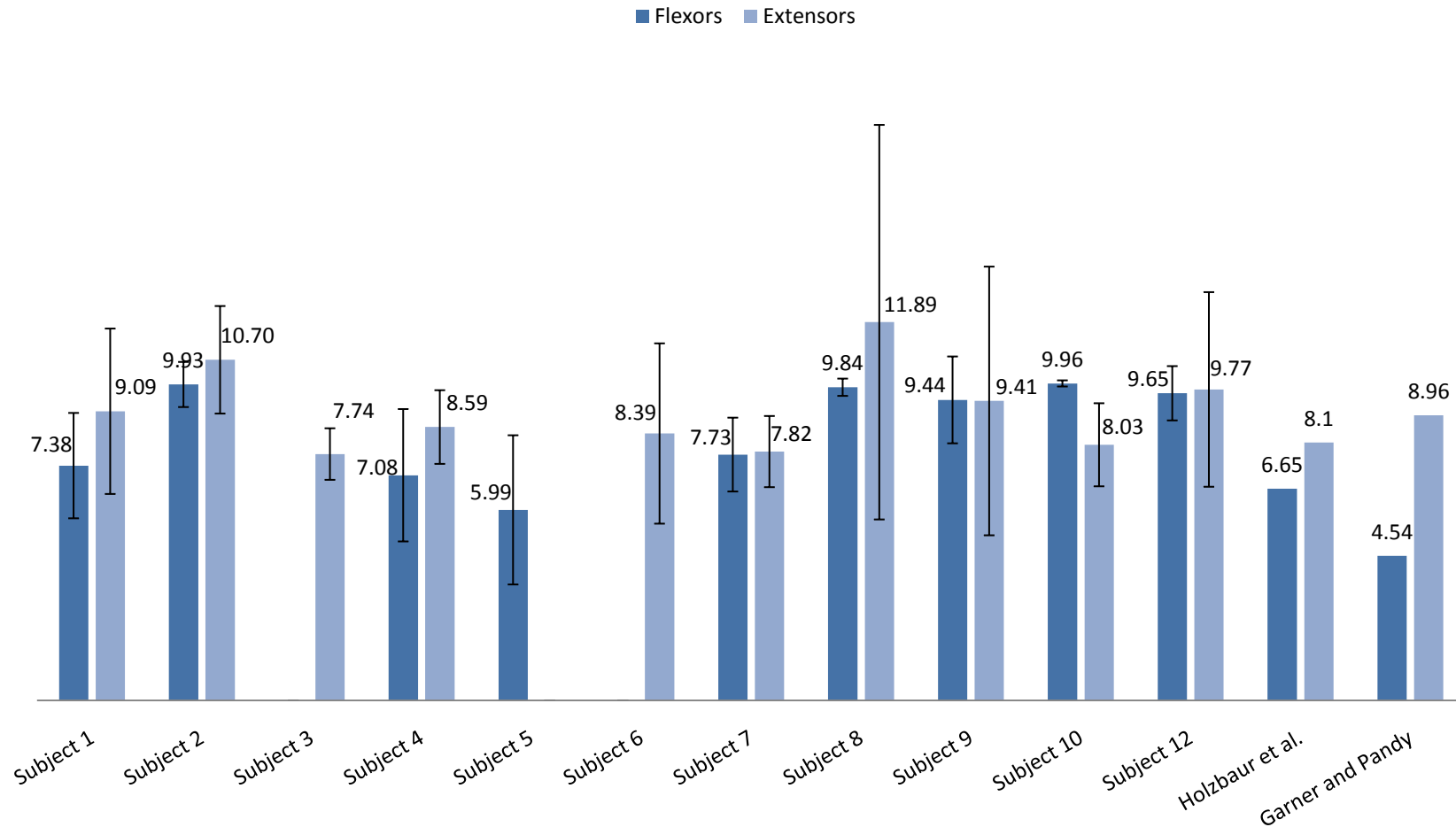


Figure 22 - L_{oM} comparison. Average estimated values (\pm SD) of flexors and extensors over each position for all of the subjects as in Table 2 compared to the L_{oM} values in (Garner and Pandey, 2001; Holzbaaur et al., 2005). Missing columns mean missing data.

Maximum Isometric Muscle Force - F_{oM} [N]

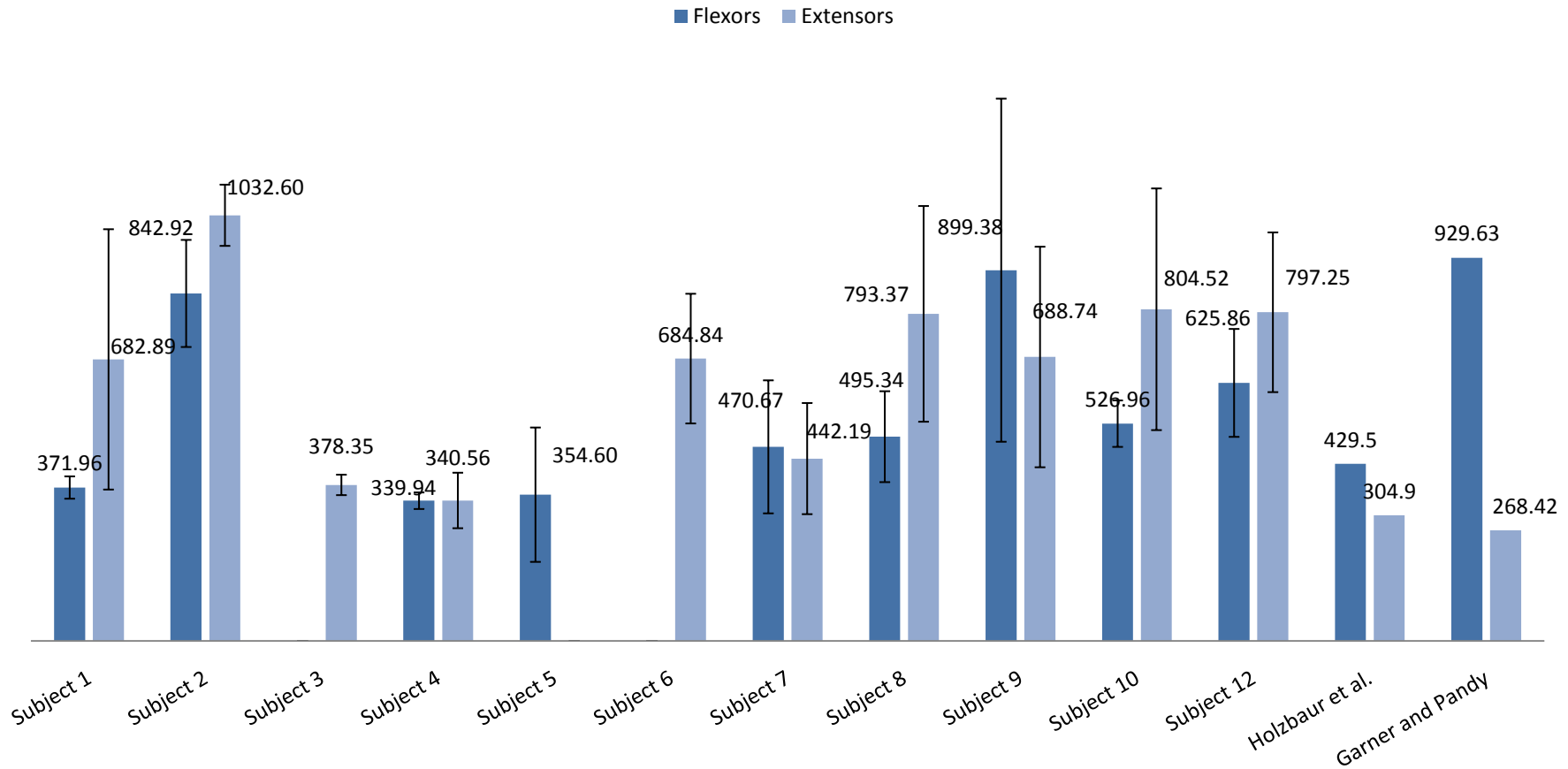


Figure 23 - F_{oM} comparison. Average estimated values (\pm SD) of flexors and extensors over each position for all of the subjects as in Table 2 compared to the F_{oM} values in (Garner and Pandey, 2001; Holzbaaur et al., 2005). Missing columns mean missing data.

Tendon Slack Length - L_{TS} [cm]

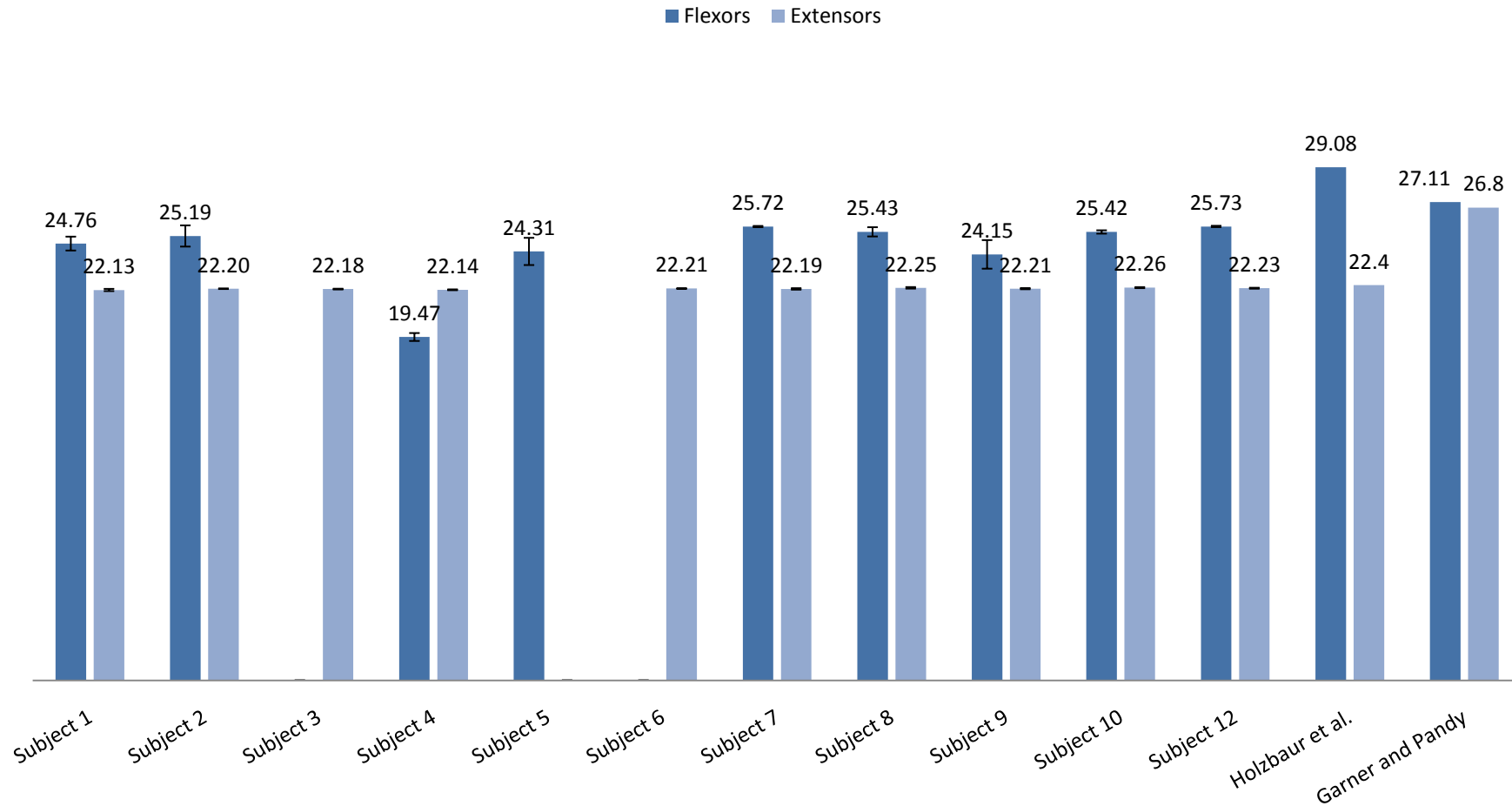


Figure 24 - L_{TS} comparison. Average estimated values (\pm SD) of flexors and extensors over each position for all of the subjects as in Table 2 compared to the L_{TS} values in (Garner and Pandy, 2001; Holzbaur et al., 2005). Missing columns mean missing data.

Optimal Physiological Muscle Length, L_{oM} [cm]

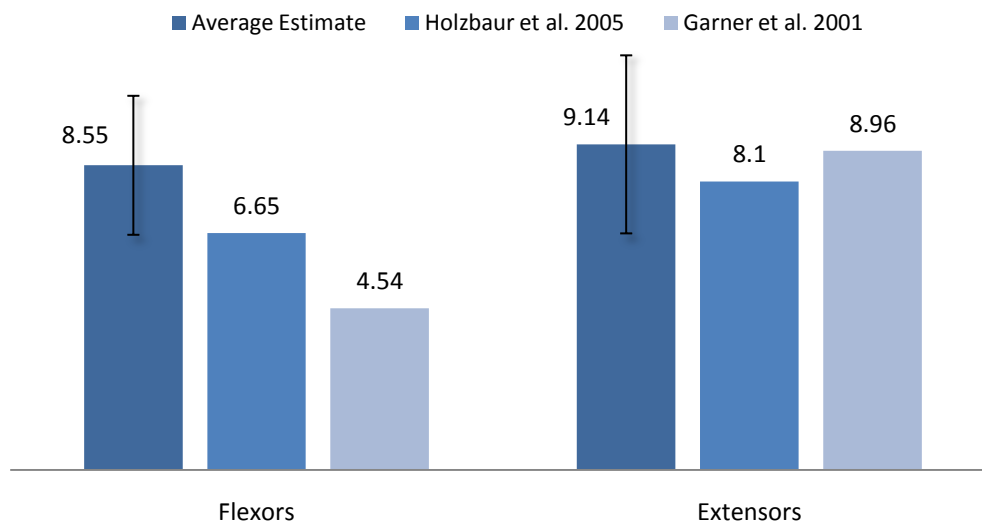


Figure 25 - L_{oM} comparison. Average estimated values (\pm SD) of L_{oM} compared to values in literature. The averages of the estimates were calculated over nine subjects for flexors and ten subjects for extensors (Table 2).

Maximum Isometric Muscle Force, F_{oM} [N]

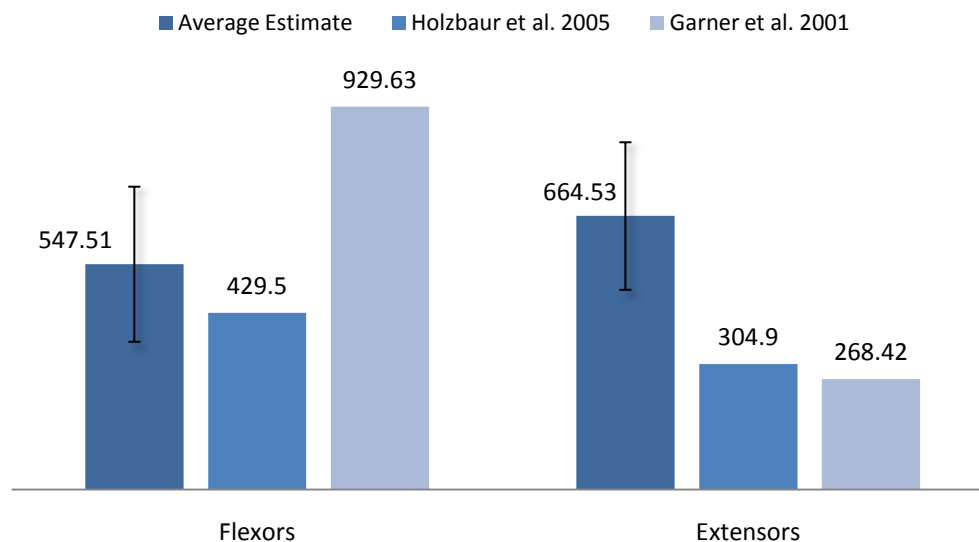


Figure 26 - F_{oM} comparison. Average estimated values (\pm SD) of F_{oM} compared to values in literature. The averages of the estimates were calculated over nine subjects for flexors and ten subjects for extensors (Table 2).

Tendon Slack Length, L_{TS} [cm]

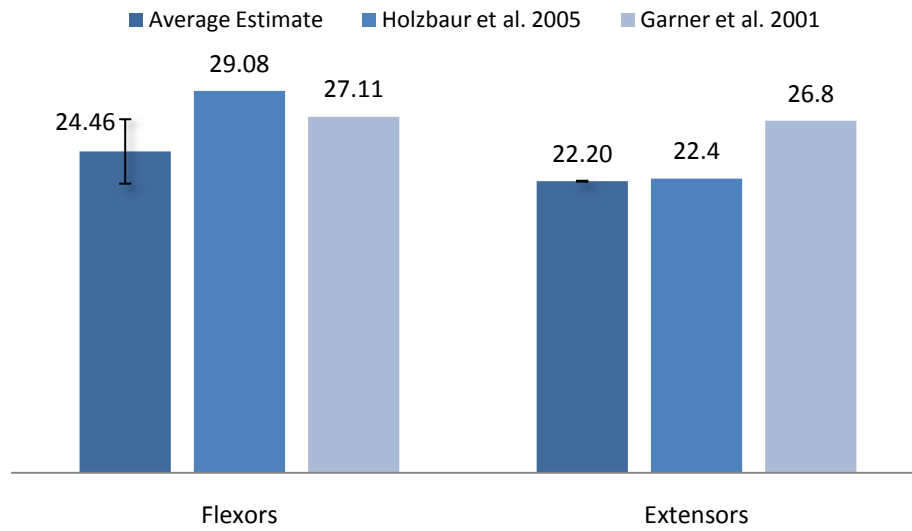


Figure 27 - L_{TS} comparison. Average estimated values (\pm SD) of L_{TS} compared to values in literature. The averages of the estimates were calculated over nine subjects for flexors and ten subjects for extensors (Table 2).

Table 3 –Estimated parameters ΔL_{MT} and MA for the 12 subjects.

Subject			Angles						Subject			Angles					
			-30°	-20°	-10°	+10°	+20°	+30°				-30°	-20°	-10°	+10°	+20°	+30°
1	ΔL_{MT} [cm]	Flex	-0.97	-1.41	-1.51	-2.25	-2.50	-2.89	7	ΔL_{MT} [cm]	Flex	-1.16	-1.50	-1.85	-2.56	-2.92	-3.28
		Ext	-0.89	-1.09	BAD	BAD	-1.84	-2.01			Ext	-0.89	-1.09	-1.29	-1.67	-1.84	-2.01
	MA [cm]	Flex	1.75	1.72	1.69	1.77	1.83	1.68		MA [cm]	Flex	1.50	1.60	1.67	2.10	2.08	2.05
		Ext	1.02	1.22	BAD	BAD	0.81	0.76			Ext	1.02	1.05	1.11	1.06	0.99	0.89
2	ΔL_{MT} [cm]	Flex	-1.00	-1.32	-1.53	-2.10	-2.38	-2.81	8	ΔL_{MT} [cm]	Flex	-1.17	-1.50	-1.73	-2.40	-2.57	-3.09
		Ext	-0.89	-1.09	-1.29	-1.67	-1.84	-2.01			Ext	-0.89	-1.09	-1.29	-1.67	-1.84	-2.01
	MA [cm]	Flex	1.77	1.96	2.02	2.05	2.05	2.02		MA [cm]	Flex	1.76	1.87	1.95	1.72	2.03	1.80
		Ext	1.25	1.22	1.05	1.05	0.97	0.93			Ext	1.04	1.19	0.96	1.06	0.99	0.88
3	ΔL_{MT} [cm]	Flex	BAD SIGNALS						9	ΔL_{MT} [cm]	Flex	-1.11	-1.32	-1.74	-2.56	Flex	-3.28
		Ext	-0.89	-1.09	-1.29	-1.84	-1.84	-2.01			Ext	-0.89	-1.09	-1.29	-1.67	-1.84	-2.01
	MA [cm]	Flex	BAD SIGNALS							MA [cm]	Flex	1.44	1.84	1.88	1.78	Flex	1.80
		Ext	1.02	1.20	1.08	0.92	0.87	0.76			Ext	1.02	1.18	0.96	0.87	0.81	0.76
4	ΔL_{MT} [cm]	Flex	BAD	-1.50	-1.62	-2.56	BAD	-3.29	10	ΔL_{MT} [cm]	Flex	-1.10	-1.41	-1.73	-2.09	-2.44	-2.59
		Ext	-0.72	-0.89	-1.29	-1.67	-1.84	-2.01			Ext	-0.88	-1.09	-1.29	-1.70	-1.34	-2.00
	MA [cm]	Flex	BAD	1.60	1.74	1.85	BAD	1.93		MA [cm]	Flex	1.84	1.96	1.92	2.10	2.03	2.06
		Ext	1.24	1.00	1.11	0.87	0.81	0.92			Ext	1.00	1.00	1.18	0.90	0.81	0.80
5	ΔL_{MT} [cm]	Flex	-0.89	-1.09	-1.29	-1.67	-1.84	-2.01	11	ΔL_{MT} [cm]	Flex	BAD SIGNALS					
		Ext	BAD SIGNALS								Ext						
	MA [cm]	Flex	1.02	1.22	1.15	0.87	0.91	0.76		MA [cm]	Flex						
		Ext	BAD SIGNALS								Ext						
6	ΔL_{MT} [cm]	Flex	BAD SIGNALS						12	ΔL_{MT} [cm]	Flex	-1.17	-1.50	-1.85	-2.56	Flex	-3.28
		Ext	-0.89	-1.09	-1.29	-1.67	-1.84	-2.01			Ext	-0.89	-1.09	-1.29	-1.67	-1.84	-2.01
	MA [cm]	Flex	BAD SIGNALS							MA [cm]	Flex	1.50	1.60	1.67	1.72	Flex	1.68
		Ext	1.02	1.22	1.15	0.87	0.91	0.76			Ext	1.25	1.22	0.96	0.87	0.81	0.89

Muscle Length Change [cm]

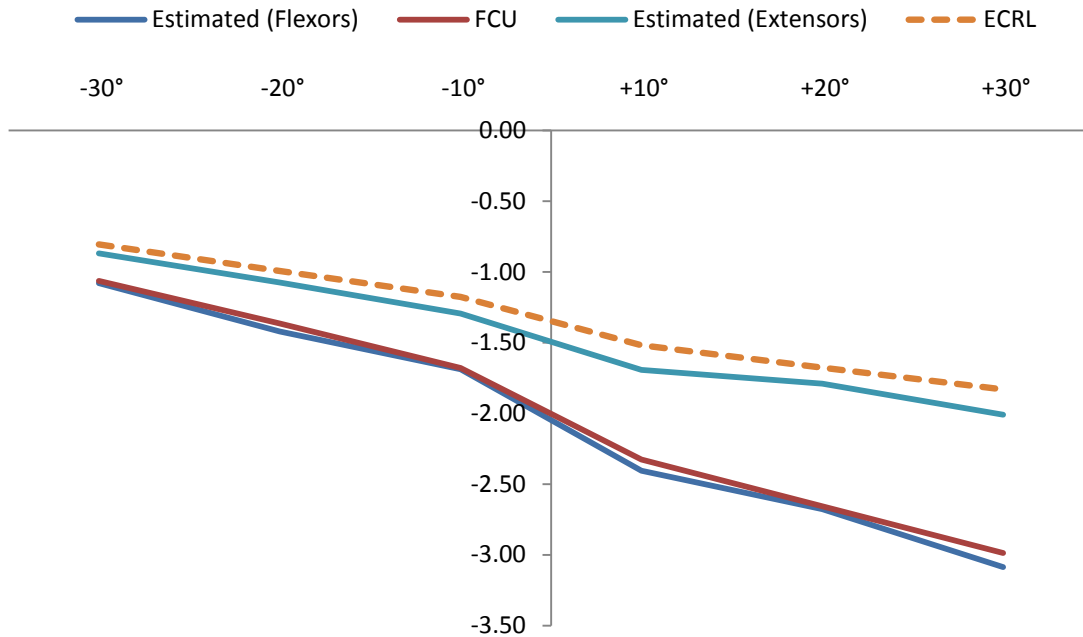


Figure 28 – Muscle length change $\Delta L_{MT}(\theta)$ as a function of the wrist angle. The figure shows the comparison between the values obtained from equations (11) and (12) as in (Lemay and Crago, 1996) for FCU and ECRL and the correspondent estimates. The sign of extensor values have been changed with respect to (Lemay and Crago, 1996).

Moment Arm [cm]

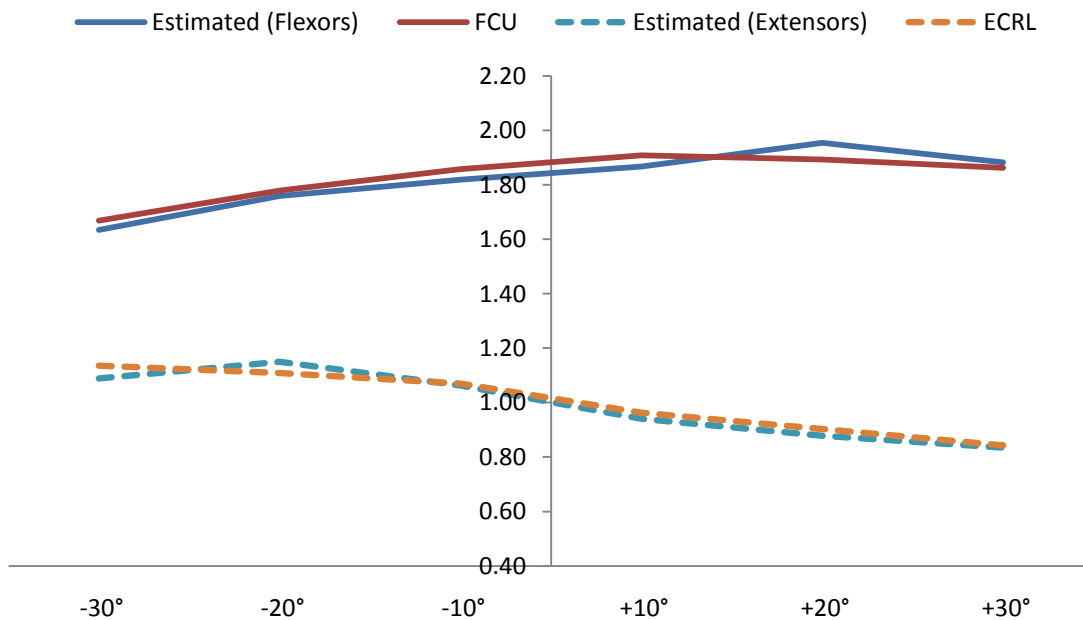


Figure 29 – Moment arm $MA(\theta)$ as a function of the wrist angle. The figure shows the comparison between the values obtained from equations (11) and (12) as in (Lemay and Crago, 1996) for FCU and ECRL and the correspondent estimates. The sign of extensor values have been changed with respect to (Lemay and Crago, 1996).

6.2 Model Validation

Once the six parameters were estimated for each muscle group, the validation phase was carried out according to the algorithm schematically shown in Figure 30. Both the estimated parameters and the EMG signals recorded with the hand positioned at 0° were used as input to the model implemented in Simulink (enched in the dashed rectangle in Figure 30), while the predicted joint moments were compared to the moments exerted by the limb and measured by means of the strain gauge load cell at the same position.

In order to quantify the goodness of the validation phase, the RMSE and the normalised RMSE (NRMSE) computed during both the estimation and validation phases between calculated and measured joint moments were compared.

The formula used to compute the RMSE was as in (26), while the NRMSE was calculated as

$$NRMSE = \frac{RMSE}{\max(M_{meas}(i))} \cdot 100 \quad (27)$$

where the denominator represents the maximum value of the measured torque in the same trial.

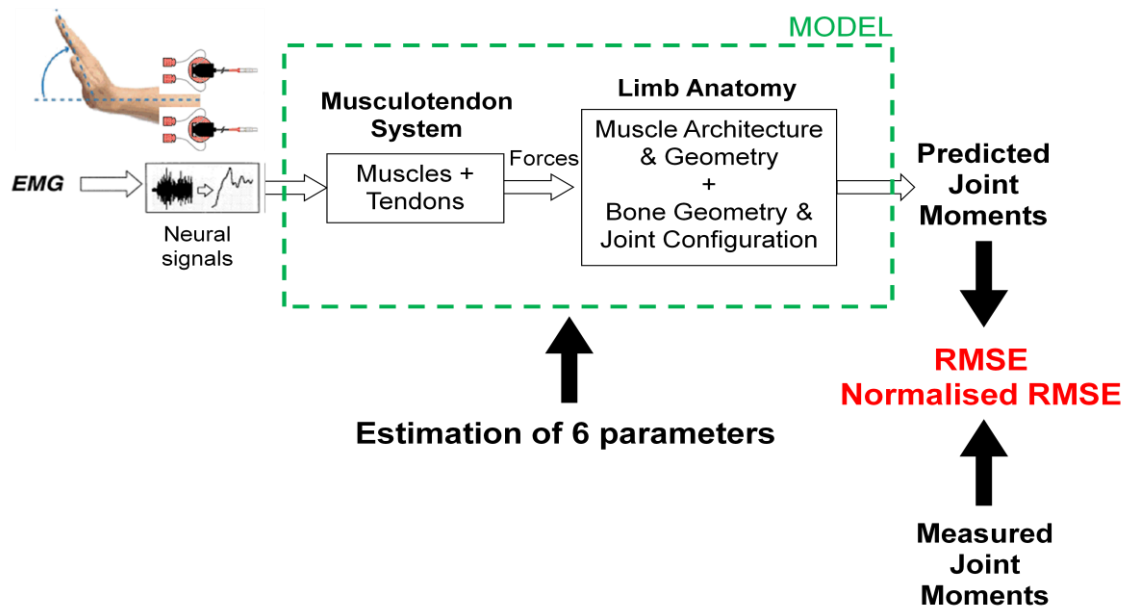


Figure 30 – Scheme of the validation process. EMGs and estimated parameters were used as input to the model, while measured and predicted torques were compared.

In order to show the outcome of the validation process for flexors and extensors, in Figure 31 and Figure 32 a comparison between joint moments calculated using the model and moments measured at 0° for subjects 8 and 12, respectively, is shown. Processed EMGs (lower curves) during the correspondent flexion and extension experiments are also shown. In Figure 31A as well as in Figure 32A, the EMGs of the flexors were used as input to the model, while the EMGs of the extensors were used as the input in Figure 31B and Figure 32B. The EMGs of the antagonists are plotted for

convenience only and were not involved at this stage of the work.¹² Appendix A contains the plots for all of the other subjects. As shown in the figures, predicted torques at rest were forced to be coincident with those measured. As for the estimation process, also in the validation phase a flexible value of the recorded EMG was used as a threshold to distinguish rest from contraction. This expedient ensured consistency of the RMSE and NRMSE calculation during both estimation and validation.

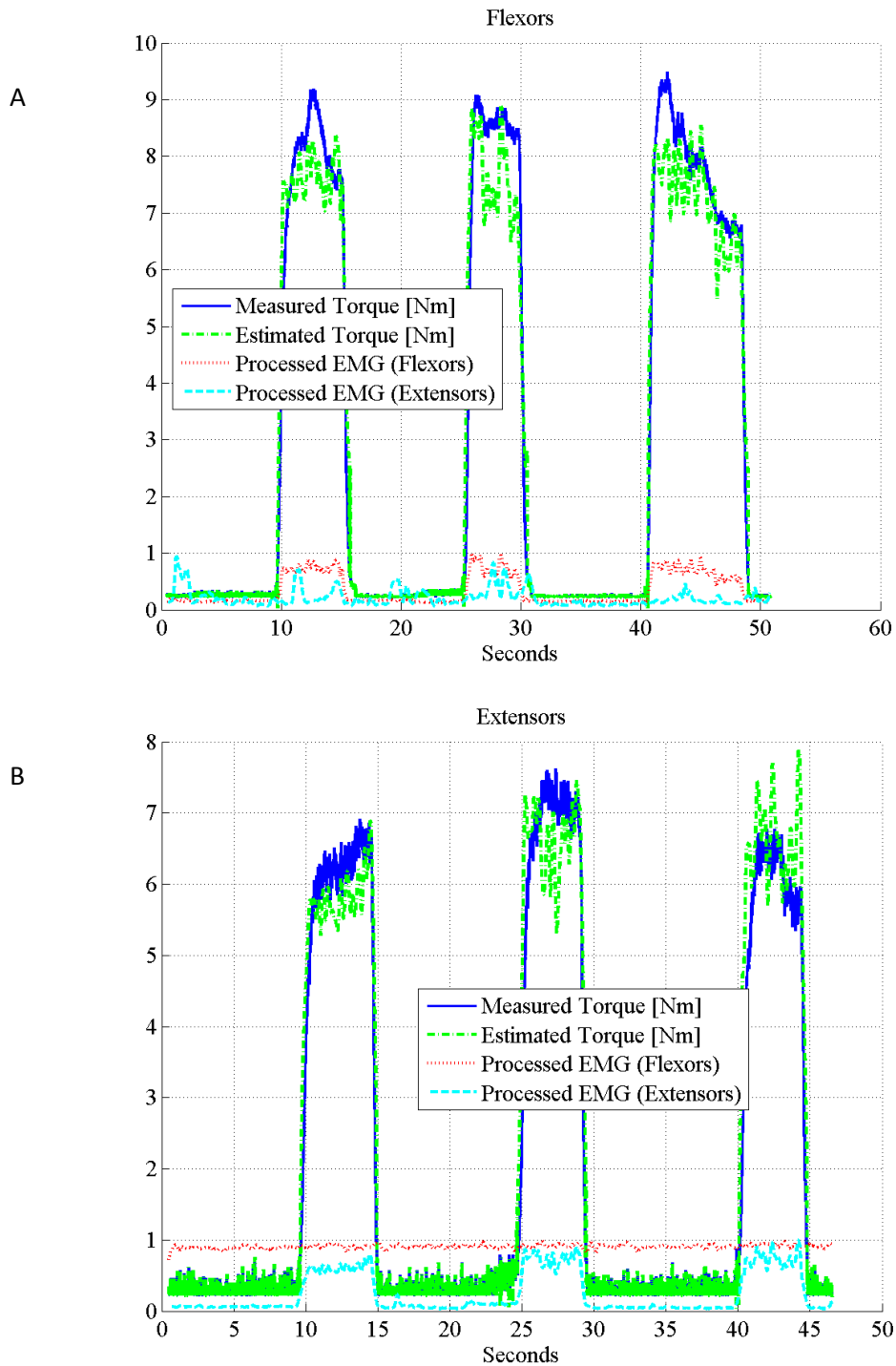


Figure 31 – Validation at 0°: Subject 8. A) Flexors; B) Extensors.

¹² A significant level of co-contraction for the antagonists could be assessed by means of equation (1) in (Delp et al., 1996). As a consequence, their influence could be taken into account.

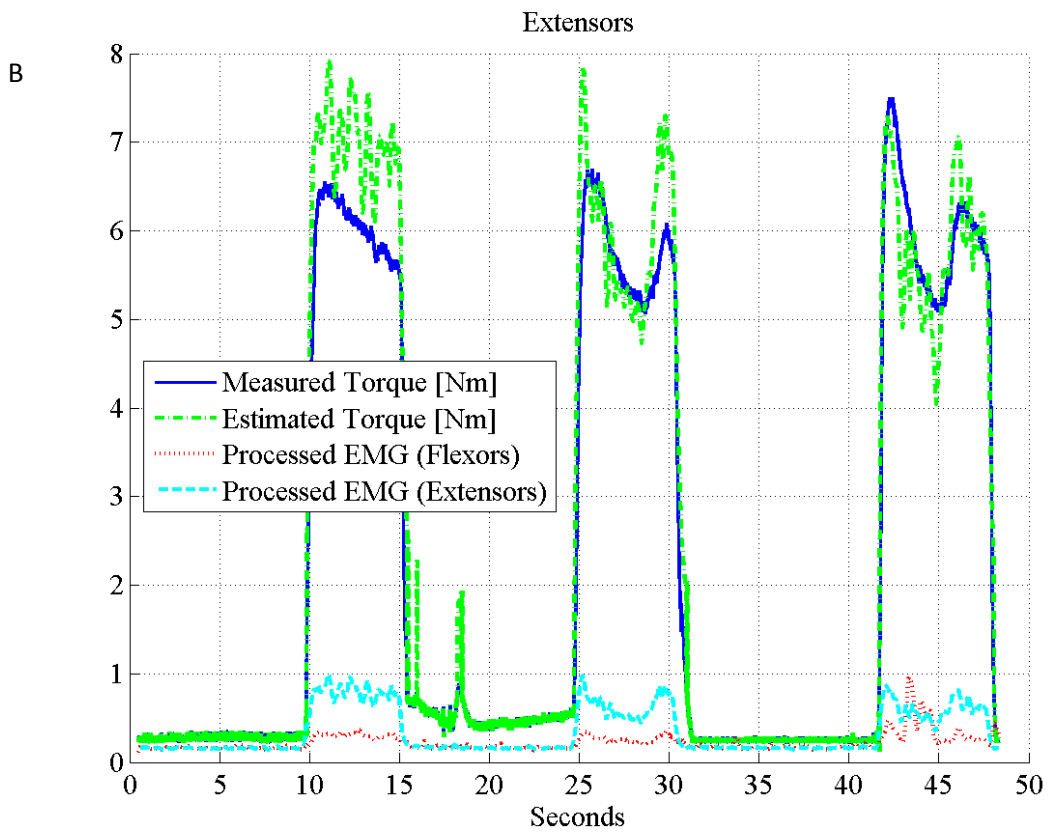
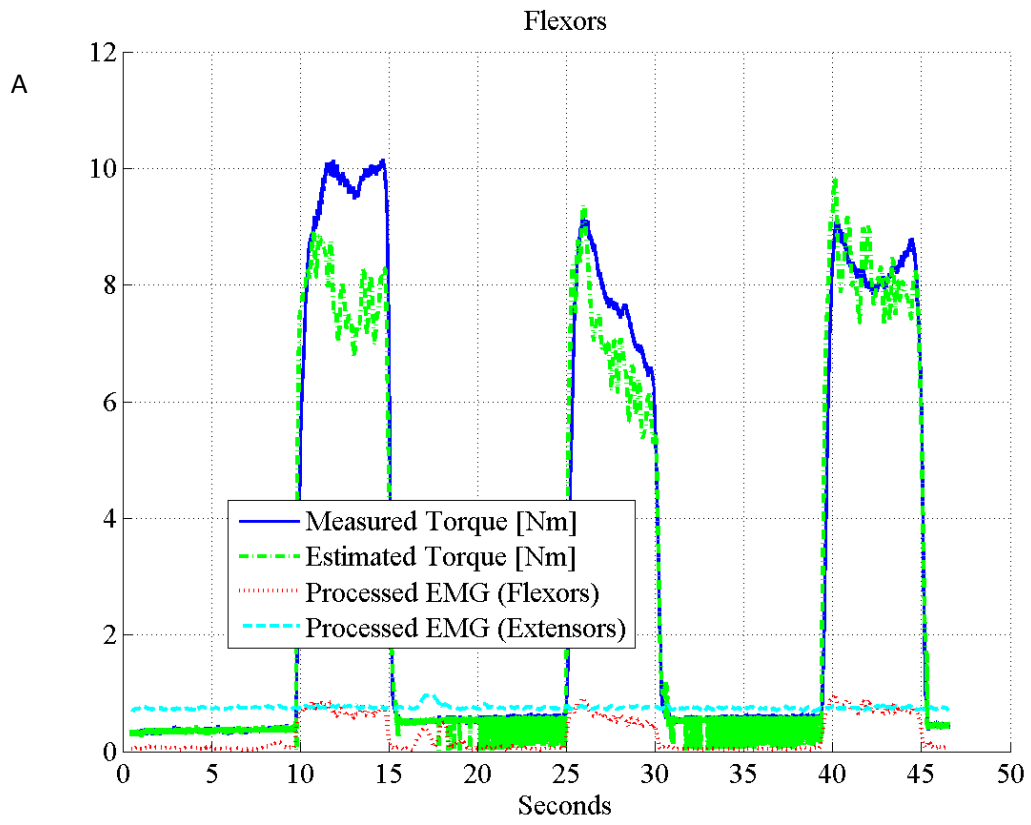


Figure 32 – Validation at 0°: Subject 12. A) Flexors; B) Extensors.

The time plots relative to subject 8 (Figure 31) and subject 12 (Figure 32) were selected as samples of the goodness of the validation process, as their RMSE and NRMSE values obtained during estimation and validation were representative of the average value for the same quantities as listed in Table 4 (for flexors) and Table 5 (for extensors). For flexors, RMSE values during estimation and validation ranged from 0.35 N to 1.30 N and from 0.44 N to 1.80 N, respectively, while NRMSE values ranged from 4.71% to 12.49% and from 6.12% to 17.07%, respectively. For extensors, RMSE values during estimation and validation ranged from 0.16 N to 0.56 N and from 0.23 N to 0.70 N, respectively, while NRMSE values ranged from 4.68% to 8.24% and from 5.40% to 11.32%, respectively.

As for values in Table 2, values of the estimation phase were calculated as an average of the values computed over six positions in the range [-30°, ..., +30°], with the exclusion of measurements at 0°. Figure 33 to Figure 36 show the same values as in Table 4 and Table 5 in a column chart format.

Table 4 – Flexors. Comparison between RMSE and NRMSE during estimation and validation.

Subject		Estimation		Validation	
		RMSE [N]	NRMSE [%]	RMSE [N]	NRMSE [%]
1	Mean	0.72	10.60%	1.08	16.43%
	±SD	0.27	3.51%		
2	Mean	0.86	6.00%	1.52	9.74%
	±SD	0.11	0.27%		
3	Mean	BAD SIGNALS		BAD SIGNALS	
	±SD	BAD SIGNALS		BAD SIGNALS	
4	Mean	0.61	12.49%	0.56	11.65%
	±SD	0.06	0.75%		
5	Mean	0.44	9.21%	0.44	8.99%
	±SD	0.19	1.43%		
6	Mean	BAD SIGNALS		BAD SIGNALS	
	±SD	BAD SIGNALS		BAD SIGNALS	
7	Mean	0.35	4.71%	0.58	7.66%
	±SD	0.09	0.87%		
8	Mean	0.88	9.42%	0.65	7.00%
	±SD	0.27	2.10%		
9	Mean	1.30	10.23%	1.80	17.07%
	±SD	0.26	1.30%		
10	Mean	0.81	7.99%	0.59	6.12%
	±SD	0.15	1.64%		
11	Mean	BAD SIGNALS		BAD SIGNALS	
	±SD	BAD SIGNALS		BAD SIGNALS	
12	Mean	0.72	8.18%	0.85	8.56%
	±SD	0.16	3.11%		

Table 5 – Extensors. Comparison between RMSE and NRMSE during estimation and validation.

Subject		Estimation		Validation	
		RMS [N]	NRMS [%]	RMS [N]	NRMS [%]
1	Mean	0.49	8.24%	0.67	11.32%
	±SD	0.12	1.67%		
2	Mean	0.56	5.96%	0.59	5.40%
	±SD	0.13	0.59%		
3	Mean	0.16	4.68%	0.34	8.70%
	±SD	0.03	0.41%		
4	Mean	0.20	6.27%	0.23	7.22%
	±SD	0.02	0.51%		
5	Mean	BAD SIGNALS		BAD SIGNALS	
	±SD	BAD SIGNALS		BAD SIGNALS	
6	Mean	0.46	7.36%	0.70	9.62%
	±SD	0.04	0.48%		
7	Mean	0.34	6.96%	0.51	9.01%
	±SD	0.03	0.81%		
8	Mean	0.42	6.31%	0.52	7.00%
	±SD	0.13	2.58%		
9	Mean	0.40	7.23%	0.43	6.78%
	±SD	0.09	1.19%		
10	Mean	0.46	6.34%	0.41	5.76%
	±SD	0.14	1.19%		
11	Mean	BAD SIGNALS		BAD SIGNALS	
	±SD	BAD SIGNALS		BAD SIGNALS	
12	Mean	0.40	5.71%	0.53	7.23%
	±SD	0.07	0.72%		

Flexors - RMSE [N]

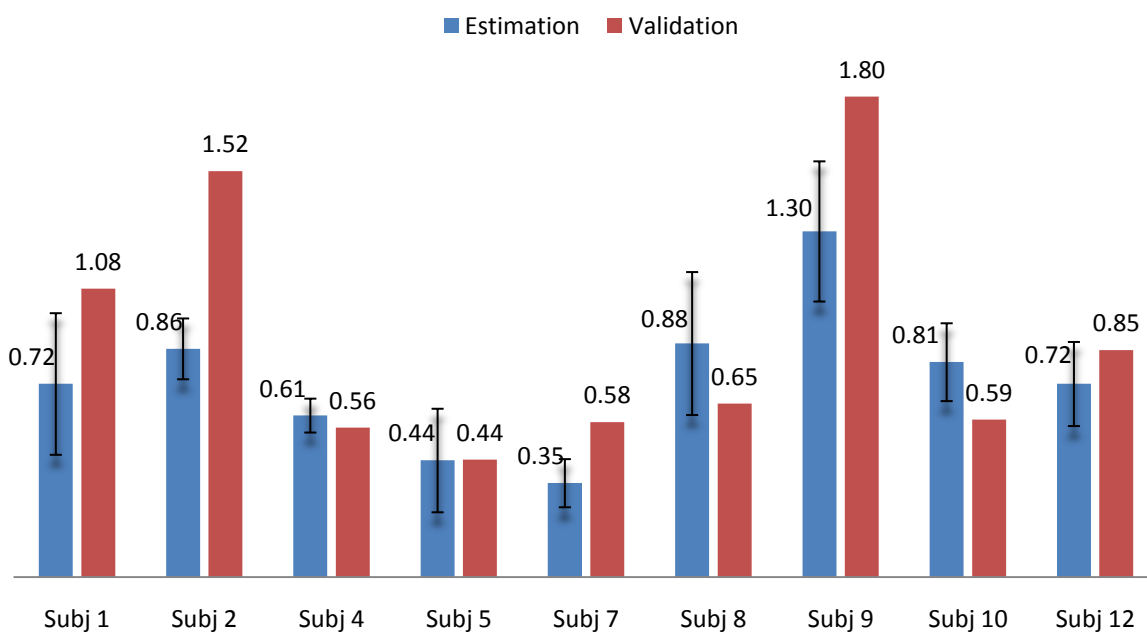


Figure 33 – Flexors. Comparison between RMSE values during estimation and validation.

Flexors - Normalised RMSE [%]

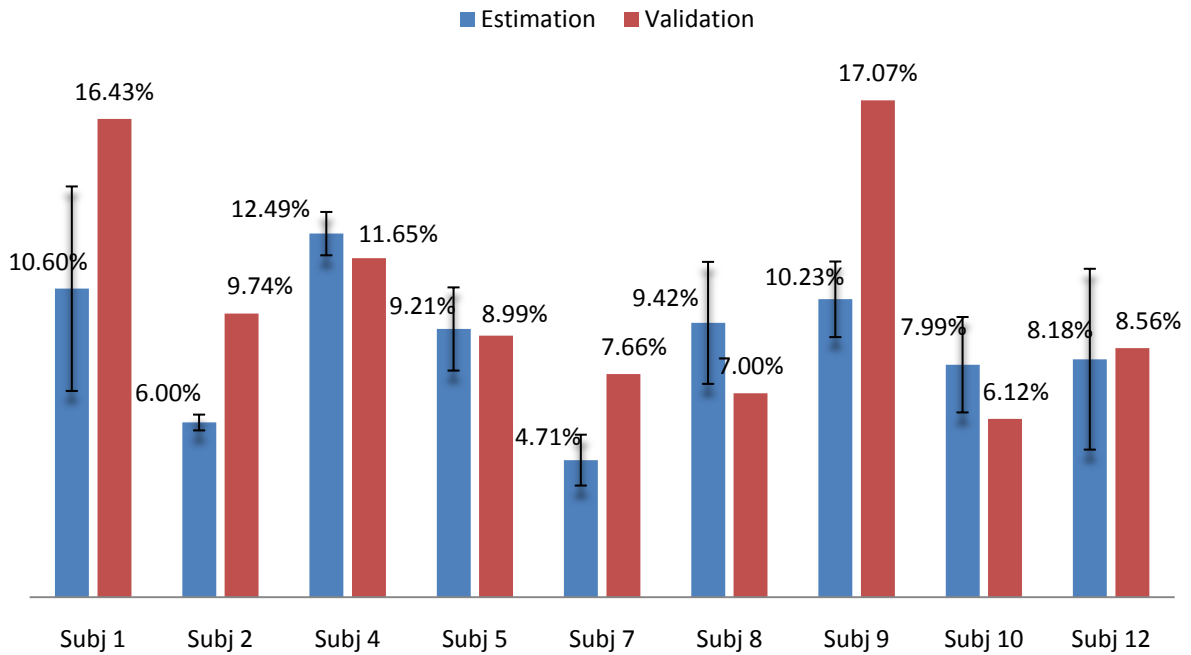


Figure 34 – Flexors. Comparison between NRMSE values during estimation and validation.

Extensors - RMSE [N]

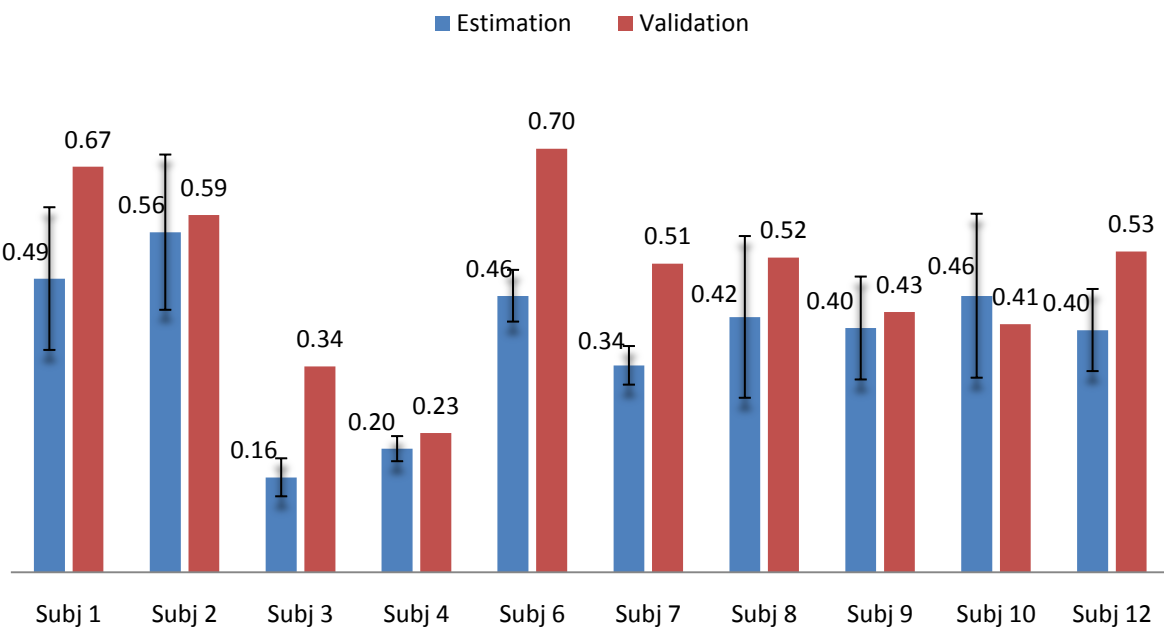


Figure 35 – Extensors. Comparison between RMSE values during estimation and validation.

Extensors -Normalised RMSE [%]

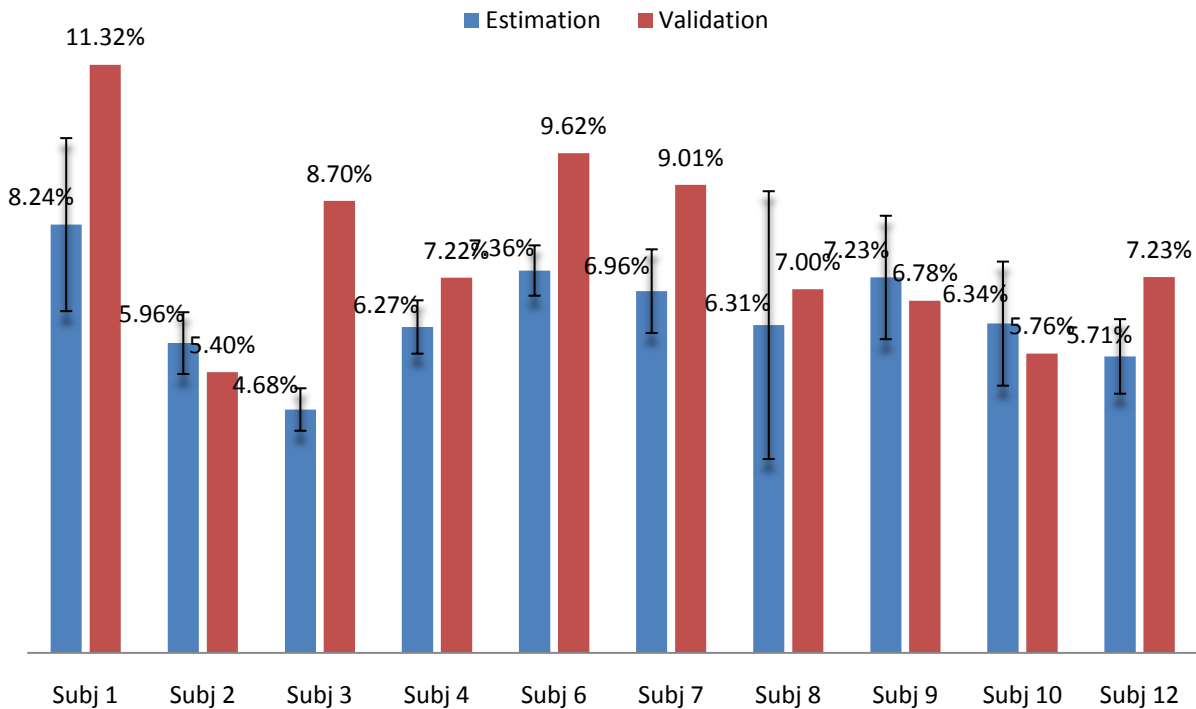


Figure 36 – Extensors. Comparison between NRMSE values during estimation and validation.

6.3 Static Values

Figure 37 and Figure 38 show a comparison between calculated and measured average moments for flexors and extensors, respectively. Particularly, average torques relative to the present work are plotted together with those from (Delp et al., 1996; Garner and Pandey, 2001; Gonzalez et al., 1997). It must be specified that the wrist as modelled in the work from Gonzalez et al. (1997) reproduced recorded data as reported in (Delp et al., 1996), while the wrist as modelled in (Garner and Pandey, 2001) was compared in the same work to measurements carried out during the same study. It is worth mentioning that the cited works were chosen as a term of comparison firstly because data were available and secondarily they contain and cross-reference data from several other sources. However, other works will be also involved for the comparison in the discussion section.

With regard to the data of the present study, for each trial at a specific position, an average value of estimated and recorded moments for a single subject was calculated over the three peak values in correspondence of the three contractions. Error bars in the same figures represent the correspondent SD. For flexors, highest individual average measured moments ranged from 6.25 Nm to 15.95 Nm and occurred between -30° and $+30^\circ$, while highest individual average calculated moments ranged from 5.72 Nm to 14.73 Nm and also occurred within the same range. The highest overall average moments computed over nine subjects were equal to 9.13 Nm and 8.67 Nm for the measured and the predicted torque, respectively, and both occurred at -30° . For extensors, highest individual average measured moments ranged from 2.71 Nm to 10.96 Nm and occurred between -10° and $+30^\circ$, while highest individual average calculated moments ranged from 3.61 Nm to 11.51 Nm and occurred within the range -20° and $+30^\circ$. In this other case, the highest overall average

moments calculated over ten subjects were equal to 6.38 Nm and 6.43 Nm for measured and predicted torque, respectively, and both occurred at +10°. Anyway, it should be noted that during flexor experiments the majority of the highest peaks occurred mainly in extended positions, while during extensor experiments they mainly occurred in flexed positions. Values for each subject at each position are listed in Appendix B.

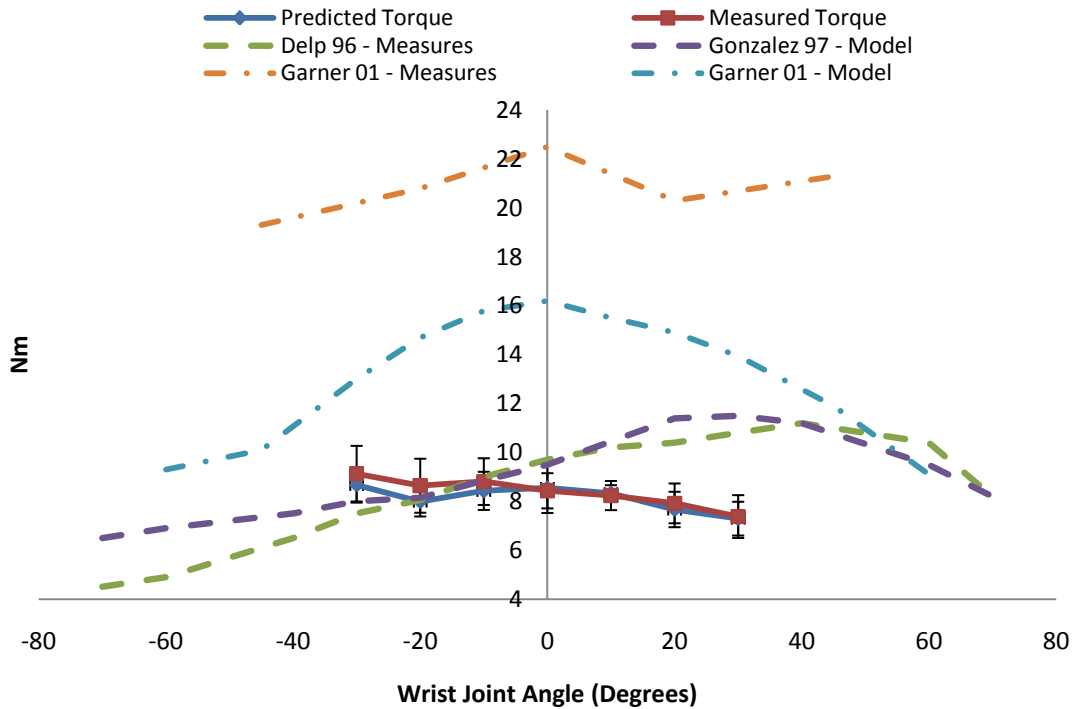


Figure 37 – Flexor torques vs. wrist joint angles. Solid lines represent average (\pm SD) maximum isometric measured and calculated moments in the present study. Each point represents the average over nine subjects. Measured values from (Delp et al., 1996) were averaged over ten subjects. Measured values from (Garner and Panday, 2001) were averaged over three subjects. Flexion angles are positive, extension angles are negative.

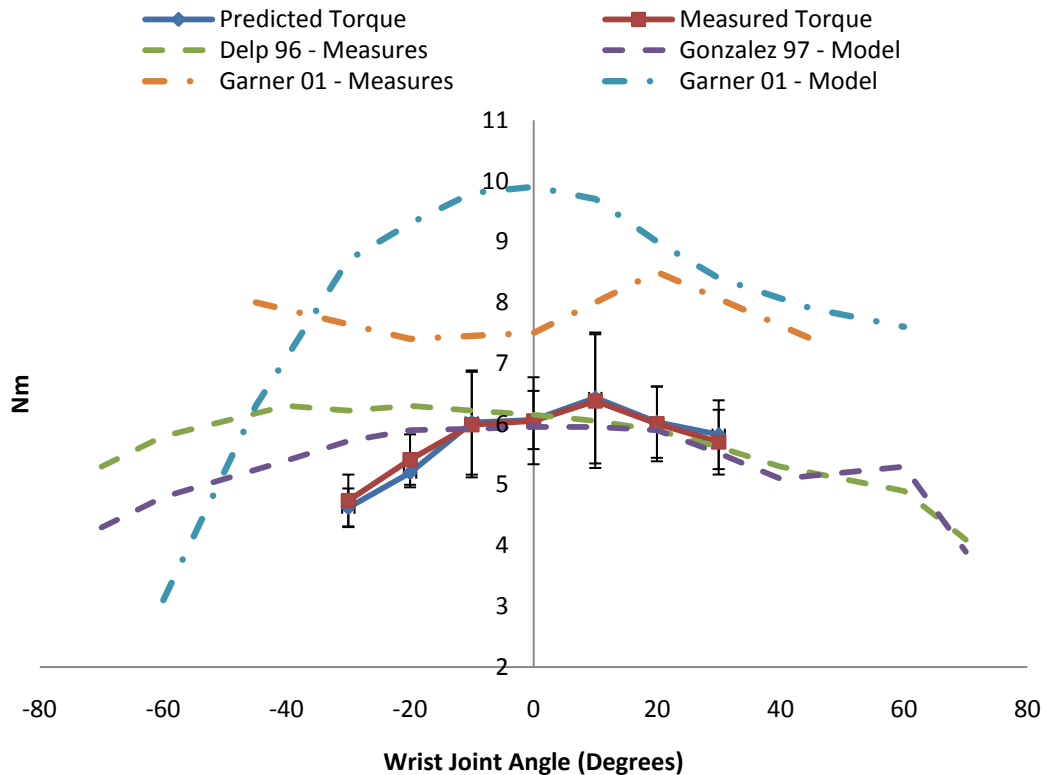


Figure 38 – Extensor torques vs. wrist joint angles. Solid lines represent average (\pm SD) maximum isometric measured and calculated moments in the present study. Each point represents the average over nine subjects. Measured values from (Delp et al., 1996) were averaged over ten subjects. Measured values from (Garner and Pandy, 2001) were averaged over three subjects. Flexion angles are positive, extension angles are negative.

Figure 39 and Figure 40 show average *MA* values together with average estimated forces at each position for flexors and extensors, respectively. In both plots, the *MA* curve refers to the average *MA* values estimated at each position for all of the subjects (Table 6). In the same figures, the Estimated Force I and II curves were respectively calculated as the ratio of average moment values of the predicted and measured torques (Figure 37 and Figure 38) to the average estimated *MA* values. As shown in Figure 39, for flexors the highest average forces were equal to 454.54 N and 558.75 N and both occurred at -30° . For extensors, instead, the highest average forces were equal to 697.49 N and 682.83 N and both occurred at $+30^\circ$. As for the moments, the highest peaks were mainly found in extension during flexor experiments and in flexion during extensor experiments. Values of forces for each subject at each position are listed in Appendix B.

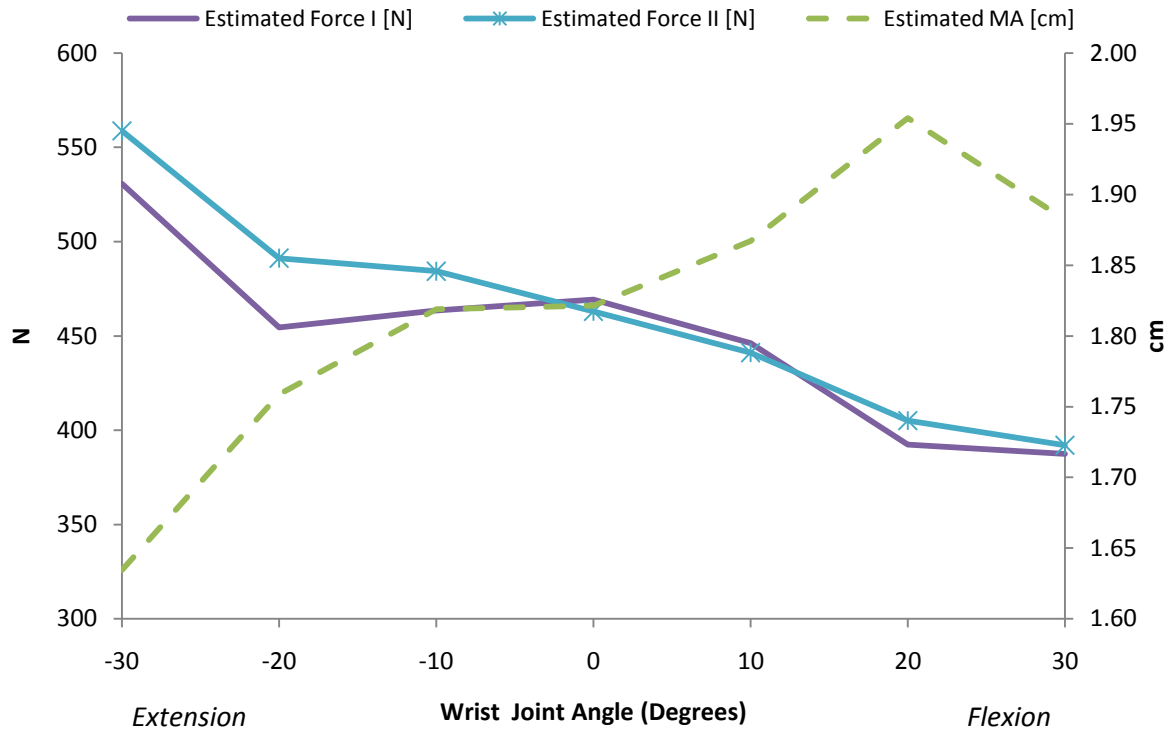


Figure 39 – Flexors. Average maximum calculated force and MAs vs. wrist joint angle. Flexion angles are positive, extension angles are negative. Average calculated over nine subjects.

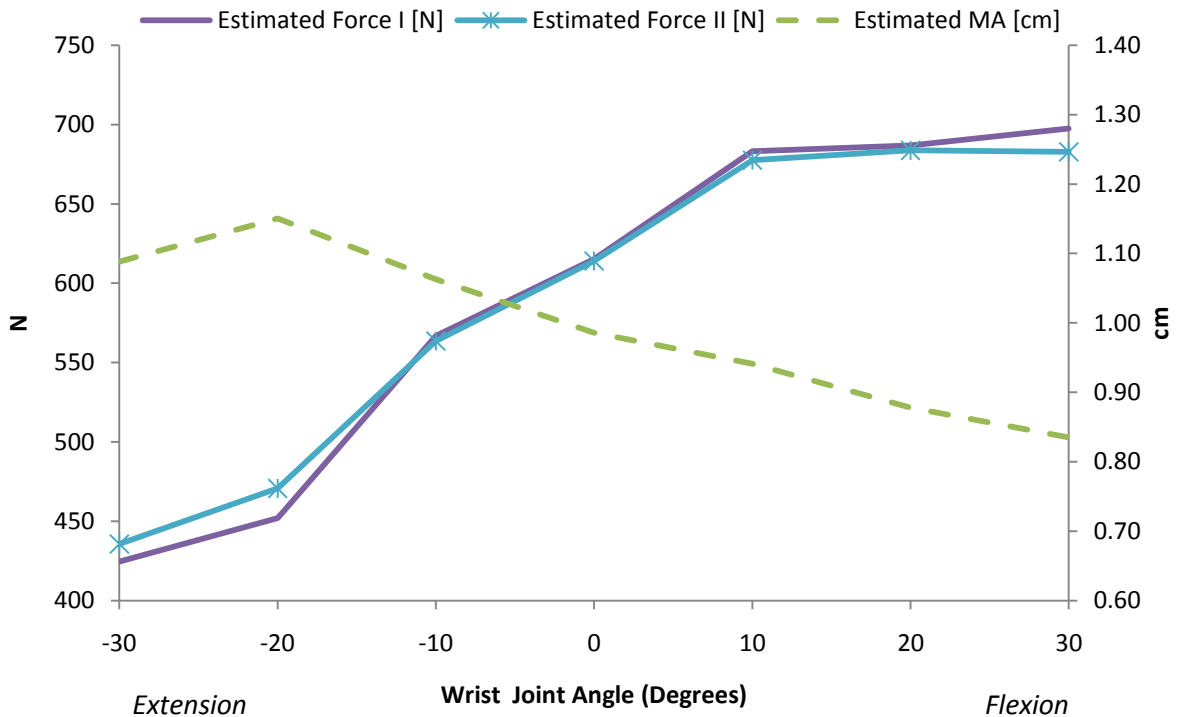


Figure 40 – Extensors. Average maximum calculated force and MAs vs. wrist joint angle. Flexion angles are positive, extension angles are negative. Average calculated over ten subjects.

Table 6 – Moment Arms and Forces.

	Angles (Degrees)						
	-30°	-20°	-10°	0°	10°	20°	30°
	Predicted Moment Arm* [cm]						
Flexors	1.63	1.76	1.82	1.82	1.87	1.95	1.88
Extensors	1.09	1.15	1.06	0.99	0.94	0.88	0.84
	Estimated Force I [N]						
Flexors	530.68	454.54	463.47	469.65	446.19	392.38	387.48
Extensors	424.69	452.14	566.87	615.22	683.12	686.79	697.49
	Estimated Force II [N]						
Flexors	558.75	491.24	484.30	463.42	441.19	405.17	392.02
Extensors	435.71	470.75	563.63	614.01	677.57	683.71	682.83

*Averages from Table 3.

6.4 Operating range of Muscle Fibres

Figure 41 shows the mean operating range of the wrist flexors and extensors on the isometric normalised force-length curve. The two diamond markers on the figure enclose the average operating range of wrist flexors, while the two triangle markers define the operating range of wrist extensors. Both the ranges were calculated by averaging the extreme values computed for each subject in the whole range of motion $\pm 30^\circ$. The operating ranges of FCU, FCR and ECRL muscles as reported in (Loren et al., 1996) and (Gonzalez et al., 1997) are adapted and overlapped on the same figure for comparison.

Plots and coordinates of the operating ranges for each subject are shown in Appendix C.

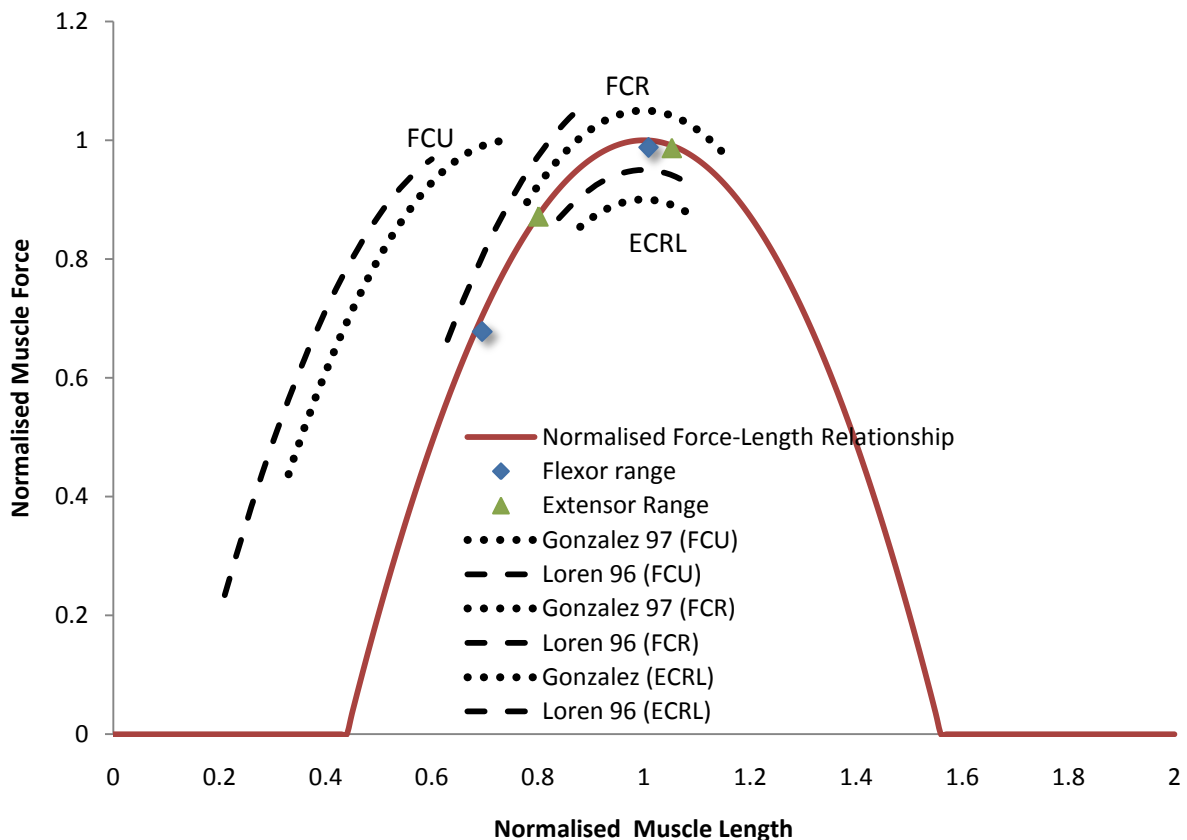


Figure 41 – Continuous line: normalised force-length relationship of muscles. Diamond markers: average operating range of wrist flexors. Triangle markers: average operating range of wrist extensors. Dotted lines: operating range of FCU and ECRL in (Gonzalez et al., 1997). Dashed lines: operating range of FCU and ECRL in (Loren et al., 1996).

Two indexes were also calculated in order to take into account the role of the tendon elasticity and the amount of excursion of the muscle fibres within the range of motion (Koo et al., 2002). The first index is the ratio of the tendon slack length to the optimal muscle length, L_{TS}/L_{OM} . This index relates to the stiffness of the wrist flexion/extension musculotendon actuators being smaller for stiffer actuators (Zajac, 1989). For flexors, the average computed over all of the subjects was equal to 2.94 (SD ± 0.53) with the highest value equal to 4.06 and the lowest value equal to 2.55. For extensors, the average was equal to 2.47 (SD ± 0.32), with the highest value equal to 2.87 and the lowest value equal to 1.87. The second index is the ratio of the optimal muscle length to the average moment arm, L_{OM}/MA_{ave} : the higher the value of this index the shorter the muscle excursion and the muscle contribution to the joint moment (Lieber, 1992). In other words, the higher its value the bigger will be the influence of the MA to the joint moment. For flexors, the average value was equal to 4.69 (SD ± 0.79), being 5.87 and 3.37 the highest and the lowest value, respectively. For extensors, the average value was equal to 9.18 (SD ± 1.23), being 11.66 and 7.66 the highest and the lowest value, respectively. The average moment arm MA_{ave} was calculated by averaging the moment arms for each subject across the range of motion.

Appendix C lists all of the values of the above mentioned parameters for each subject.

7. Discussion

This preliminary model of one degree of freedom wrist joint (flexion/extension) involves simplifications. First, it was based on the assumption that flexors act as a lumped muscle group and no distinction was made between the various flexors involved in wrist flexion. Regarding the extensors, only the ECRL contribution was taken into account and the extension action was ascribed to this latter muscle only. This certainly biased the results showed, and better results could be obtained with more measurements available. Secondly, no other EMGs were acquired, thus eventual contributions from other muscles during MVCs could not be discriminated. Figure 32A is representative of such a situation: even though the magnitude of the envelope EMG was similar throughout the experiment for each contraction, the measured torque in correspondence of the first one was bigger than the other two and the predicted torque failed to mimic it. With measurements of EMGs from other muscles, it could be verified whether an additional contribution to the total exerted moment was provided during the first contraction. Additionally, the level of co-contraction of the antagonists could be taken into account as well. Thirdly, no bone surface geometry, joint kinematics or muscle path geometry was considered. To overcome this limitation, the present study could be integrated with commercially available software such as SIMM (MusculoGraphics Inc., Chicago, USA) or AnyBody (AnyBody Technology, Aalborg, Denmark), even though these software provides musculoskeletal anatomy and function of average adult subjects which should be scaled to fit an individual's size and body proportions (Lloyd et al., 2009; Winby et al., 2008). To be mentioned are also new dynamic imaging techniques which would provide a detailed description of musculoskeletal dynamics, complex muscle architecture, joint kinematics and muscle MAs as well as

muscle tissue deformation in presence of diseases (Blemker et al., 2007). Though, this latter approach is not mature yet. Lastly, the model was validated using healthy subjects only. Future work might include the use of the model with data gathered from patients affected by sensory-motor interaction diseases so that it would be possible to compare its outcome and how this is influenced by changes occurring in the musculoskeletal system.

With regard to the results, Figure 22 to Figure 27 show that the average estimates of L_{OM} , F_{OM} and L_{TS} are in agreement with physiological values as reported in (Garner and Pandy, 2001; Holzbaur et al., 2005). Figure 26 shows an overestimated F_{OM} for extensors. This might be explained by considering that the total torque exerted during the experiments was ascribed to ECRL only. Among the three parameters, L_{TS} showed to be the less sensitive (Figure 24) and different optimisation algorithms could be tested to improve the parameter identification process. It is worth mentioning that the works from Garner and Pandy (2001) and Holzbaur et al. (2005) were selected and used to carry out the comparison for the wide range of values referred, reviewed and reported therein. Furthermore, Figure 31 to Figure 36 as well as Table 4 and Table 5 show that once the estimated parameters are used as input to the model in order to predict the measured torque in a different position, the simulated torque mimics the measured one with values of RMSE and NRMSE comparable to those found during the estimation phase.

Figure 37 shows a shallower trend with regard to the flexor moment variability when this is compared to data from (Delp et al., 1996; Gonzalez et al., 1997; Holzbaur et al., 2005; Loren et al., 1996). In these latter works, the moment decays faster going from flexion to extension for the same angular range. Moreover, in the works from (Delp et al., 1996; Gonzalez et al., 1997; Holzbaur et al., 2005) flexor moment peaks were mainly located in the flexed region. These authors argue that the biomechanics of the joint (i.e. *MA*s) together with the muscle properties (i.e. *PCSA*) would be the main causes limiting the capability of flexors (extensors) to exert moments in extended (flexed) positions higher than in flexed (extended) positions. On the other hand, in (Garner and Pandy, 2001) the highest peak was located at 0° , while data recorded during the present study showed the highest values being in extended positions as also reported in (Loren et al., 1996) and in (Hutchins, 1993). With regard to the extensors, Figure 38 shows lower torque values than those relative to flexors, as generally found in the literature. The measured highest peak was recorded at a slightly flexed position ($+10^\circ$), which contrasts with findings in (Delp et al., 1996; Gonzalez et al., 1997; Holzbaur et al., 2005; Loren et al., 1996) where peaks were mainly located in the extension region. However, measures in (Garner and Pandy, 2001) show a similar outcome as the one in the present work with the highest peaks occurring in flexion. Nevertheless, it is worth noting how the outcome of the modelled wrist joint closely follows the measurements gathered during this study.

As Figure 39 and Figure 40 show, the trend of the force curves contrasts that of the *MA*s: at an increasing (decreasing) force corresponds a decreasing (increasing) *MA*. A comparison between the two figures shows on average lower estimated flexor forces with respect to estimated extensor forces, even though flexor moments resulted higher than the extensor ones. This might be explained by looking at Figure 41 and considering the values of the ratios L_{TS}/L_{OM} and L_{OM}/MA_{ave} . Figure 41 shows that flexors were found to operate mainly on the ascending limb of the normalised force-length relationship with larger muscle length change than extensors which, instead, were characterised by a narrower range of motion at the top of the same curve. This confirms findings in (Gonzalez et al., 1997; Loren et al., 1996), even though in these latter works *FCU* was found to operate also at shorter lengths. On the other hand, the range of motion of *FCR* in (Loren et al., 1996) was found to operate in a region which overlaps the one of the present work, while the modelled

FCR operating range in (Gonzalez et al., 1997) was located on the plateau region of the force-length relationship. However, it must be emphasised that the results shown refer to FCU, FCR and FDS lumped together and the range of motion used during the experiments was smaller than the ones in the two cited works. With regard to the range of motion of ECRL, its location at the top of the curve in correspondence of slightly longer muscle lengths confirms results in (Gonzalez et al., 1997; Loren et al., 1996). The behaviour described for both flexors and extensors is thus in accordance with values of the two ratio indexes. Indeed, a smaller L_{TS}/L_{OM} ratio for extensors indicates stiffer musculotendon actuators with smaller muscle excursion predominantly located in the upper part of the ascending limb, hence higher forces, as also found in (Loren et al., 1996; Zajac, 1989). At the same time, extensors were also characterised by a bigger L_{OM}/MA_{ave} ratio (Gonzalez et al., 1997; Loren et al., 1996). As a consequence, a major role to the joint moment was played by MAs more than muscle forces: even though extensors were characterised by higher forces than flexors, extensor torques resulted lower because of lower values of MA .

8. Conclusions

The present model showed its potential as an *in vivo* method to estimate musculotendon parameters. In particular, it was found that:

1. The values of the estimated parameters varied in a physiologically realistic range (see section '6.1 *Estimated Values*' and in particular Figure 25 to Figure 27);
2. The model was able to simulate the measured torques with values of RMSE and NRMSE comparable to those calculated during the estimation phase (see section '6.2 *Model Validation*' and Figure 37 and Figure 38).
3. The range of motion of the muscle fibres as well as the influence of tendon elasticity and MA were consistent with findings in the literature (see section '6.4 *Operating range of*' and Figure 41).

With the aim to obtain a robust and reliable model to be used as a benchmark for characterising biomechanical parameters of the musculotendon system, the limitations of the present study ought to be, however, properly tackled. The following actions should be thus considered for future work:

1. Inclusion and distinction of the maximum possible number of muscles involved in the motor task under study and acquisition of their EMGs. This would allow one to map the single contribution (e.g. agonist or antagonist) of each musculotendon actuator during any prescribed task.
2. An improved and detailed description of musculoskeletal dynamics, complex muscle architecture, joint kinematics and muscle MAs . In the first instance, a better description could be introduced by the use of commercial software such as SIMM (MusculoGraphics Inc., Chicago, USA) or AnyBody (AnyBody Technology, Aalborg, Denmark). On the other hand, these software tools provide models of an average adult human whose values have been derived from cadaveric studies, thus the necessity to scale an individual's size and body proportions arises (Lloyd et al., 2009; Winby et al., 2008). A further step toward a patient-specific musculoskeletal modelling would be the integration of this approach with imaging technologies (e.g. MRI) (Blemker et al., 2007).

3. To test the model on patients in order to verify its efficacy in estimating subject-specific musculotendon parameters in presence of pathologies. This could be useful for diagnosis of musculoskeletal injuries, customisation of rehabilitation or monitoring of its outcome.
4. Improvement of the optimisation algorithm should be sought as well. The values of the estimated parameters showed a certain degree of dependency upon their initial values, hence the use of optimisation algorithms which provide the possibility to monitor with more accuracy their outcome is advised. Finally, a comprehensive sensitivity analysis was not carried out.

It is worth noting that improvements such as those specified above would benefit the model in a general sense. Indeed, even though this study was conducted on the wrist joint, the same approach and hierarchical and topological organisation could be transferred to different joints, being anatomy the main aspect to be adapted.

On a longer term, the musculoskeletal model developed with the present approach could be completed with models of the sensory organs (as specified in section '3.3 *Nervous System*'). The resulting entire neuromusculoskeletal model could be then exploited as an investigational tool to discriminate between biomechanical and neural causes of musculoskeletal disorders or diseases affecting the nervous system. Indeed, pathological conditions could be inferred by analysing deviations of the indexes as those cited herein from healthy values. This would provide additional insights into the dynamic interactions among the elements involved in the execution of motor tasks that would be difficult or even impossible to obtain from physiological studies alone (Pearson et al., 2006). In conjunction with models of neurophysiologic pathways, it may be possible to understand how the central nervous system controls movement and how commands from the peripheral receptors are taken into account and cooperate with movement strategies.

Along this path, it will be also possible to guide clinical experimentation as well as clinical diagnosis. Indeed, causes or mechanisms involved in patient's pathological condition can be hypothesised and clinically verified. Manipulation of elements of the peripheral and central nervous system by means of rehabilitation techniques which integrate electrical therapy and exercise-active movements have showed success in enhancing motor re-learning following damage to the central nervous system (Popovic et al., 2009). On the other hand, the mechanisms underlying the therapeutic approaches and the consequent effects of neuromuscular rehabilitation are still unknown (Jung et al., 2009). Thus, the potential of this research in terms of clinical application is evident: by means of the neuromusculoskeletal model not only the nature and the cause of the impairment in a patient can be inferred, but a customised therapy regime can be planned, prescribed and monitored.

Acknowledgements

I would like to thank Dr. David Simpson for his help with the EMG linear envelope processing and Ruth Turk for her help with the test rig and the placement of the electrodes. Financial support provided by EPSRC (Platform Grant in Structural Acoustics) is also acknowledged.

References

- Blemker, S.S., Asakawa, D.S., Gold, G.E., Delp, S.L., 2007. Image-based musculoskeletal modeling: applications, advances, and future opportunities. *J Magn Reson Imaging* 25,441-451.
- Buchanan, T.S., Lloyd, D.G., Manal, K., Besier, T.F., 2004. Neuromusculoskeletal modeling: estimation of muscle forces and joint moments and movements from measurements of neural command. *J Appl Biomech* 20,367-395.
- Buchthal, F., Schmalbruch, H., 1970. Contraction times and fibre types in intact human muscle. *Acta Physiol Scand* 79,435-452.
- Delp, S.L., Grierson, A.E., Buchanan, T.S., 1996. Maximum isometric moments generated by the wrist muscles in flexion-extension and radial-ulnar deviation. *J Biomech* 29,1371-1375.
- Delp, S.L., Loan, J.P., 1995. A graphics-based software system to develop and analyze models of musculoskeletal structures. *Comput Biol Med* 25,21-34.
- Delp, S.L., Loan, J.P., Hoy, M.G., Zajac, F.E., Topp, E.L., Rosen, J.M., 1990. An interactive graphics-based model of the lower extremity to study orthopaedic surgical procedures. *IEEE Trans Biomed Eng* 37,757-767.
- Erdemir, A., McLean, S., Herzog, W., van den Bogert, A.J., 2007. Model-based estimation of muscle forces exerted during movements. *Clin Biomech (Bristol, Avon)* 22,131-154.
- Frigon, A., Rossignol, S., 2006. Experiments and models of sensorimotor interactions during locomotion. *Biol Cybern* 95,607-627.
- Garner, B.A., Pandy, M.G., 2001. Musculoskeletal model of the upper limb based on the visible human male dataset. *Comput Methods Biomech Biomed Engin* 4,93-126.
- Garner, B.A., Pandy, M.G., 2003. Estimation of musculotendon properties in the human upper limb. *Ann Biomed Eng* 31,207-220.
- Gonzalez, R.V., Buchanan, T.S., Delp, S.L., 1997. How muscle architecture and moment arms affect wrist flexion-extension moments. *J Biomech* 30,705-712.
- Hildebrand, F.B., 1968. *Finite-Difference Equations and Simulations*. Englewood Cliffs, New Jersey: Prentice-Hall.
- Holzbaur, K.R., Murray, W.M., Delp, S.L., 2005. A model of the upper extremity for simulating musculoskeletal surgery and analyzing neuromuscular control. *Ann Biomed Eng* 33,829-840.
- Holzbaur, K.R., Murray, W.M., Gold, G.E., Delp, S.L., 2007. Upper limb muscle volumes in adult subjects. *J Biomech* 40,742-749.
- Hutchins, E.L., 1993. *The musculoskeletal geometry of the human elbow and wrist: An analysis using torque-angle relationships*. Austin: University of Texas at Austin.
- Jung, R., Belanger, A., Kanchiku, T., Fairchild, M., Abbas, J.J., 2009. Neuromuscular stimulation therapy after incomplete spinal cord injury promotes recovery of interlimb coordination during locomotion. *J Neural Eng* 6,55010.
- Khoo, M.C.K., 1999. *Physiological Control Systems: Analysis, Simulation, and Estimation*. New York: Wiley, John & Sons, Inc.
- Koo, T.K., Mak, A.F., 2005. Feasibility of using EMG driven neuromusculoskeletal model for prediction of dynamic movement of the elbow. *J Electromyogr Kinesiol* 15,12-26.
- Koo, T.K., Mak, A.F., 2006. A neuromusculoskeletal model to simulate the constant angular velocity elbow extension test of spasticity. *Med Eng Phys* 28,60-69.
- Koo, T.K., Mak, A.F., Hung, L.K., 2002. In vivo determination of subject-specific musculotendon parameters: applications to the prime elbow flexors in normal and hemiparetic subjects. *Clin Biomech (Bristol, Avon)* 17,390-399.
- Lan, N., 2002. Stability analysis for postural control in a two-joint limb system. *IEEE Trans Neural Syst Rehabil Eng* 10,249-259.
- Lan, N., Li, Y., Sun, Y., Yang, F.S., 2005. Reflex regulation of antagonist muscles for control of joint equilibrium position. *IEEE Trans Neural Syst Rehabil Eng* 13,60-71.

- Langhorne, P., Coupar, F., Pollock, A., 2009. Motor recovery after stroke: a systematic review. *Lancet Neurol* 8,741-754.
- Lemay, M.A., Crago, P.E., 1996. A dynamic model for simulating movements of the elbow, forearm, and wrist. *J Biomech* 29,1319-1330.
- Lieber, R.L., 1992. *Skeletal muscle structure and function - implications for rehabilitation and sports medicine*. Baltimore: Williams & Wilkins.
- Lin, C.C., Crago, P.E., 2002. Structural model of the muscle spindle. *Ann Biomed Eng* 30,68-83.
- Lloyd, D., Besier, T., Winby, C., Buchanan, T.S., 2009. Neuromusculoskeletal modelling and simulation of tissue loading in lower extremities. In: *Routledge Handbook of Biomechanics and Human Movement Science* (Hong Y, Bartlett R, eds). London and New York: Taylor & Francis Group.
- Loren, G.J., Shoemaker, S.D., Burkholder, T.J., Jacobson, M.D., Friden, J., Lieber, R.L., 1996. Human wrist motors: biomechanical design and application to tendon transfers. *J Biomech* 29,331-342.
- Mendez, J., Keys, A., 1960. Density and composition of mammalian muscle. *Metabolism, Clinical and Experimental* 9,184-188.
- Merletti, R., Parker, P. eds, 2004. *Electromyography: Physiology, Engineering, and Non-Invasive Applications*. Hoboken, New Jersey: John Wiley & Sons, Inc.
- Mileusnic, M.P., Brown, I.E., Lan, N., Loeb, G.E., 2006. Mathematical models of proprioceptors. I. Control and transduction in the muscle spindle. *J Neurophysiol* 96,1772-1788.
- Milner-Brown, H.S., Stein, R.B., Yemm, R., 1973. The contractile properties of human motor units during voluntary isometric contractions. *J Physiol* 228,285-306.
- Paul, C., Bellotti, M., Jezernik, S., Curt, A., 2005. Development of a human neuro-musculo-skeletal model for investigation of spinal cord injury. *Biol Cybern* 93,153-170.
- Pearson, K., Ekeberg, O., Buschges, A., 2006. Assessing sensory function in locomotor systems using neuro-mechanical simulations. *Trends Neurosci* 29,625-631.
- Peckham, P.H., Knutson, J.S., 2005. Functional electrical stimulation for neuromuscular applications. *Annu Rev Biomed Eng* 7,327-360.
- Popovic, D.B., Sinkaer, T., Popovic, M.B., 2009. Electrical stimulation as a means for achieving recovery of function in stroke patients. *NeuroRehabilitation* 25,45-58.
- Prochazka, A., 1996. Proprioceptive feedback and movement regulation. In: *Exercise: Regulation and Integration of Multiple Systems* (Rowell L, Sheperd J, eds). New York: American Physiological Society; 89-127.
- Prochazka, A., Gillard, D., Bennett, D.J., 1997a. Implications of positive feedback in the control of movement. *J Neurophysiol* 77,3237-3251.
- Prochazka, A., Gillard, D., Bennett, D.J., 1997b. Positive force feedback control of muscles. *J Neurophysiol* 77,3226-3236.
- Schmidt, R.F., 1978. *Fundamentals of neurophysiology*, 2d ed. New York: Springer-Verlag.
- Shao, Q., Buchanan, T.S., 2008. A biomechanical model to estimate corrective changes in muscle activation patterns for stroke patients. *J Biomech* 41,3097-3100.
- Sinkjaer, T., Haugland, M., Inmann, A., Hansen, M., Nielsen, K.D., 2003. Biopotentials as command and feedback signals in functional electrical stimulation systems. *Med Eng Phys* 25,29-40.
- Song, D., Lan, N., Loeb, G.E., Gordon, J., 2008. Model-based sensorimotor integration for multi-joint control: development of a virtual arm model. *Ann Biomed Eng* 36,1033-1048.
- Taylor, A., Durbaba, R., Ellaway, P.H., Rawlinson, S., 2006. Static and dynamic gamma-motor output to ankle flexor muscles during locomotion in the decerebrate cat. *J Physiol* 571,711-723.
- Vallbo, A.B., al-Falahe, N.A., 1990. Human muscle spindle response in a motor learning task. *J Physiol* 421,553-568.
- Winby, C.R., Lloyd, D.G., Kirk, T.B., 2008. Evaluation of different analytical methods for subject-specific scaling of musculotendon parameters. *J Biomech* 41,1682-1688.
- Winter, D., 2005. *Biomechanics and motor control of human movement*, 3rd ed: Wiley.

- Winters, J.M., Stark, L., 1988. ESTIMATED MECHANICAL-PROPERTIES OF SYNERGISTIC MUSCLES INVOLVED IN MOVEMENTS OF A VARIETY OF HUMAN JOINTS. *Journal of Biomechanics* 21,1027-1041.
- Yamaguchi, G., 2001. *Dynamic Modeling of Musculoskeletal Motion: A Vectorized Approach for Biomechanical Analysis in Three Dimensions*, 1st ed. New York: Springer-Verlag.
- Yamaguchi, G., Sawa, A., Moran, D., Fessler, M., Winters, J., 1990. A survey of human musculotendon actuator parameters. In: *Multiple Muscle Systems Biomechanics and Movement Organization* (Winters J, Woo J, eds). Berlin: Springer.
- Zajac, F.E., 1989. Muscle and tendon: properties, models, scaling, and application to biomechanics and motor control. *Crit Rev Biomed Eng* 17,359-411.

Appendix A

Time plots for flexors and extensors.

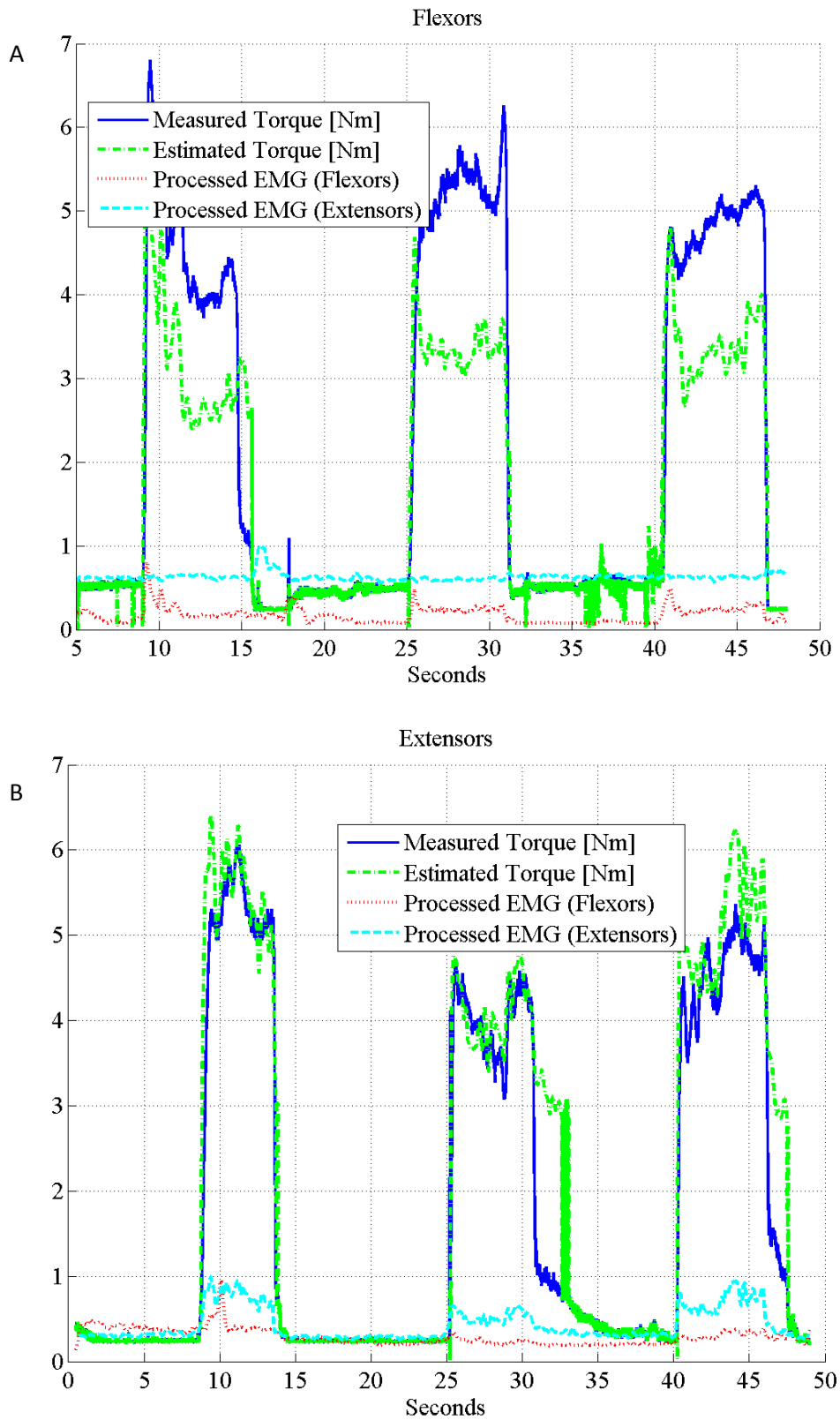


Figure 42 – Subject 1. A) Flexors (the first 5 seconds of this data set were cut off due to artefacts); B) Extensors.

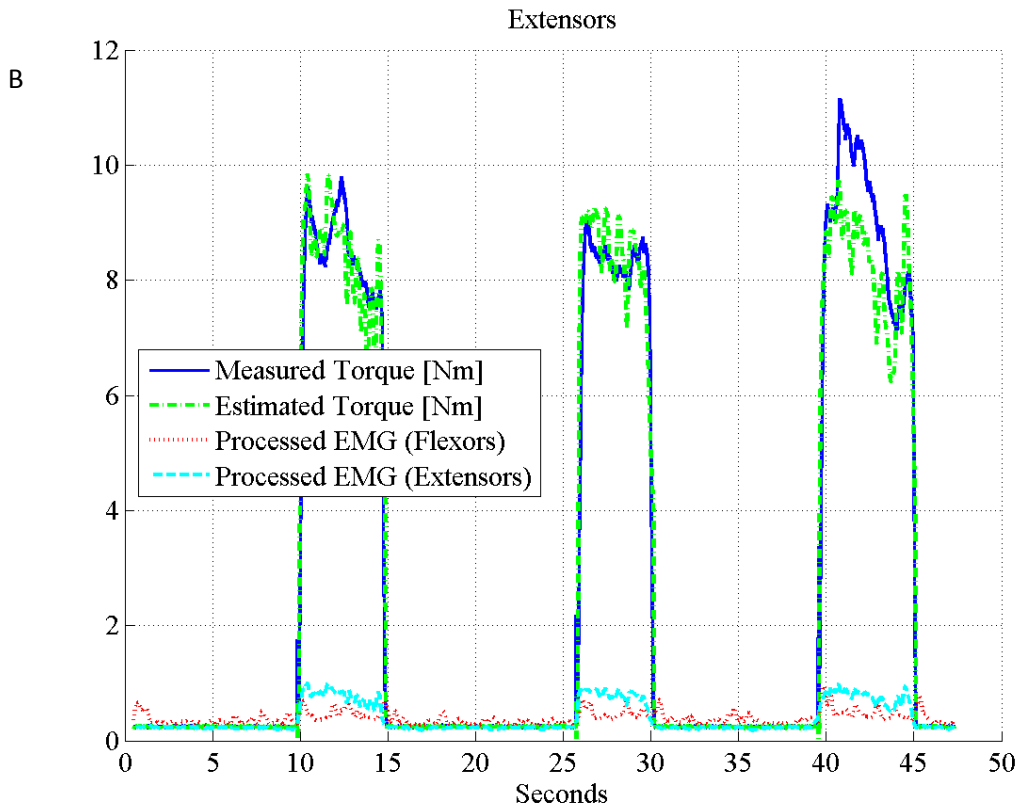
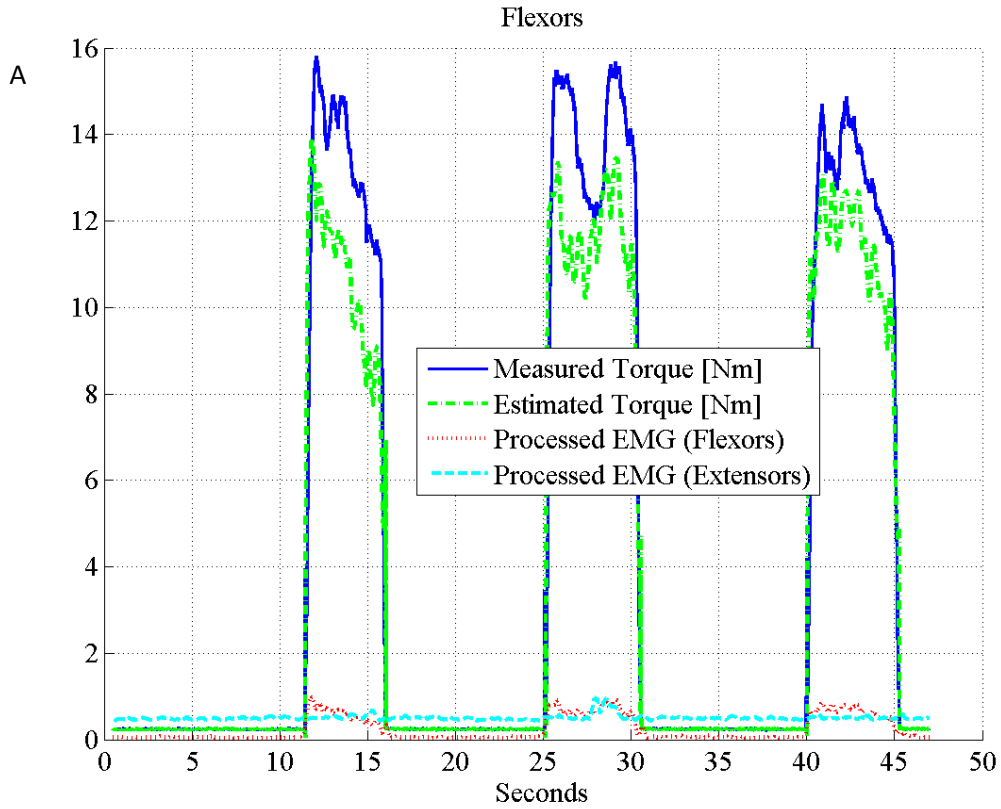


Figure 43 – Subject 2. The validation was carried out using one of the five trials available. A) Flexors; B) Extensors.

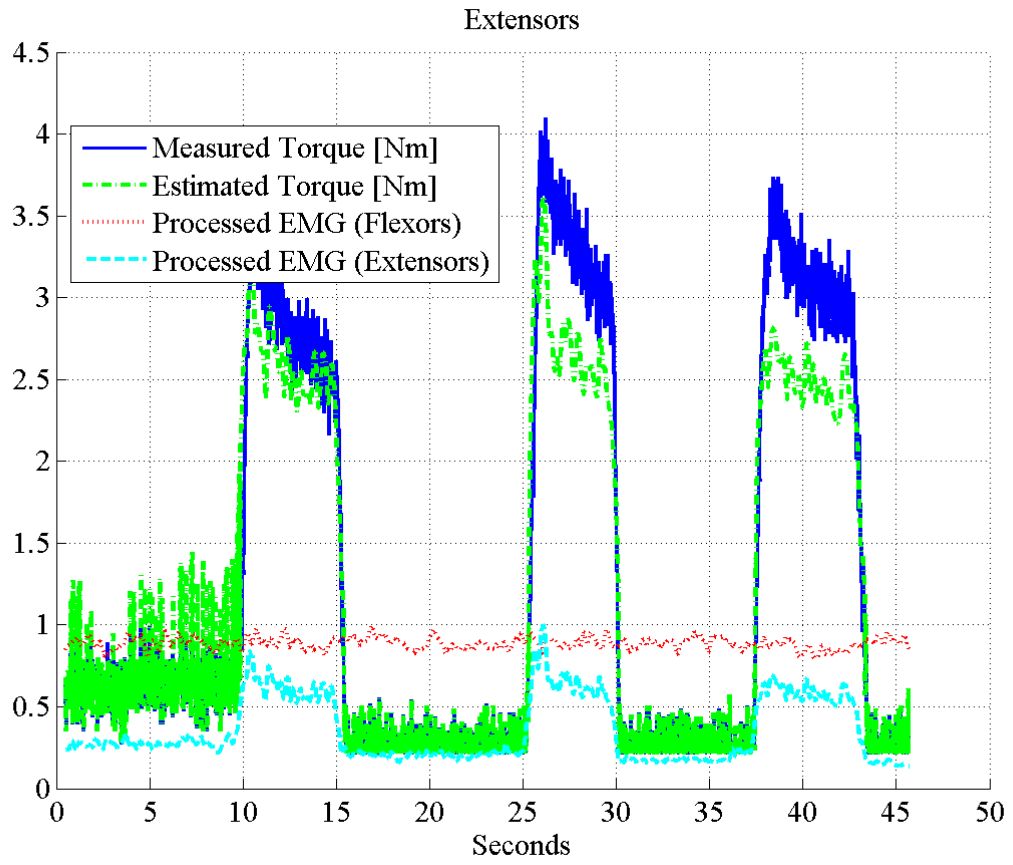


Figure 44 – Subject 3. Extensors only.

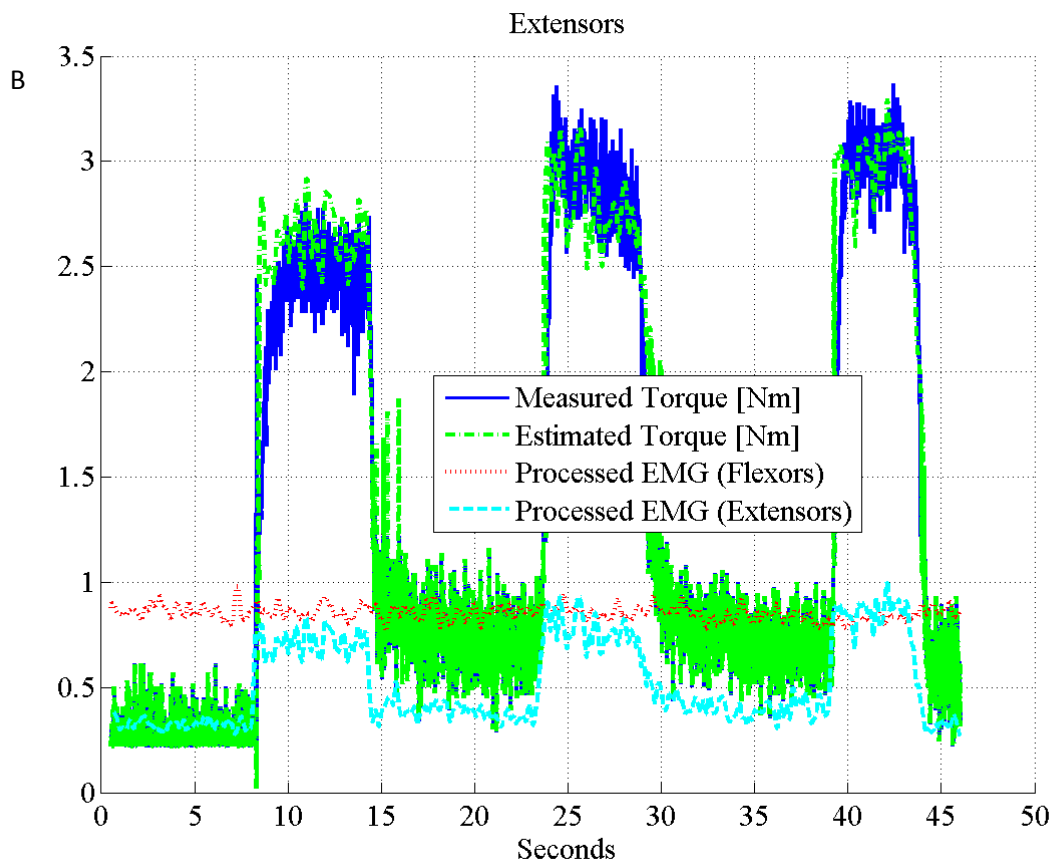
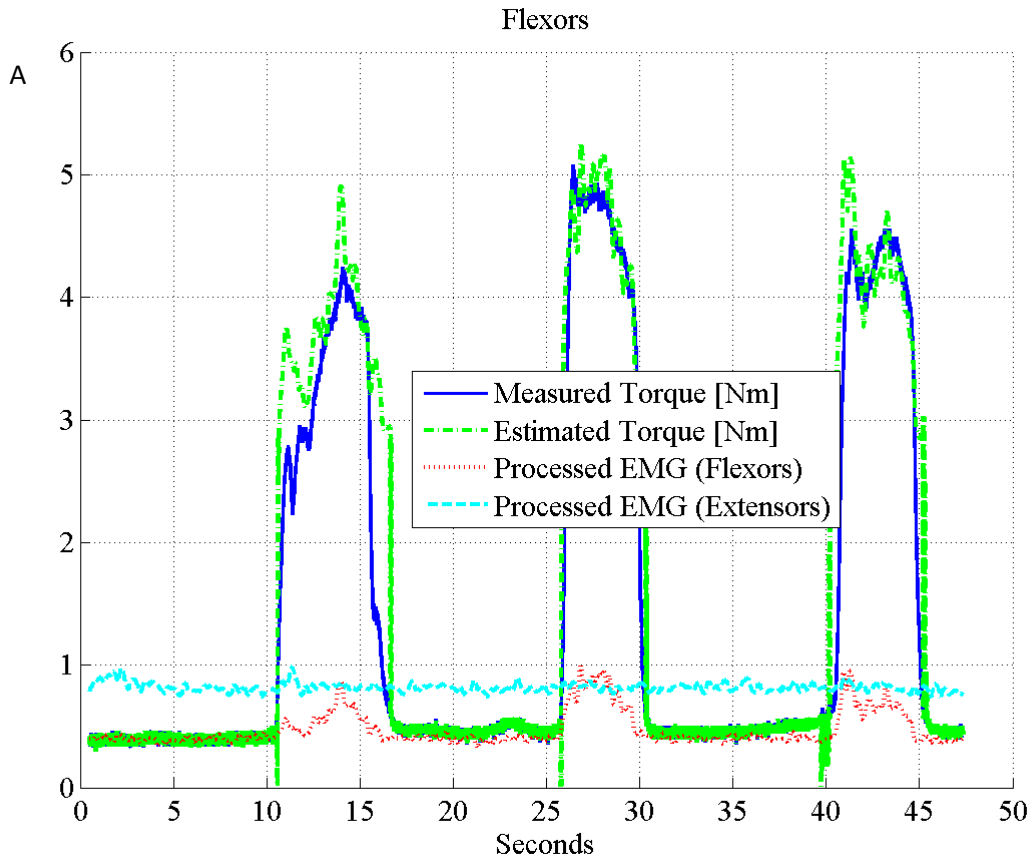


Figure 45 – Subject 4. A) Flexors; B) Extensors.

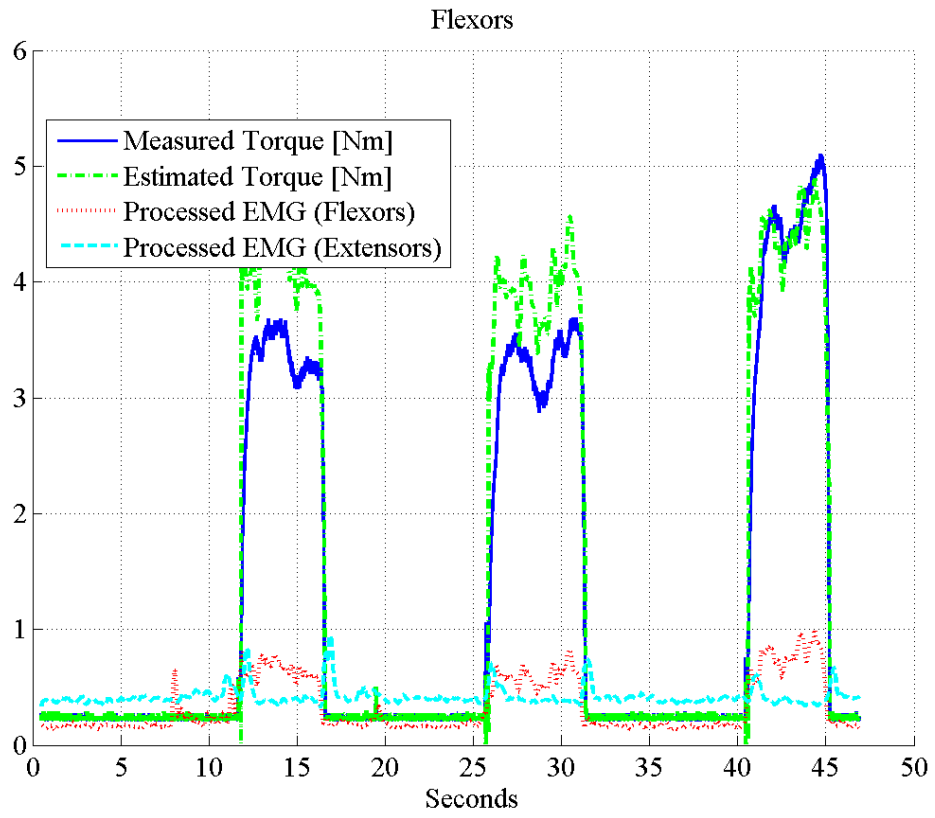


Figure 46 – Subject 5. Flexors only.

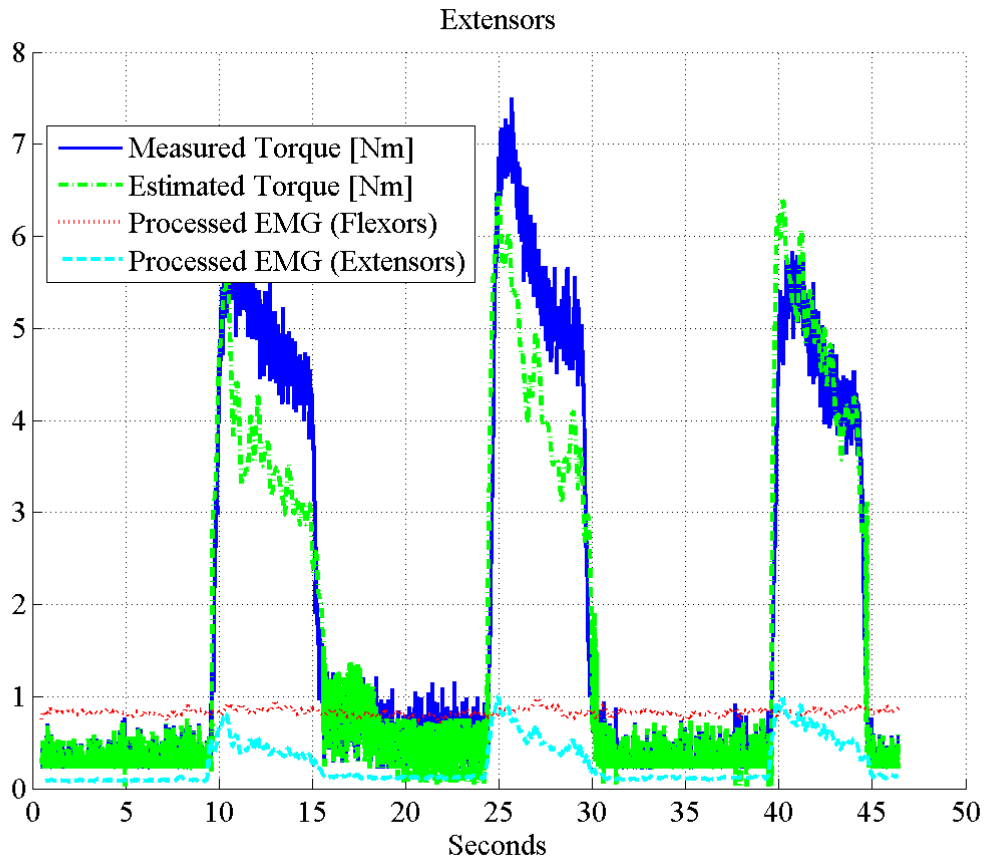


Figure 47 – Subject 6. Extensors only.

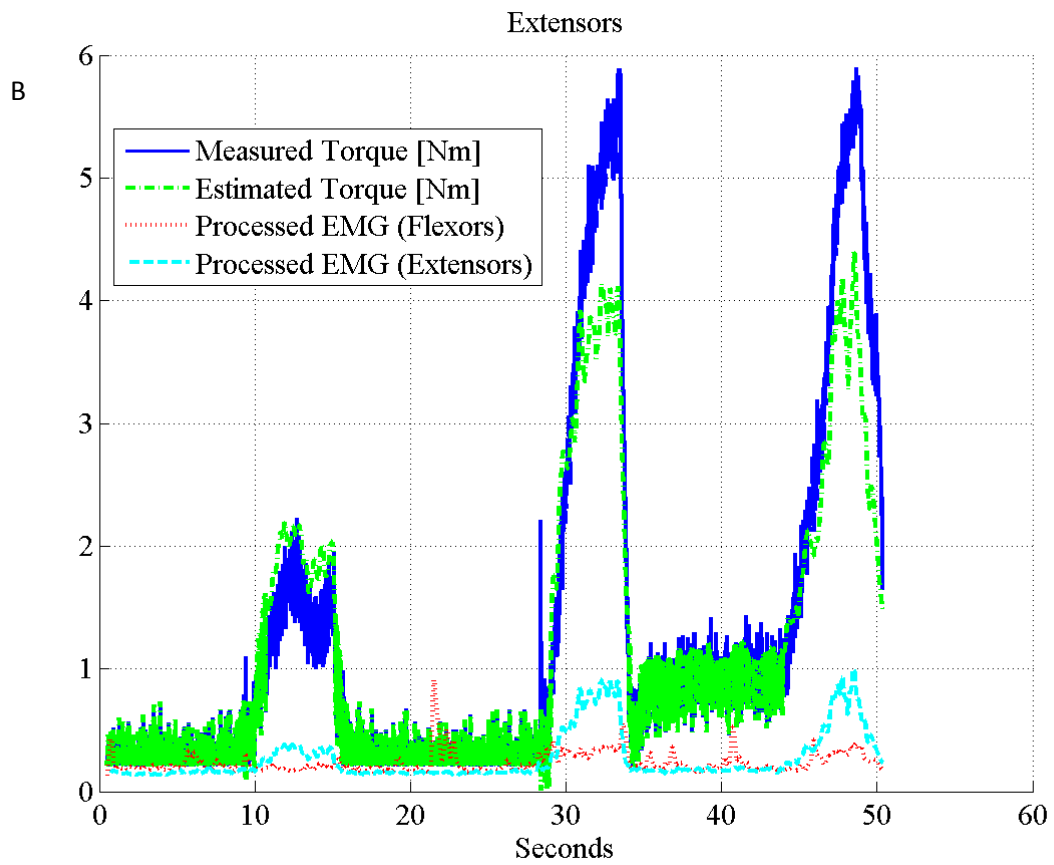
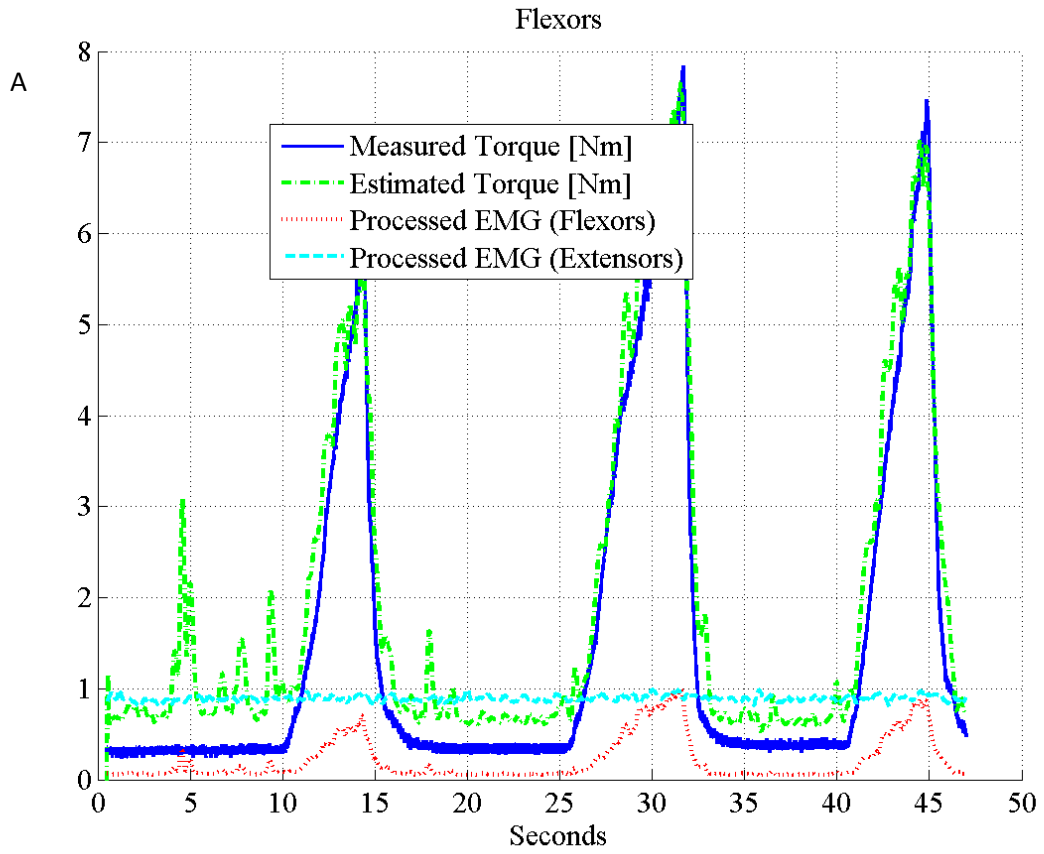


Figure 48 – Subject 7. A) Flexors; B) Extensors.

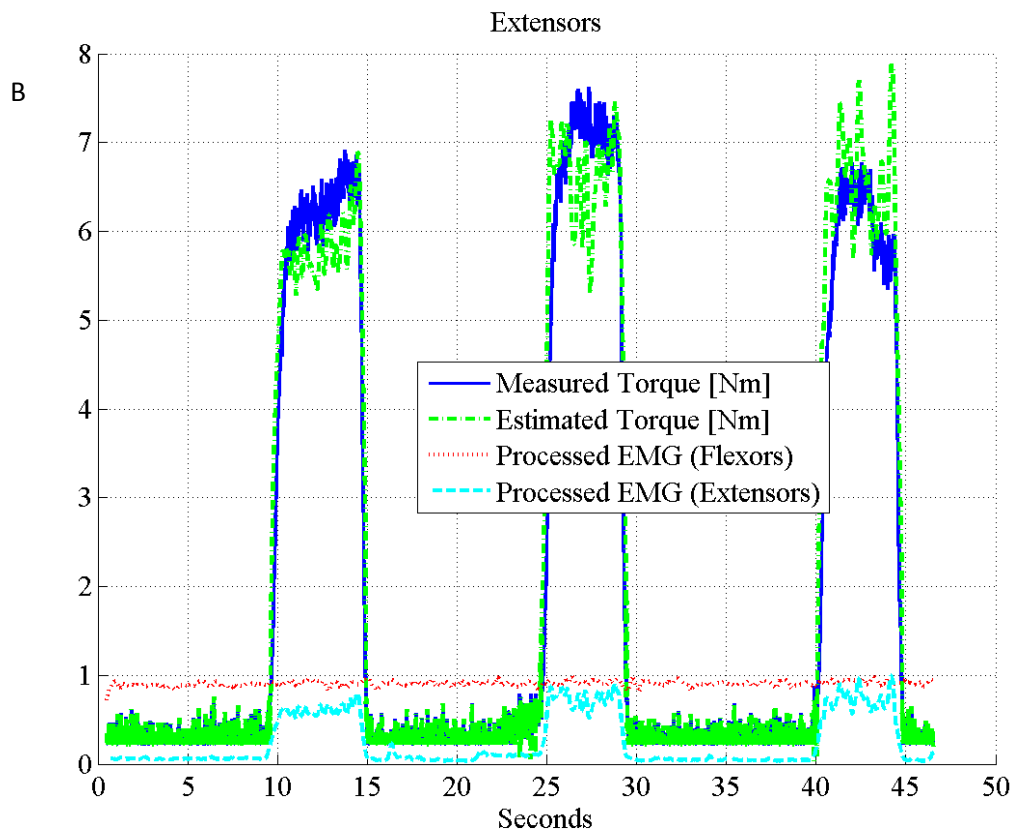
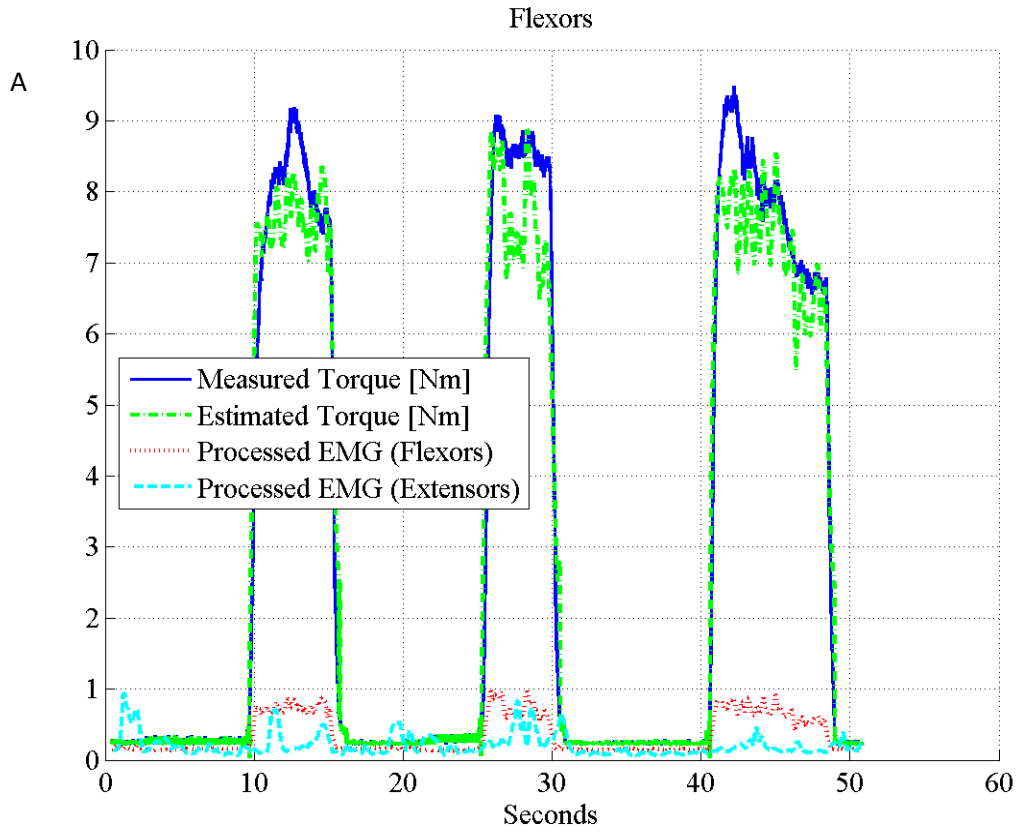


Figure 49 – Subject 8. A) Flexors; B) Extensors.

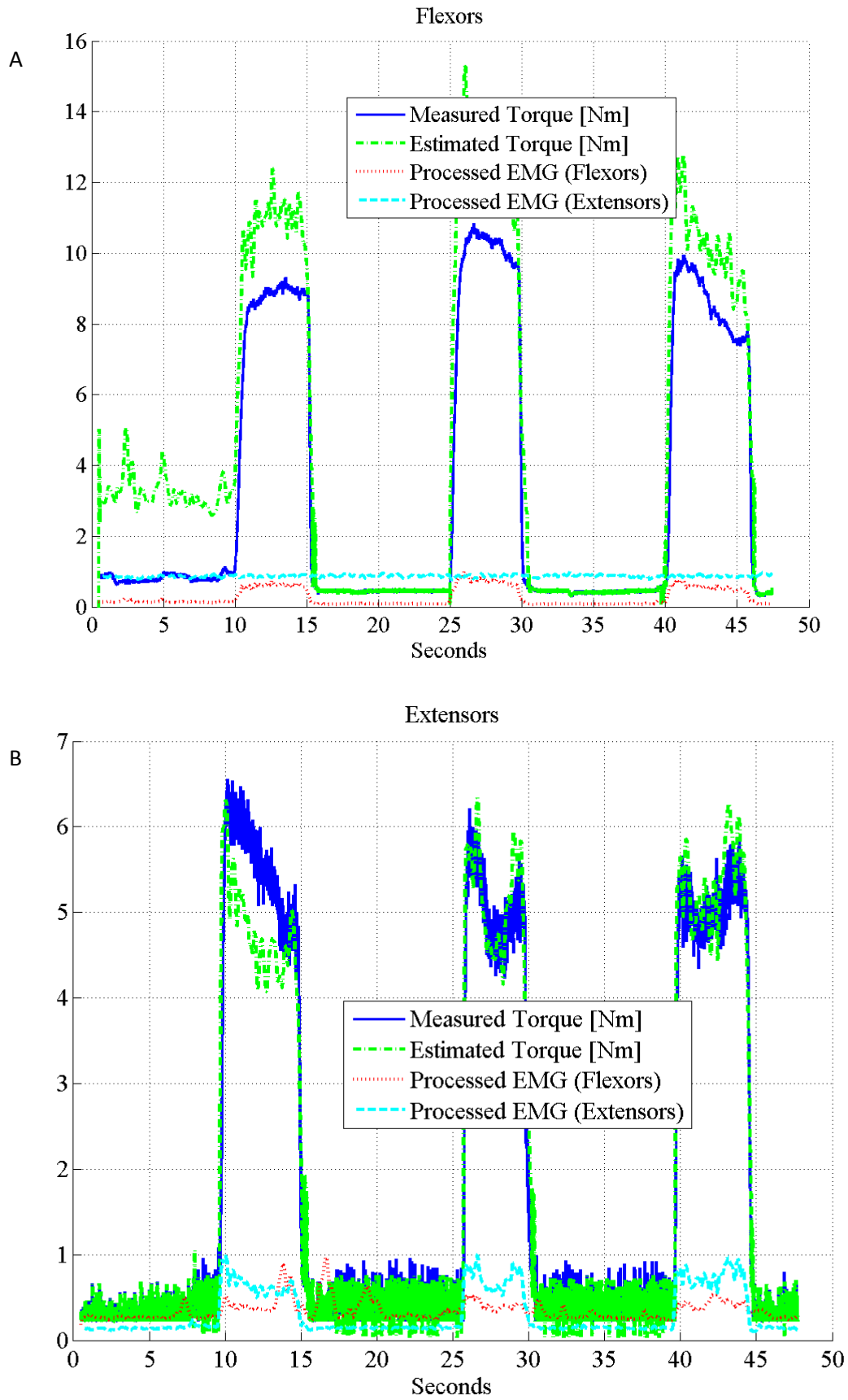


Figure 50 - Subject 9. A) Flexors; B) Extensors.

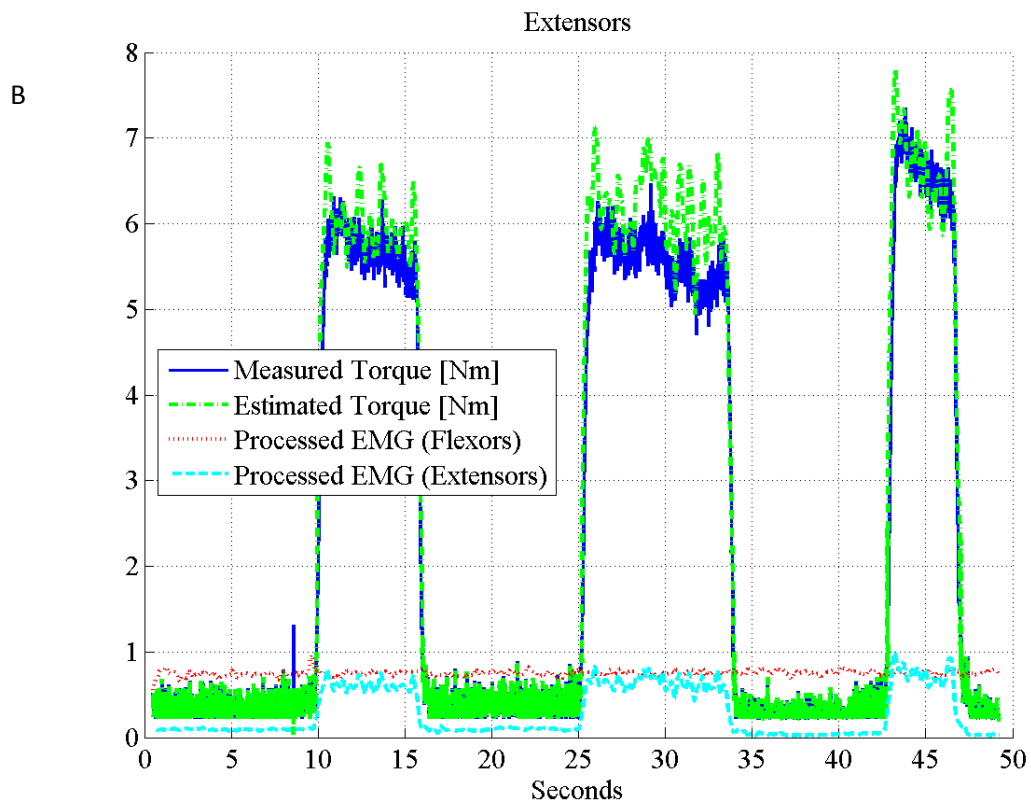
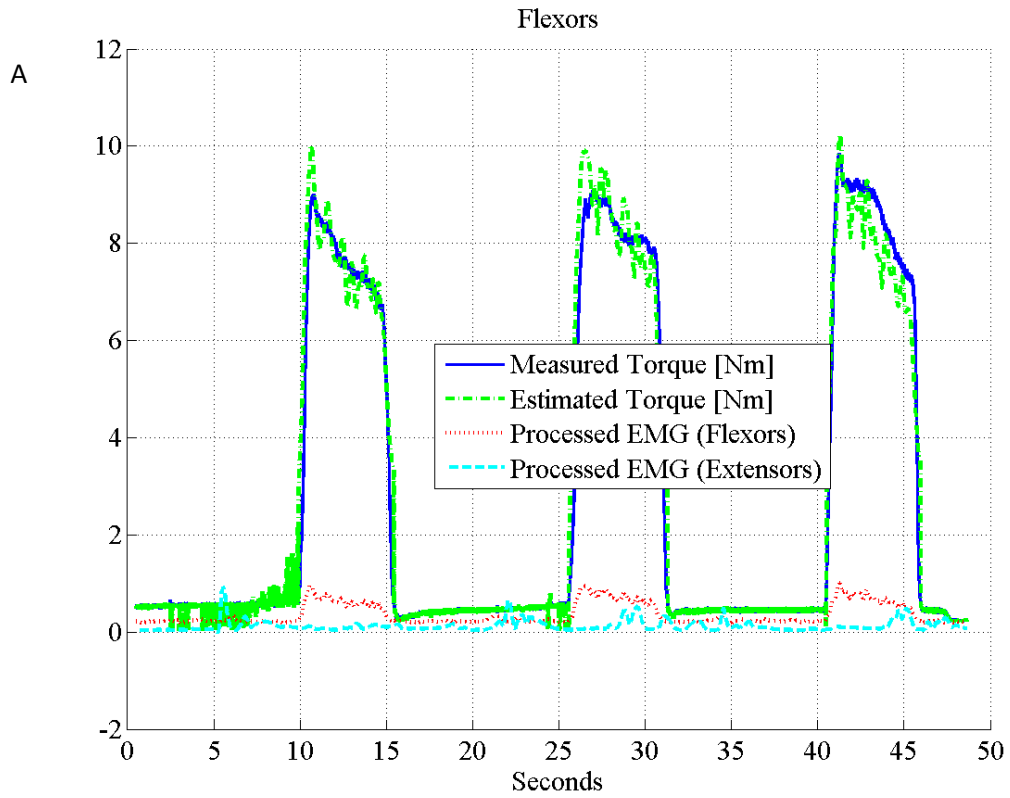


Figure 51 – Subject 10. A) Flexors; B) Extensors.

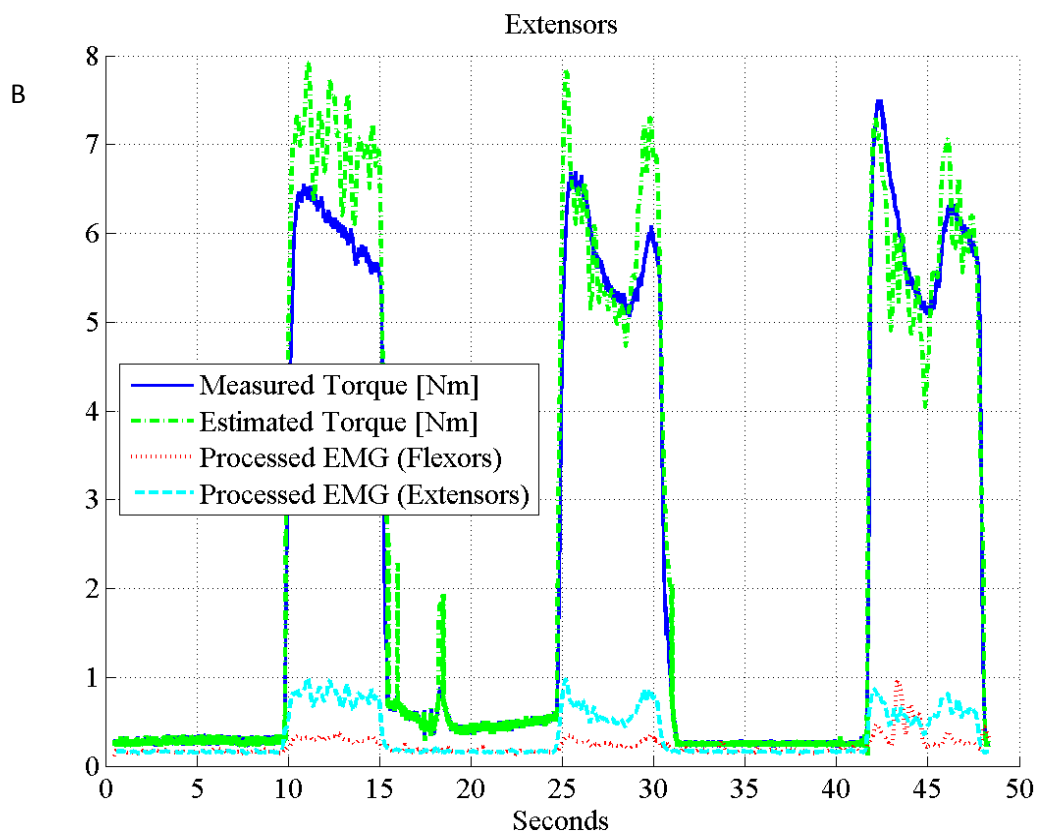
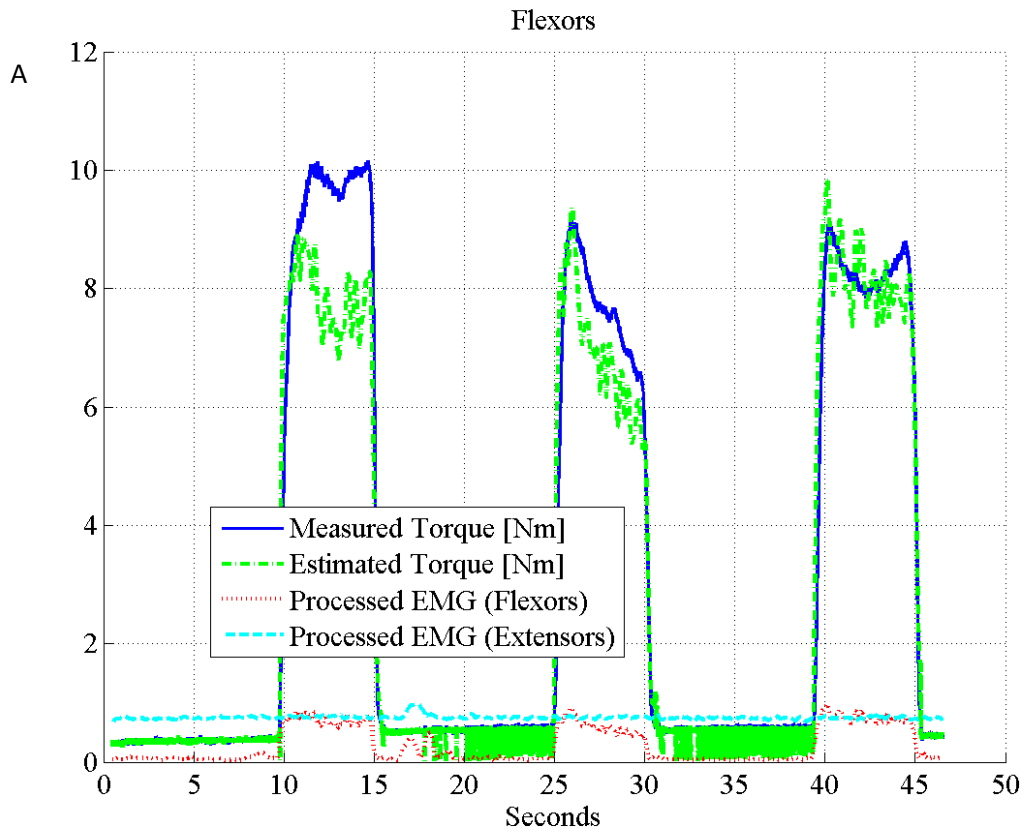


Figure 52 – Subject 12. A) Flexors; B) Extensors.

Appendix B

Mean and standard deviation (SD) values of predicted and measured torques and estimated muscle force for flexors and extensors.

Subject		Predicted Torque [Nm] – Flexors							
		Angle (degrees)							
		-30°	-20°	-10°	0°	10°	20°	30°	
1	Mean	6.27	6.33	5.48	5.4	5.34	5.56	4.69	
	±SD	0.42	0.25	0.64	0.46	0.4	0.34	0.97	
2	Mean	13.03	12.73	15.03	13.48	13.96	11.24	11.78	
	±SD	0.8	0.32	0.34	0.42	0.42	0.45	0.28	
3	Mean	BAD SIGNALS							
	±SD	BAD SIGNALS							
4	Mean	N/A	4.47	5.69	5.1	5.1	N/A	2.99	
	±SD	N/A	0.26	0.23	4.63	0.04	N/A	0.79	
5	Mean	1.99	3.12	4.00	4.53	4.7	3.91	5.72	
	±SD	0.17	0.31	0.19	0.37	0.2	0.19	0.47	
6	Mean	BAD SIGNALS							
	±SD	BAD SIGNALS							
7	Mean	9.42	6.77	7.77	6.89	4.4	4.05	5.24	
	±SD	1.14	0.38	0.41	0.85	0.1	1.05	0.59	
8	Mean	8.04	8.95	7.72	8.6	8.84	7.07	7.04	
	±SD	0.64	1.36	1.31	0.26	0.33	0.12	0.45	
9	Mean	14.37	12.98	10.86	13.49	11.43	10.54	10.93	
	±SD	1.19	2.13	0.67	1.57	0.6	2.6	0.78	
10	Mean	9.6	9.63	9.95	10.05	10.17	8.64	9.61	
	±SD	0.97	0.42	1.51	0.16	0.33	0.74	0.77	
11	Mean	BAD SIGNALS							
	±SD	BAD SIGNALS							
12	Mean	6.67	6.97	9.37	9.38	11.04	10.33	7.64	
	±SD	0.47	0.08	1.72	0.48	0.55	0.31	1.12	
		Mean	8.67	7.99	8.43	8.55	8.33	7.67	7.29
		±SD	0.73	0.61	0.78	1.02	0.33	0.73	0.69

Measured Torque [Nm] – Flexors

Subject		Angle (degrees)						
		-30°	-20°	-10°	0°	10°	20°	30°
1	Mean	7.03	6.56	6.52	6.12	5.1	6.4	5.1
	±SD	0.33	1.68	1.22	0.76	0.36	0.45	1.02
2	Mean	13.21	14.21	15.76	15.45	14.7	12.43	11.47
	±SD	1.49	1.8	0.57	0.5	0.64	0.64	0.36
3	Mean	BAD SIGNALS						
	±SD	BAD SIGNALS						
4	Mean	N/A	4.59	5.57	4.63	4.72	N/A	3.85
	±SD	N/A	0.57	1.07	0.42	0.36	N/A	0.8
5	Mean	2.13	3	4.42	4.16	4.88	4.12	6.25
	±SD	0.08	0.71	0.89	0.82	0.19	0.5	1.94
6	Mean	BAD SIGNALS						
	±SD	BAD SIGNALS						
7	Mean	9.85	7.22	8.14	7.05	5.33	4.75	6.01
	±SD	1.29	0.45	0.44	1.06	0.22	1.58	1.16
8	Mean	8.1	9.67	8.79	9.25	8.92	6.92	7.35
	±SD	0.99	1.46	0.96	0.22	2.71	0.52	0.99
9	Mean	15.95	15.83	10.65	10.4	9.88	10.35	9.66
	±SD	2.93	2.12	0.57	0.76	0.56	1.08	0.36
10	Mean	9.93	9.66	10.95	9.32	10.06	8.44	8.9
	±SD	0.84	1.03	1.45	0.46	0.07	1.05	0.2
11	Mean	BAD SIGNALS						
	±SD	BAD SIGNALS						
12	Mean	6.86	7.02	8.48	9.52	10.55	9.93	7.82
	±SD	1.15	0.12	1.43	1.48	0.26	0.69	1.05
Mean		9.13	8.64	8.81	8.43	8.24	7.92	7.38
±SD		1.14	1.10	0.96	0.72	0.60	0.81	0.88

Predicted Force [N] – Flexors

Subject		Angle (degrees)						
		-30°	-20°	-10°	0°	10°	20°	30°
1	Mean	358.1	367.47	323.56	309.04	288.47	303.46	239.68
	±SD	23.91	14.61	39.05	26.53	2.25	15.58	16.7
2	Mean	765.55	648.51	781.7	694.62	697.02	539.69	609.33
	±SD	46.91	17.24	17.77	21.33	21.21	21.94	14.2
3	Mean	BAD SIGNALS						
	±SD	BAD SIGNALS						
4	Mean	N/A	278.62	326.79	286.24	274.88	N/A	154.69
	±SD	N/A	16.53	13.36	9.54	2.24	N/A	41.02
5	Mean	143.04	176.23	237.68	261.92	272.7	199.07	296.1
	±SD	8.64	5.9	10.72	12.76	10.99	9.68	24.4
6	Mean	BAD SIGNALS						
	±SD	BAD SIGNALS						
7	Mean	627	405	464.67	375.68	209.06	194.54	255.27
	±SD	76.27	21.79	24.22	47.03	4.61	50.1	25.61
8	Mean	455.73	477.8	394.93	463.97	512.91	348.2	390.5
	±SD	35.85	73.29	66.37	14.05	19.67	5.81	24.67
9	Mean	806.33	729.03	562.1	756.89	594.33	578.46	649.2
	±SD	67.1	119.84	34.93	88.33	31.29	142.82	46.25
10	Mean	521.08	490.57	517.57	504.68	483.57	418.78	465.82
	±SD	53.01	20.89	78.81	7.73	16.06	36.24	37.22
11	Mean	BAD SIGNALS						
	±SD	BAD SIGNALS						
12	Mean	443.9	435.03	559.89	567.58	644.77	606.58	454.92
	±SD	30.63	5.03	102.76	28.83	32.1	18.27	65.91
Mean		515.09	445.36	463.21	468.96	441.97	398.60	390.61
±SD		42.79	32.79	43.11	28.46	15.60	37.56	32.89

Predicted Torque [Nm] – Extensors

Subject		Angle (degrees)						
		-30	-20	-10	0	10	20	30
1	Mean	3.6	5.66	BAD	5.81	BAD	5.49	7.89
	±SD	0.31	0.15		0.89		0.48	0.17
2	Mean	6.8	7.9	9.34	9.92	11.51	10.16	9.33
	±SD	0.7	0.21	0.33	0.3	0.43	0.26	0.39
3	Mean	3.5	3.82	3.57	3.21	3.31	3	2.35
	±SD	0.26	0.37	0.2	0.4	0.21	0.37	0.17
4	Mean	2.87	3.61	3.6	3.13	3.17	2.87	2.42
	±SD	0.22	0.4	0.39	0.19	0.27	0.18	0.28
5	Mean	BAD SIGNALS						
	±SD	BAD SIGNALS						
6	Mean	5.17	5.25	6.1	6.32	5.45	6.07	5.26
	±SD	0.9	0.52	0.62	0.5	1.04	1.44	1.05
7	Mean	3.92	4.08	4.28	3.58	2.94	3.68	5.25
	±SD	0.08	0.1	0.21	1.2	0.28	0.51	0.64
8	Mean	4.67	4.43	7.33	7.41	8.65	9.04	7.24
	±SD	0.18	0.24	0.15	0.5	0.74	0.82	1.38
9	Mean	4.09	4.55	5.59	6.3	7.42	5.02	4.84
	±SD	0.1	0.09	0.16	0.03	1.77	0.63	0.58
10	Mean	5.3	5.7	6.27	7.29	8.16	7.7	7.08
	±SD	0.23	0.11	0.84	0.44	0.87	0.69	0.96
11	Mean	BAD SIGNALS						
	±SD	BAD SIGNALS						
12	Mean	6.3	7.01	8.14	7.69	7.25	7.27	6.58
	±SD	0.2	0.24	0.67	0.34	0.16	0.48	0.04
Mean		4.62	5.20	6.02	6.07	6.43	6.03	5.82
±SD		0.32	0.24	0.86	0.48	1.08	0.59	0.57

Measured Torque [Nm] – Extensors

Subject		Angle (degrees)						
		-30	-20	-10	0	10	20	30
1	Mean	3.94	6.18	BAD	5.39	BAD	5.25	7.12
	±SD	0.79	1		0.7		0.42	0.54
2	Mean	6.71	7.74	9.38	10	10.96	10.23	9.76
	±SD	0.6	0.23	0.51	1.06	0.25	0.6	0.71
3	Mean	3.67	3.85	3.76	3.85	3.52	2.97	2.58
	±SD	0.12	0.11	0.04	0.21	0.16	0.5	0.15
4	Mean	3.04	3.42	3.46	3.19	3.53	2.93	2.71
	±SD	0.16	0.33	0.29	0.3	0.8	0.28	0.45
5	Mean	BAD SIGNALS						
	±SD	BAD SIGNALS						
6	Mean	4.94	5.23	6.03	6.5	5.76	5.75	5.16
	±SD	1.18	0.71	0.65	0.88	1.22	1.6	0.73
7	Mean	4.55	4.95	5.03	4.67	3.85	4.5	5.5
	±SD	0.3	0.16	0.13	2.12	1.2	0.83	0.45
8	Mean	4.54	5.2	6.74	7.1	8.3	8.74	6.92
	±SD	0.12	0.49	0.64	0.45	0.33	0.67	0.6
9	Mean	4.2	4.9	5.56	6.21	7.26	5.49	4.55
	±SD	0.21	0.48	0.63	0.36	1.45	0.56	0.23
10	Mean	5.44	5.69	6.33	6.71	7.22	7.19	6.38
	±SD	0.29	0.38	0.28	0.57	0.56	0.49	1.03
11	Mean	BAD SIGNALS						
	±SD	BAD SIGNALS						
12	Mean	6.39	6.99	7.62	6.92	6.99	6.98	6.34
	±SD	0.49	0.26	0.51	0.51	0.03	0.21	0.44
Mean		4.74	5.42	5.99	6.05	6.38	6.00	5.70
±SD		0.43	0.42	0.87	0.72	1.10	0.62	0.53

Predicted Force [N] – Extensors

Subject		Angle (degrees)						
		-30	-20	-10	0	10	20	30
1	Mean	351.39	463.2	BAD	610.99	BAD	677.04	1037.3
	±SD	29.85	11.87		94.22		58.75	21.52
2	Mean	543.74	646.79	888.71	918.13	1095.8	1046.7	1002.4
	±SD	56.01	17.02	31.4	27.96	40.82	26.29	41.57
3	Mean	343.49	317.83	330.31	327	359.62	345.5	308.26
	±SD	25.62	30.38	18.54	40.91	23.28	42.24	22.8
4	Mean	231.47	360.12	329.85	281.61	364.11	353.19	263.15
	±SD	17.57	39.31	7.46	17.33	31.16	22.41	30.69
5	Mean	BAD SIGNALS						
	±SD	BAD SIGNALS						
6	Mean	506.55	430.09	530.2	637.71	625.9	666.22	692.09
	±SD	88.11	41.96	53.81	50.92	120.13	157.83	138.56
7	Mean	383.91	388.27	385.25	350.24	117.91	371.89	589.61
	±SD	8.45	9.84	18.74	137.17	26.74	51.33	72.38
8	Mean	448.9	461	763.17	739.24	815.63	912.52	822.1
	±SD	17.37	25.08	15.73	49.77	69.69	83.02	156.64
9	Mean	400.42	385.38	582.36	677.6	851.94	660.13	635.62
	±SD	10.54	8.2	17.03	3.59	204.03	83.18	76.67
10	Mean	423.97	570.14	531.5	735.95	906.08	950.57	885.06
	±SD	18.22	11.16	70.73	44.73	96.45	85	119.43
11	Mean	BAD SIGNALS						
	±SD	BAD SIGNALS						
12	Mean	503.89	574.47	846.77	768.28	832.95	897	738.56
	±SD	15.92	20.1	69.83	34.38	18.06	59.59	4.32
Mean		413.77	459.73	576.46	604.68	663.33	688.08	697.42
±SD		28.77	21.49	30.83	50.10	63.54	66.96	68.46

Appendix C

Range of motion coordinates, L_{TS}/L_{OM} , L_{OM}/MA , PCSA and muscle stress values (σ).

Flexors

Subject		Range of Motion Coordinates	L_{TS}/L_{OM}	L_{OM}/MA	PCSA [cm ²]	σ [N/cm ²]
1	Lm/Lm0	0.9865 0.6559	3.36	4.24	19.77	18.82
	Fm/Fm0	0.9994 0.6223				
2	Lm/Lm0	1.019 0.7822	2.59	4.88	15.25	55.26
	Fm/Fm0	0.9989 0.8488				
3	Lm/Lm0	BAD SIGNALS	BAD SIGNALS	BAD SIGNALS	BAD SIGNALS	BAD SIGNALS
	Fm/Fm0	BAD SIGNALS	BAD SIGNALS	BAD SIGNALS	BAD SIGNALS	BAD SIGNALS
4	Lm/Lm0	0.927 0.6008	2.75	3.98	20.61	16.49
	Fm/Fm0	0.983 0.4919				
5	Lm/Lm0	0.9869 0.5435	4.06	3.37	24.36	14.56
	Fm/Fm0	0.9995 0.3355				
6	Lm/Lm0	BAD SIGNALS	BAD SIGNALS	BAD SIGNALS	BAD SIGNALS	BAD SIGNALS
	Fm/Fm0	BAD SIGNALS	BAD SIGNALS	BAD SIGNALS	BAD SIGNALS	BAD SIGNALS
7	Lm/Lm0	1.164 0.6072	3.33	4.21	18.88	24.93
	Fm/Fm0	0.9141 0.5081				
8	Lm/Lm0	0.9654 0.7599	2.58	5.31	14.82	33.42
	Fm/Fm0	0.9962 0.81				
9	Lm/Lm0	0.98 0.7502	2.56	5.29	15.45	58.23
	Fm/Fm0	0.9987 0.801				
10	Lm/Lm0	1.005 0.8081	2.55	5.02	14.64	35.99
	Fm/Fm0	0.9999 0.8826				
11	Lm/Lm0	BAD SIGNALS	BAD SIGNALS	BAD SIGNALS	BAD SIGNALS	BAD SIGNALS
	Fm/Fm0	BAD SIGNALS	BAD SIGNALS	BAD SIGNALS	BAD SIGNALS	BAD SIGNALS
12	Lm/Lm0	0.9647 0.7496	2.67	5.87	15.11	41.42
	Fm/Fm0	0.996 0.8001				
Mean Lm/Lm0		1.0089 0.6953	2.94	4.69	17.66	33.23
Mean Fm/Fm0		0.9878 0.6778	0.53	0.79	3.43	16.17

Extensors

Subject		Range of Motion Coordinates		L_{TS}/L_{OM}	L_{OM}/MA	PCSA [cm²]	σ [N/cm²]
1	Lm/Lm0	1.043	0.8522	2.44	9.53	4.12	165.66
	Fm/Fm0	0.9842	0.9303				
2	Lm/Lm0	1.11	0.78	2.07	9.93	3.50	295.09
	Fm/Fm0	0.9614	0.8457				
3	Lm/Lm0	0.9988	0.7404	2.87	7.94	4.84	78.20
	Fm/Fm0	1	0.7852				
4	Lm/Lm0	1.02	0.8184	2.58	8.66	4.36	78.11
	Fm/Fm0	0.9988	0.8949				
5	Lm/Lm0	BAD SIGNALS		BAD SIGNALS	BAD SIGNALS	BAD SIGNALS	BAD SIGNALS
	Fm/Fm0	BAD SIGNALS		BAD SIGNALS	BAD SIGNALS	BAD SIGNALS	BAD SIGNALS
6	Lm/Lm0	1.08	0.8006	2.65	8.47	4.47	153.35
	Fm/Fm0	0.9998	0.8732				
7	Lm/Lm0	0.9854	0.8106	2.84	7.66	4.79	92.31
	Fm/Fm0	0.9993	0.8856				
8	Lm/Lm0	1.09	0.8145	1.87	11.66	3.15	251.79
	Fm/Fm0	0.9742	0.8903				
9	Lm/Lm0	1.095	0.7995	2.36	10.07	3.98	173.04
	Fm/Fm0	0.971	0.8718				
10	Lm/Lm0	1.028	0.7801	2.77	8.12	4.66	172.55
	Fm/Fm0	0.9974	0.8459				
11	Lm/Lm0	BAD SIGNALS		BAD SIGNALS	BAD SIGNALS	BAD SIGNALS	BAD SIGNALS
	Fm/Fm0	BAD SIGNALS		BAD SIGNALS	BAD SIGNALS	BAD SIGNALS	BAD SIGNALS
12	Lm/Lm0	1.078	0.8172	2.27	9.77	3.83	208.00
	Fm/Fm0	0.9807	0.8935				
Mean Lm/Lm0		1.0528	0.8014	2.47	9.18	4.17	166.81
Mean Fm/Fm0		0.9867	0.8716	0.32	1.23	0.54	69.08

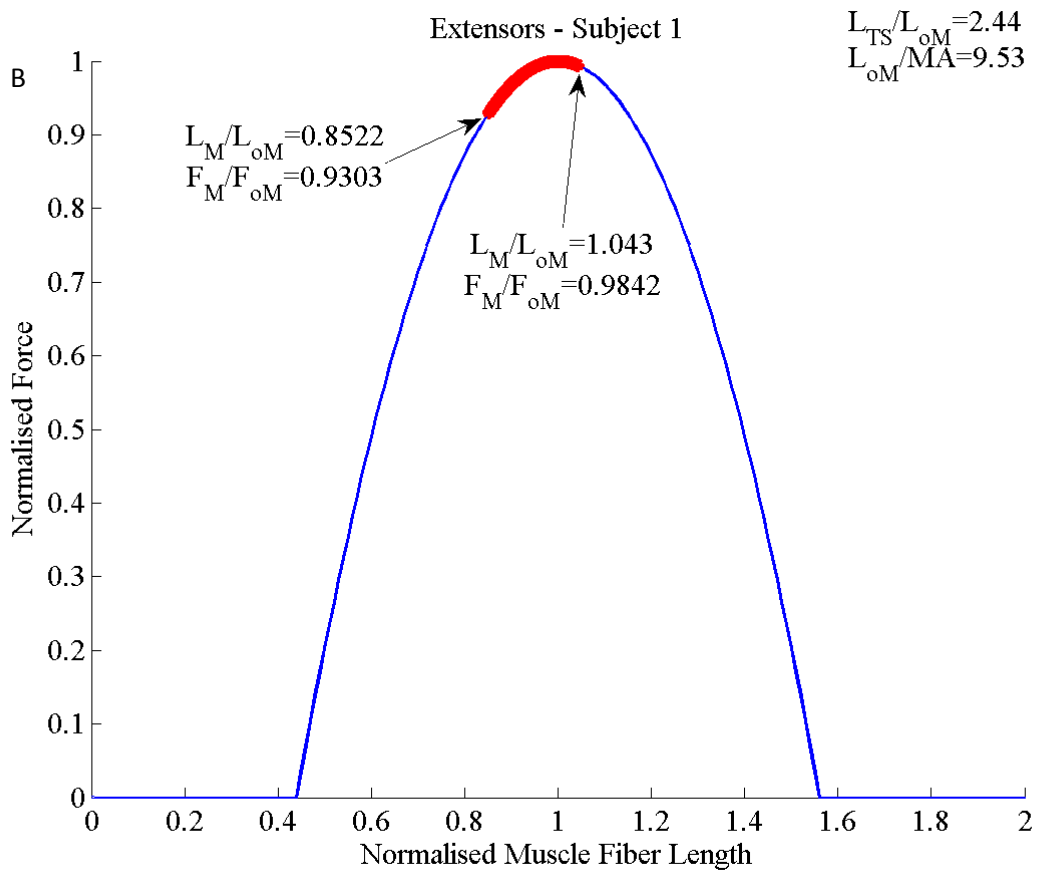
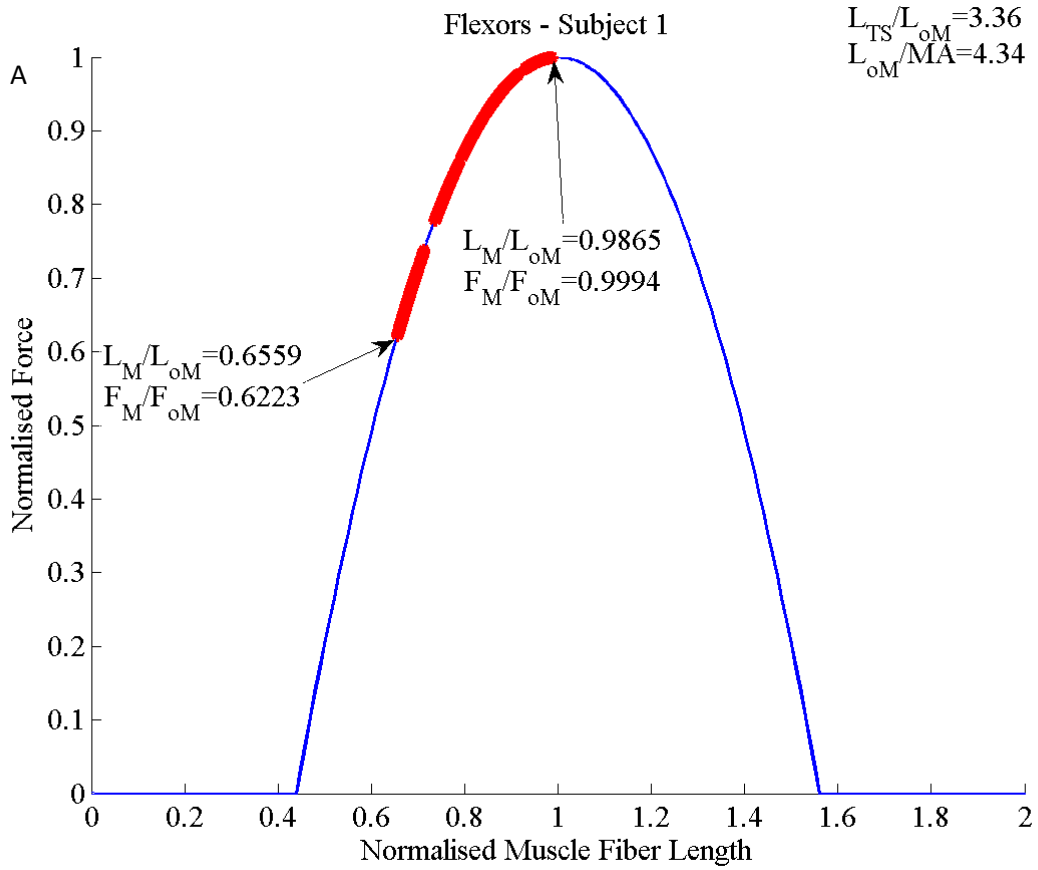


Figure 53

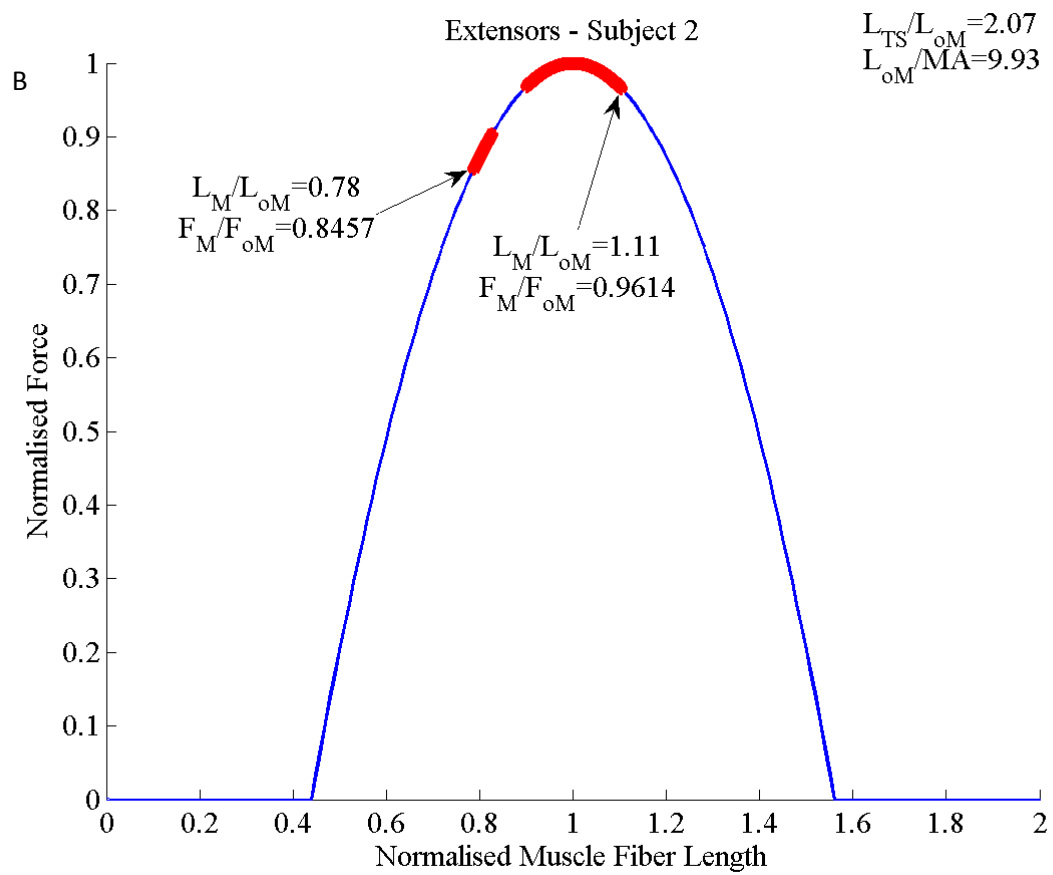
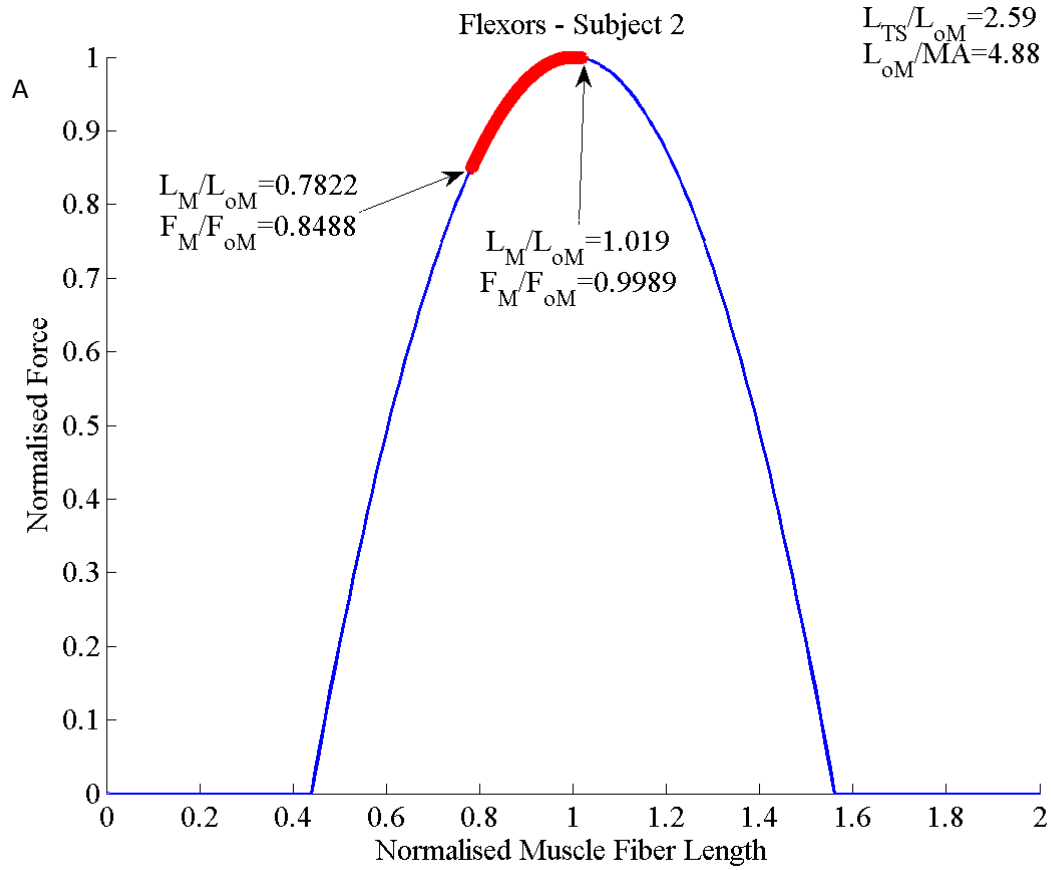


Figure 54

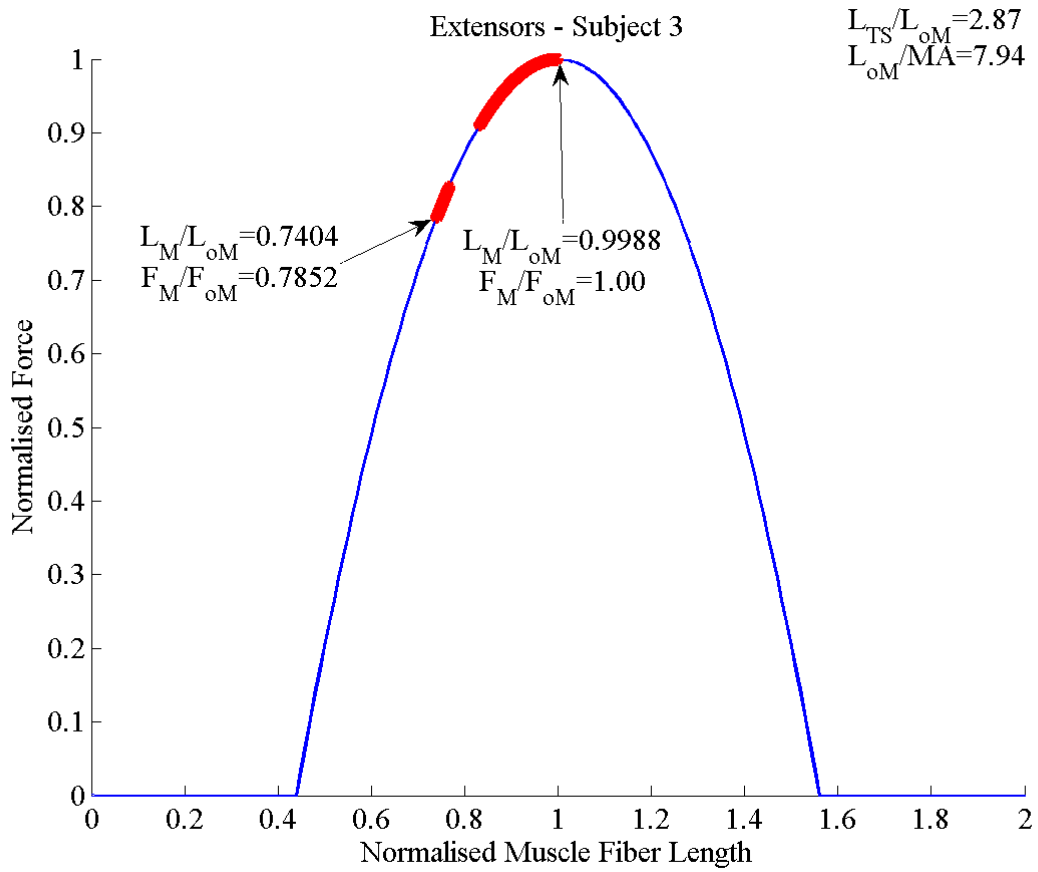


Figure 55

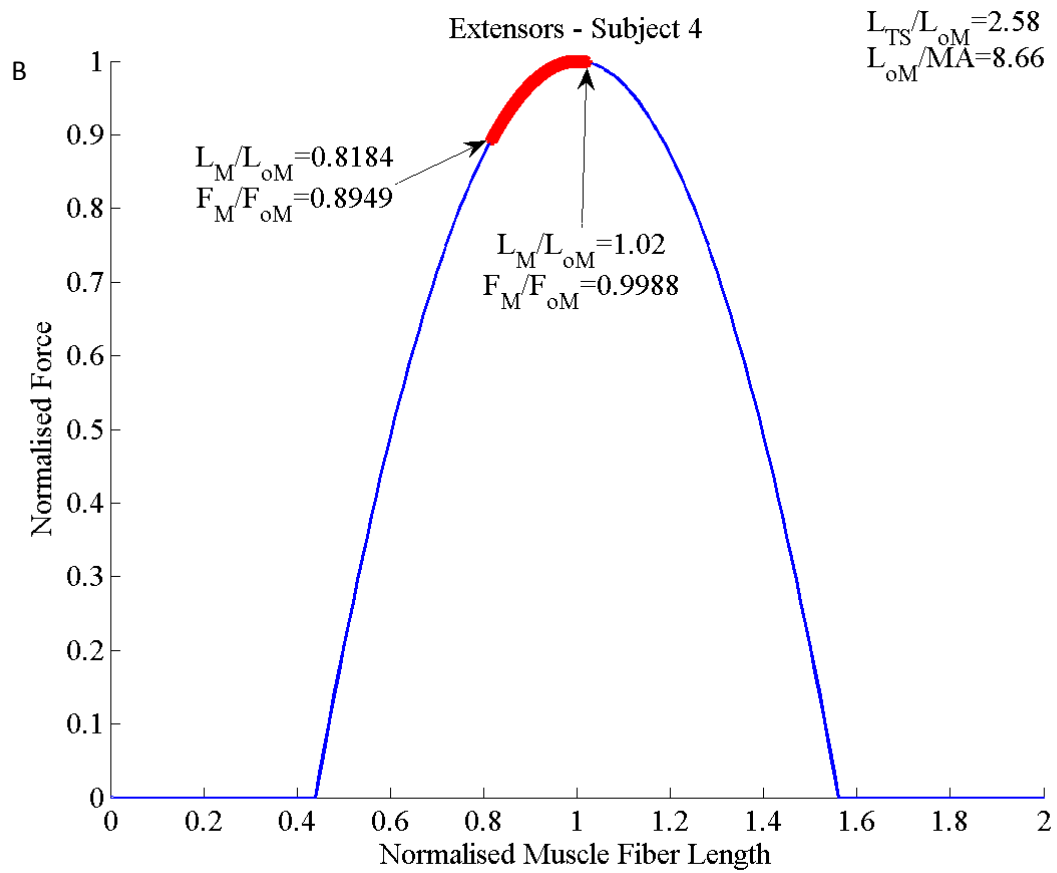
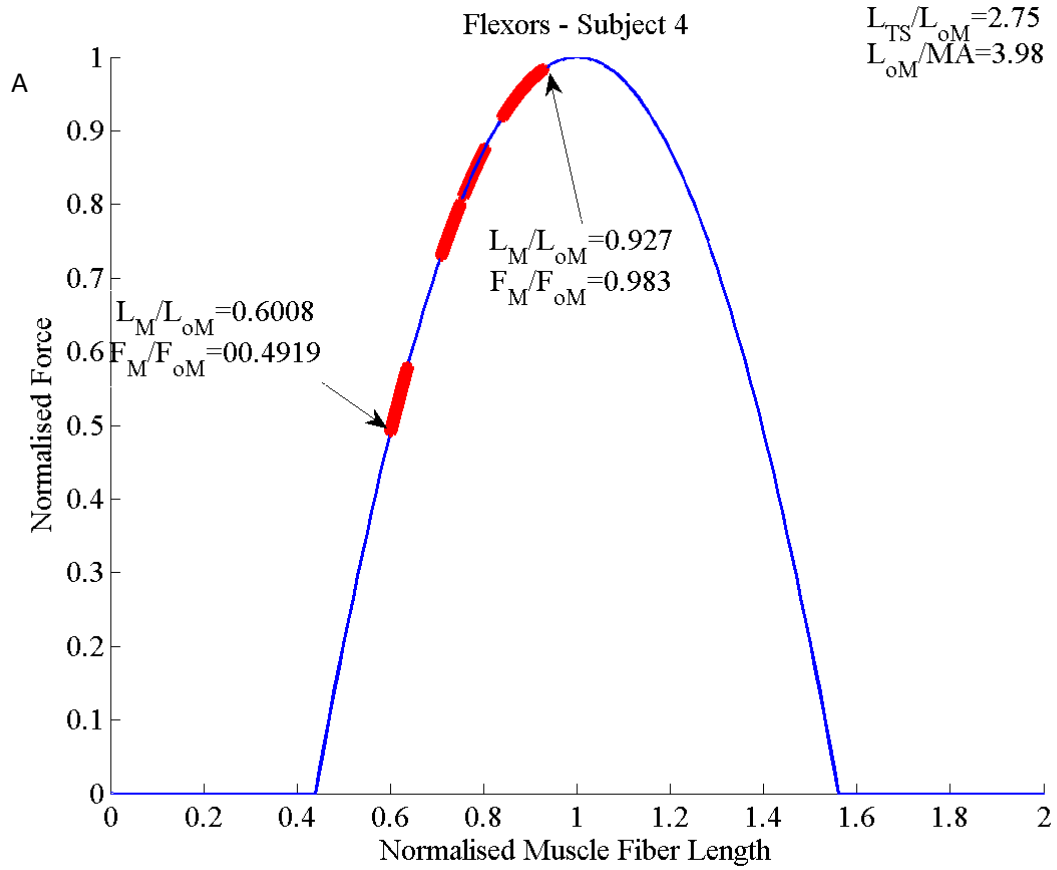


Figure 56

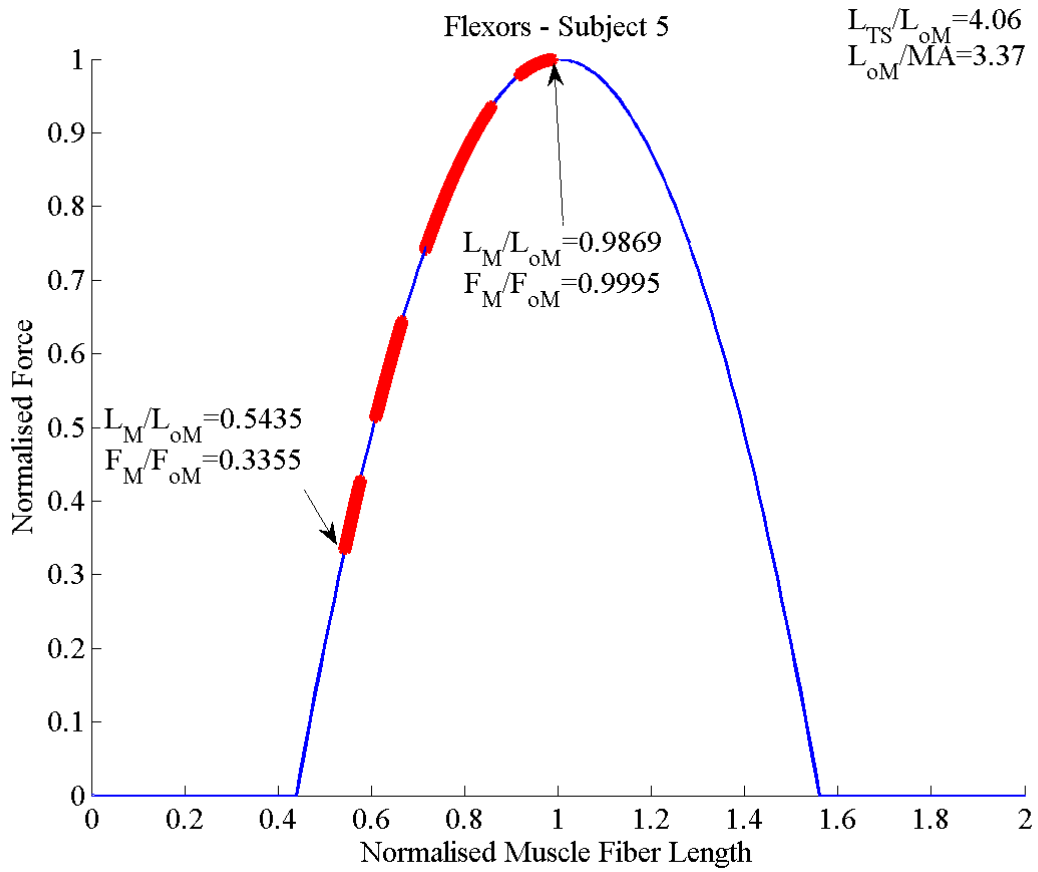


Figure 57

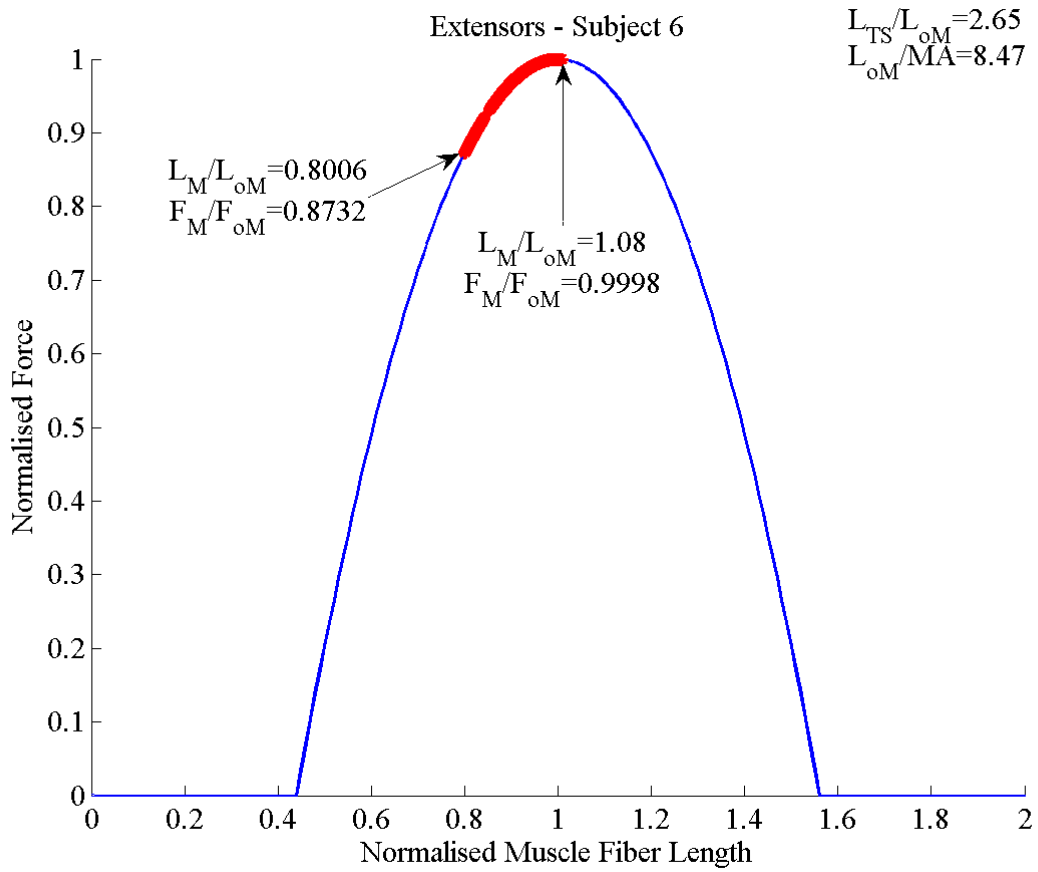


Figure 58

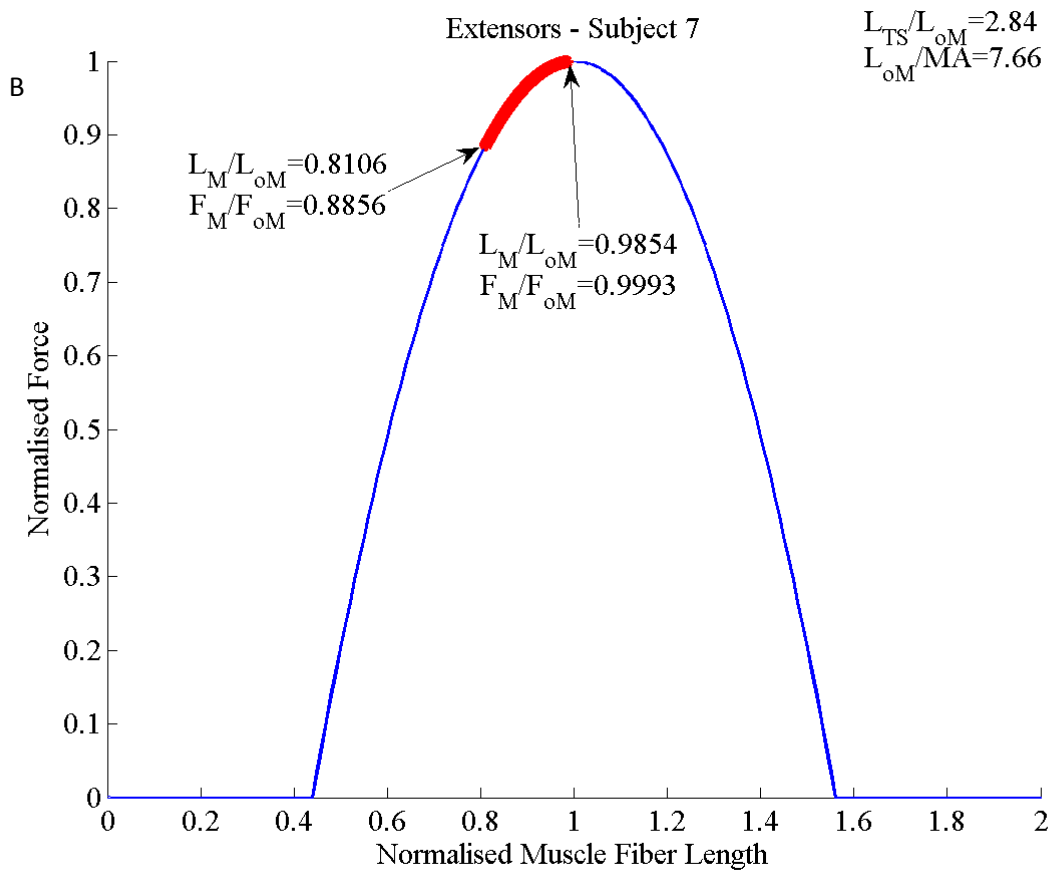
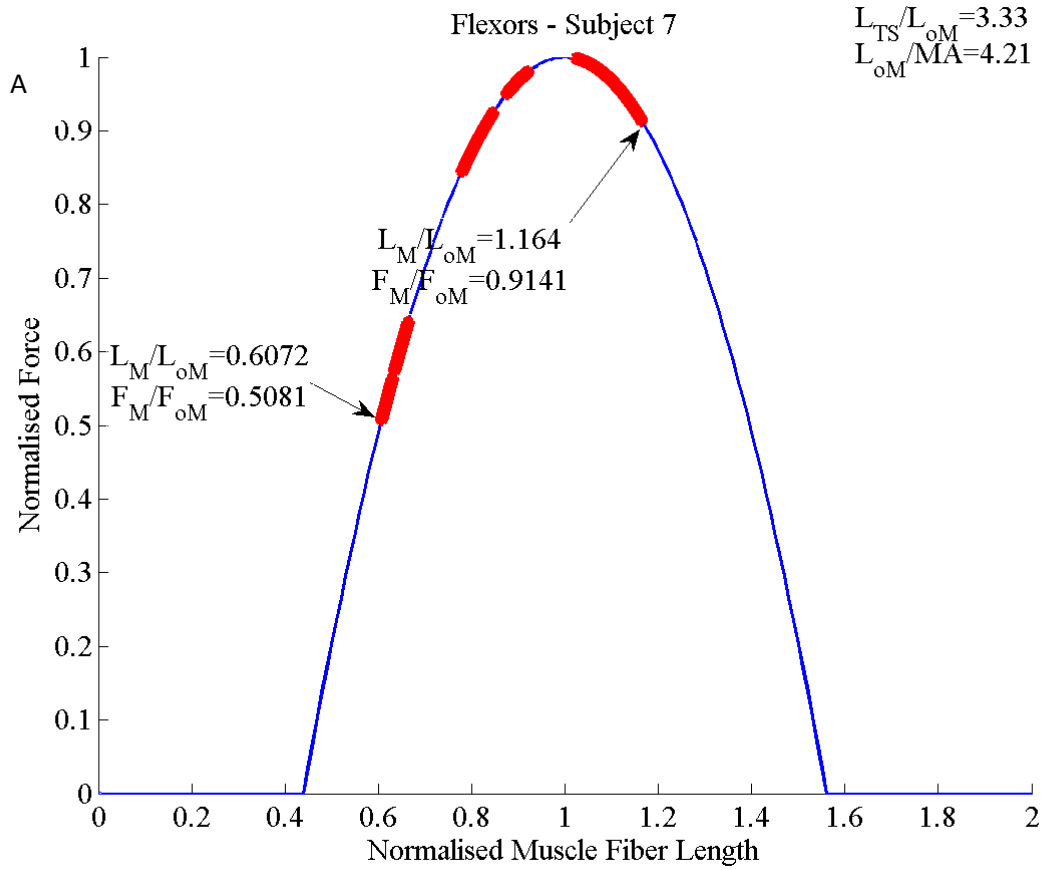


Figure 59

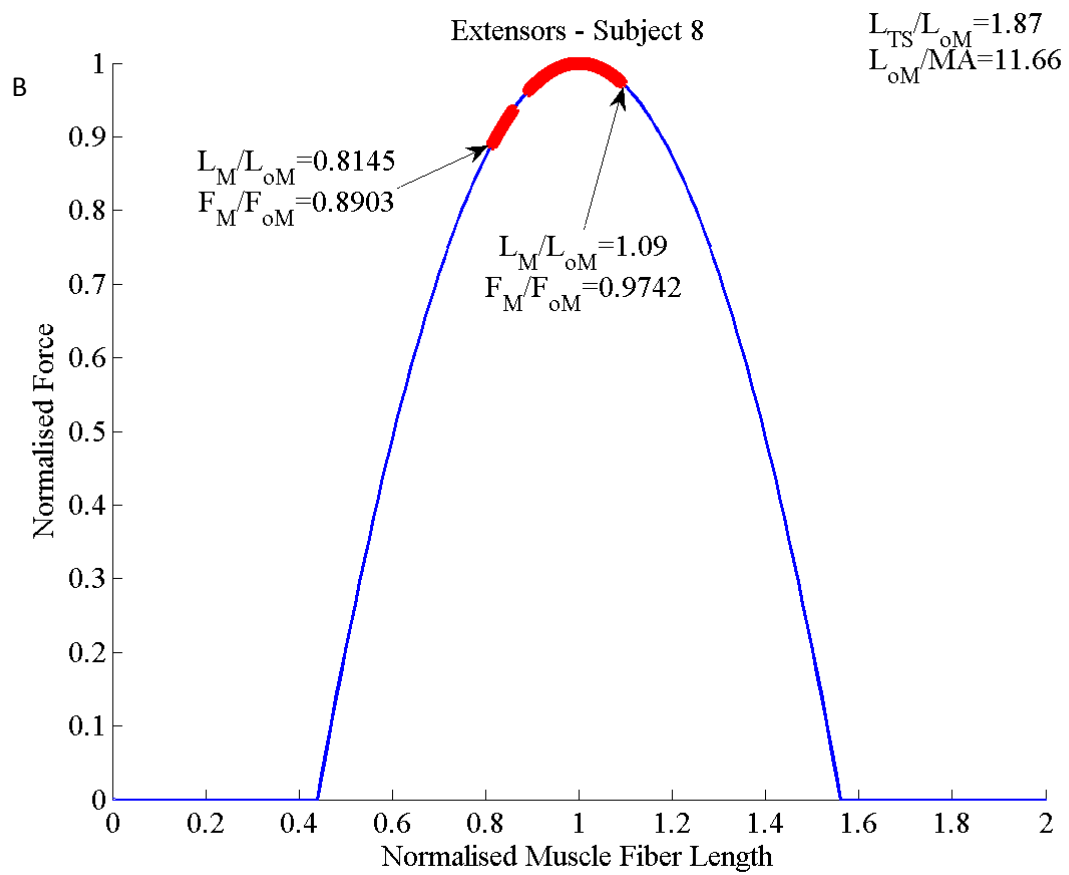
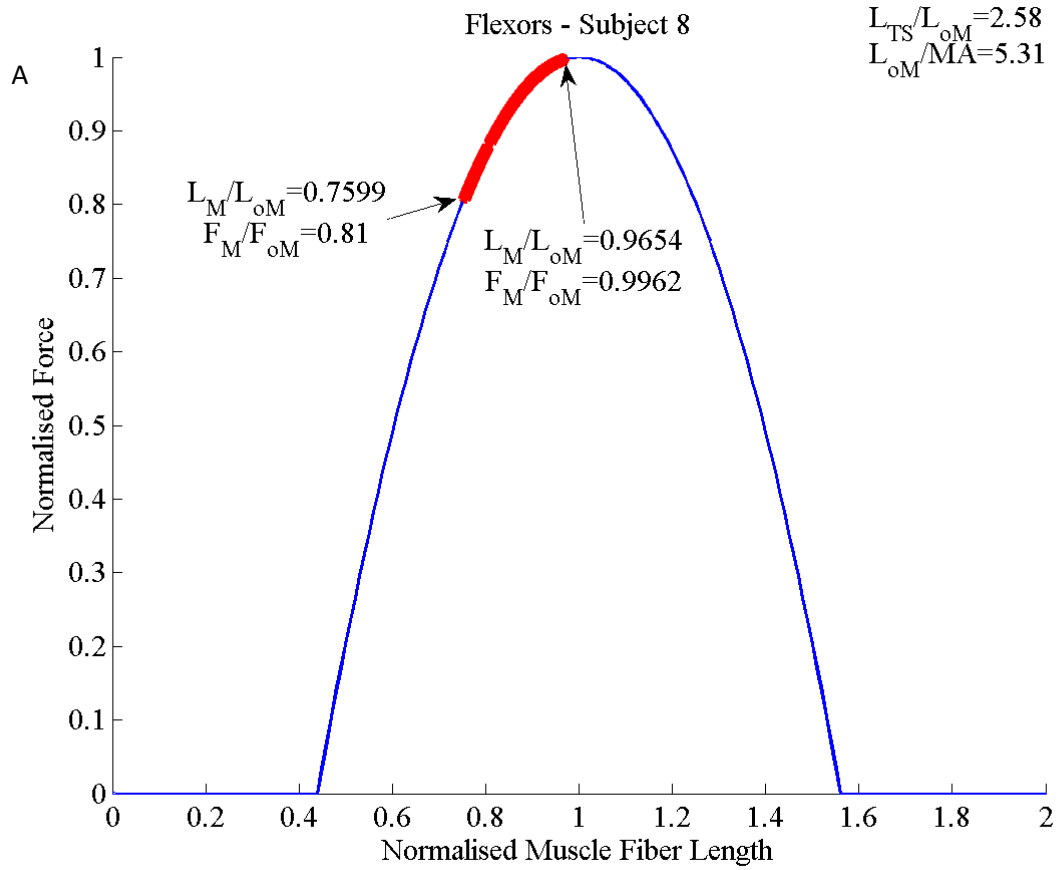


Figure 60

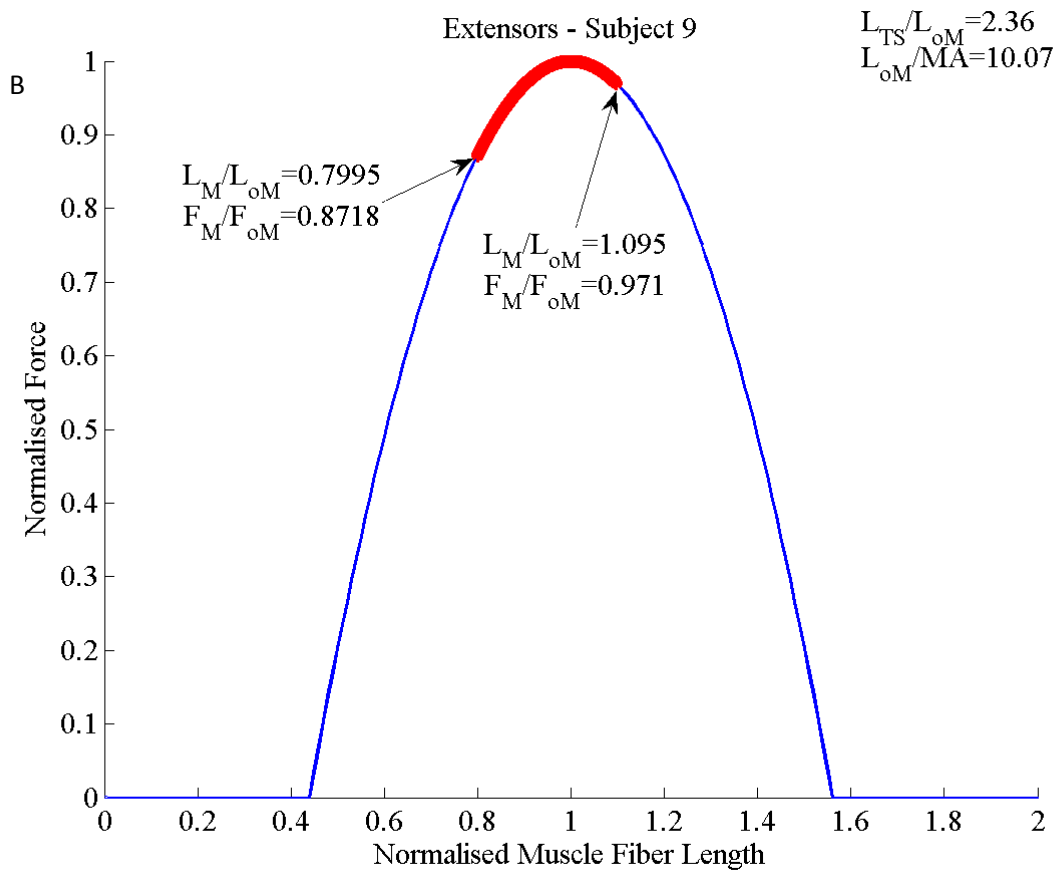
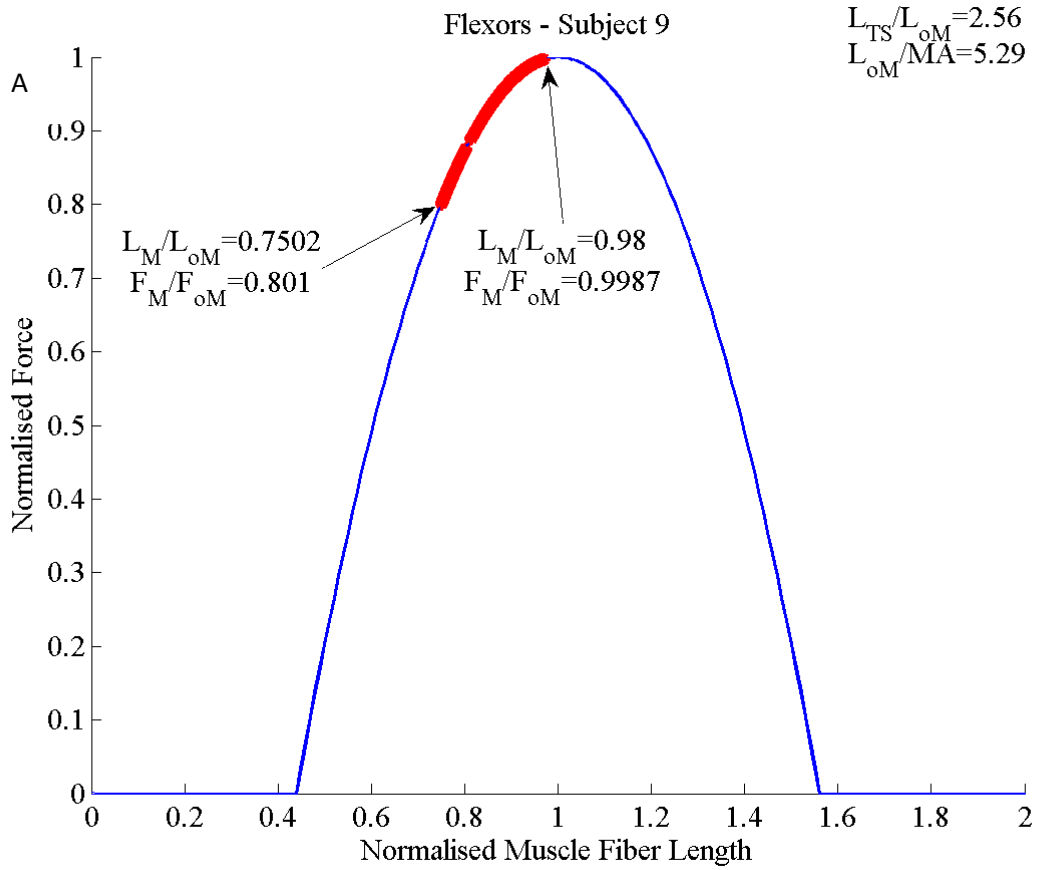


Figure 61

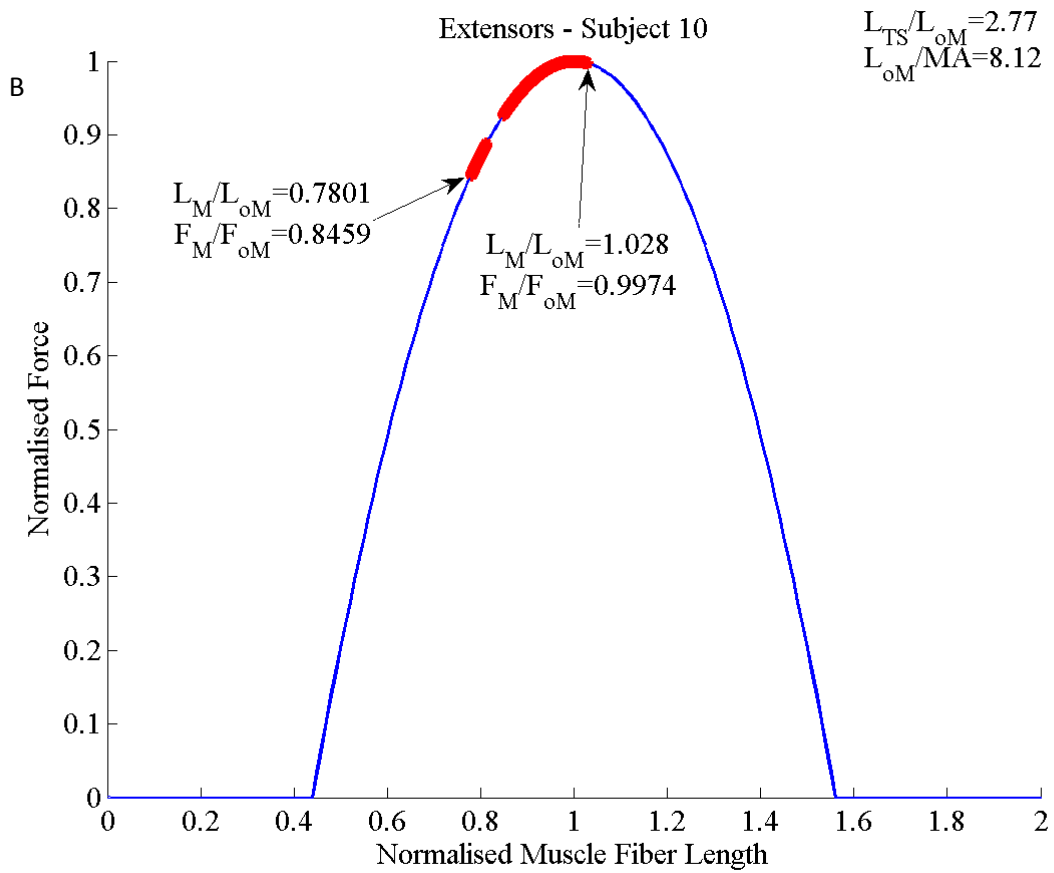
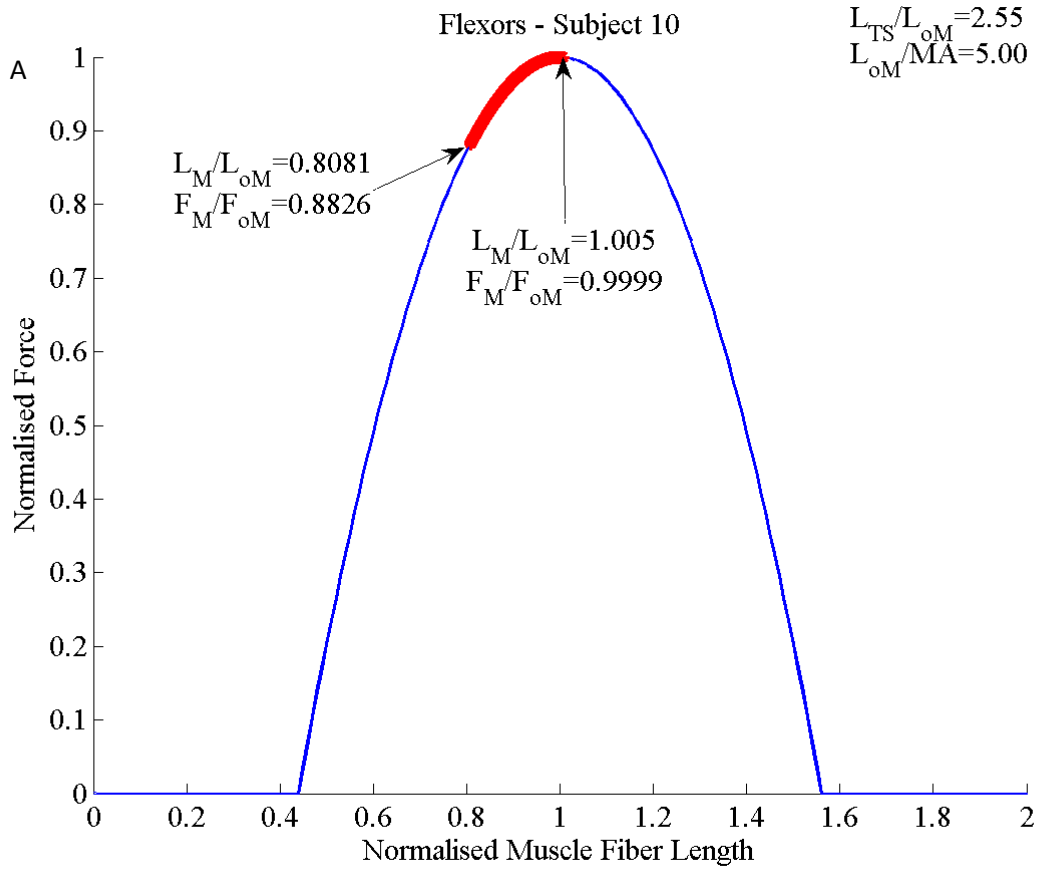


Figure 62

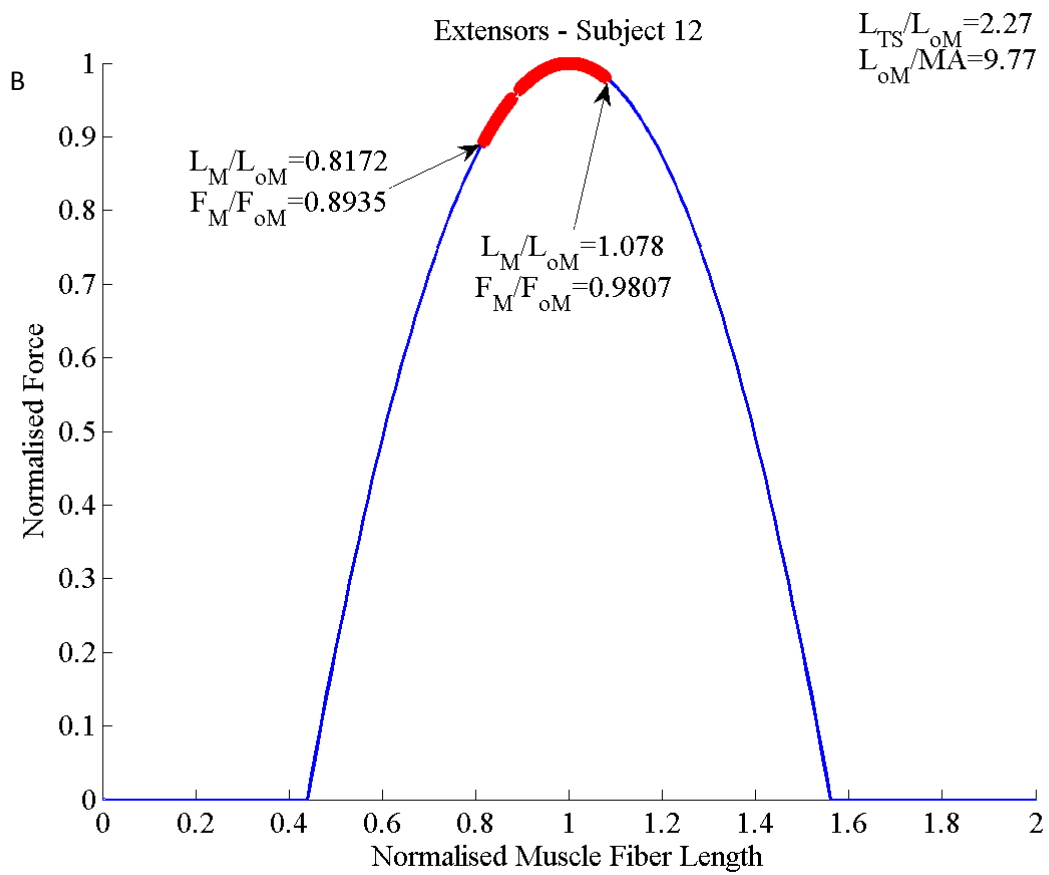
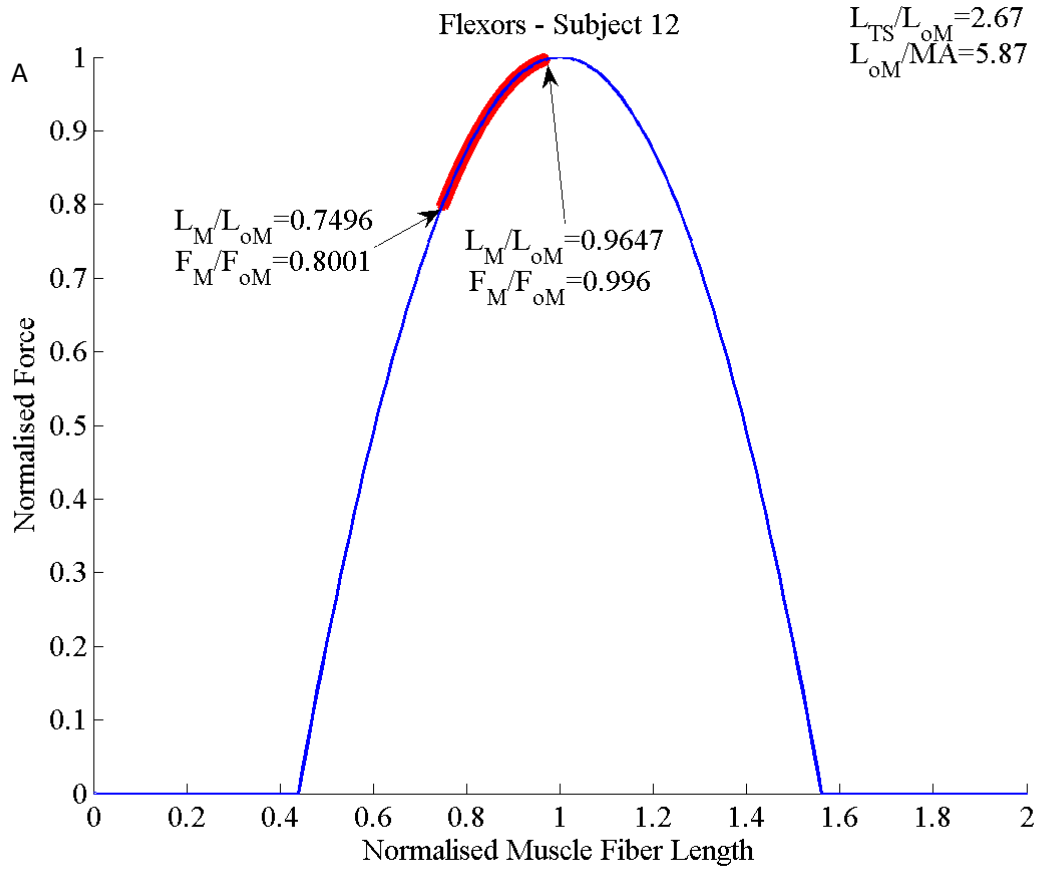


Figure 63